MODULATION OF DORSAL HIPPOCAMPUS FIELD CA1 PYRAMIDAL CELL EXCITABILITY BY AN ASCENDING RELAY FROM HYPOTHALAMIC SUPRAMAMMILLARY NUCLEUS

JIANG FENGLI

A THESIS SUBMITTED FOR

THE DEGREE OF DOCTOR OF PHILOSOPHY

DEPARTMENT OF PHYSIOLOGY

NATIONAL UNIVERSITY OF SINGAPORE

2004

ACKNOWLEDGEMENTS

This research work was carried out at the Department of Physiology, National University of Singapore. I would like to express my deepest and sincerest gratitude to my supervisor, Associate Professor Sanjay Khanna, for his patient guidance and suggestions, criticisms, and friendly encouragement throughout the course of my Ph.D training.

I also express my thanks to Ms. Esther Chang, Senior Laboratory Officer, for the technical support provided.

Finally, I am forever indebted to my parents and my wife for their understanding, endless patience and encouragement during my difficult moments.

TABLE OF CONTENTS

LIST OF FIGURES

LIST OF ABBREVIATIONS

CA	cornu ammonis
CHAT	choline acetyltransferase
CSD	current source density
dfEPSP	dendritic field excitatory postsynaptic potential
EEG	electroencephalogram
EPSC	excitatory postsynaptic current
EPSP	excitatory postsynaptic potential
fEPSP	field excitatory postsynaptic potential
FFT	fast Fourier Transform
Fr	fasciculus retroflexus
GABA	gamma aminobutyric acid
Hz	hertz
i.p.	intraperitoneal
kg	kilogram
LDT	laterodorsal tegmental nucleus
LTP	long-term potentiation
lSUM	lateral supramammillary region
MB	mammillary body

MFB	medial forebrain bundle
mg	milligram
mm	millimeter
min	minute
ml	milliliter
μg	microgram
μl	microliter
mSUM	medial supramammillary region
ms	millisecond
mV	millivolt
MS-VLDBB	medial septum-vertical limb of diagonal band of Broca
PH	posterior hypothalamus
PS	population spike
PPT	pedunculopontine tegmental nucleus
RSA	rhythmic slow activity
RPO	reticular pontis oralis nucleus
sfEPSP	somatic field excitatory postsynaptic potential
SUM	supramammillary region
SUMX	supramammillary decussation

LIST OF PUBLICATIONS

1. Jiang, F. and Khanna, S. (2004) Reticular stimulation evokes suppression of CA1 synaptic responses and generation of theta through separate mechanisms. *Eur. J. Neurosci*. 19(2): 295-308.

2. Khanna, S., Chang, L.S., Jiang, F. and Koh, H.C. (2004) Nociception-driven decreased induction of Fos protein in ventral hippocampus field CA1 of the rat. *Brain Res.* 1004(1-2): 167-176.

3. Jiang, F. and Khanna, S. (in preparation) Cholinergic mechanisms in supramammillary region mediate suppression of CA1 pyramidal cell synaptic excitability.

ABSTRACTS

1. Jiang, F., Khanna, S. and H. Wong, P.T. (2001) Effect of posterior hypothalamic microinjection of procaine on hippocampal nociceptive responses. Society for Neuroscience's 31st Annul Meeting. Prog#: 280.9, November 10-15, San Diego, CA, USA.

2. Jiang, F. and Khanna, S. (2002) Ascending relay mediating hippocampal nociceptive responses. 1st NNI-NUS *N*euroscience *S*ymposium. D-2, March 14-16, Singapore.

SUMMARY

Reticular stimulation-induced hippocampal theta involves a relay to the hippocampus via the posterior hypothalamus-supramammillary (PH-SUM) region and then the medial septum-vertical limb of diagonal band of Broca (MS-VLDBB). Interestingly, sensory- or behavior-induced theta is accompanied by suppression of hippocampal field CA1 synaptic responses. Given the links between theta activity and synaptic responses in CA1, it was hypothesized that the theta generating stimulation, such as that of the region of the reticular pontis oralis (RPO) nucleus (or reticular stimulation) will evoke a suppression of CA1 synaptic excitability that is mediated via a neural relay involving the PH-SUM and the MS-VLDBB regions. Additionally, the role of the PH-SUM region in regulating CA1 excitability was assessed with direct chemical stimulation of the region.

The experiments were performed on urethane anaesthetized rats. Reticular stimulation induced a suppression of the CA1 pyramidal cell population spike and the corresponding dendritic field excitatory postsynaptic potential evoked by field CA3 stimulation. However, this suppression was observed at stimulation intensity below the threshold for generation of CA1 theta and was maximal at the threshold for theta. The frequency and amplitude of theta waves, by contrast, increased further with increasing reticular stimulation voltage. The foregoing suggested that mechanisms underlying reticularly-elicited suppression and generation of theta were dissociated.

Neural inactivation by microinjection of the local anaesthetic procaine (20%w/v, 0.1-0.2 µl) or the inhibitory ligand gamma aminobutyric acid (0.8 M, 0.5 µl) in the PH-SUM, especially the

ipsilateral medial SUM region, or the MS-VLDBB region, attenuated both suppression and theta generation. However, and as with effect of reticular stimulation, the effects of microinjection on suppression and theta were not always in parallel. In this regards: (1) the effect of inactivation of medial SUM and the medial forebrain bundle (MFB; a fibre bundle with brainstem/diencephalic afferents travelling to the hippocampal formation) on reticularly-elicited population spike (PS) suppression preceded the loss of theta rhythm; (2) microinjection of procaine into MS-VLDBB region, especially in the lateral regions, attenuated suppression with no apparent loss of theta; (3) while the onset of effect of MS-VLDBB procaine on suppression paralleled the decrease in amplitude of RPO elicited theta, the population spike suppression recovered to control even though the amplitude of theta remained strongly reduced; and (4) the recovery of PS suppression from microinjection of GABA in the medial SUM region preceded the recovery of theta amplitude. Put together, the above suggests that separate neural elements in close anatomical proximity to theta-related neurons in SUM and MS-VLDBB regions mediate reticularly-elicited suppression.

Consistent with the notion that separate neural elements, at least in part, mediate CA1 suppression, the effect of microinjection of GABA on RPO elicited PS suppression was observed from relatively fewer sites as compared to the effect of the agent on theta activation. In this context, microinjections into the medial SUM region attenuated both PS suppression and theta activation, whereas microinjection into the lateral SUM region and lateral-ventral sites in PH did not affect suppression although the RPO elicited theta amplitude was reduced. Similarly, microinjection into the MFB did not affect suppression. The lack of effect of GABA from lateral SUM and MFB regions contrasts with the robust attenuation of suppression following procaine microinjection at these sites. The foregoing pattern of effect with GABA is compatible with the

view that the influence of SUM GABA on CA1 suppression is due to a selective affect of the agent on synaptic transmission in the medial region. Perhaps, the medially positioned neurons send their axons laterally to join MFB which might explain, at least in part, the efficacy of lateral microinjection of procaine on suppression.

To further investigate whether neuronal mechanism in the SUM region mediate CA1 pyramidal cell suppression, the medial or leteral region of SUM was chemically excited with local microinjection of the cholinergic agonist, carbachol (carbamoylcholine chloride). Results indicated that carbachol microinjected at concentrations of 0.0285-, 0.854- or 3.42-mM evoked concentration–dependent suppression of CA1 population spike. As with RPO stimulation, the carbachol-induced suppression of CA1 pyramidal cell excitability was accompanied by decrease in the slope of the corresponding somatic field excitatory postsynaptic potential. The carbachol-induced suppression of CA1 pyramidal cell excitability was antagonized by systemically administrated cholinergic-muscarinic antagonist, atropine (5 mg/kg, i.p.), though the antagonist did not antagonize the suppression and theta induced by tail pinch. Taken together, the foregoing indicates that cholinergic mechanisms in the SUM region influence CA1 pyramidal cell excitability.

The suppression of CA1 population spike with microinjection of 0.0285 mM carbachol was observed in absence of theta, whereas with the higher concentrations of carbachol the suppression was accompanied by theta activation. While the maximal suppression evoked with higher concentrations of carbachol was greater than the maximal suppression evoked on RPO stimulation, the maximal RPO stimulation-evoked theta peak frequency and peak power was significantly greater than that evoked at maximal suppression with the higher concentrations of

carbachol. Both suppression and theta activation observed with microinjection of 0.854 mM carbachol were reversibly attenuated by inactivation of the MS-VLDBB region with microinjection of procaine, indicating that the suppression evoked by direct activation of SUM was also mediated by the MS-VLDBB region.

On probing the PH-SUM region with the lower concentration of carbachol (0.0285 mM), it was observed that the microinjection into the lateral SUM, but not medial SUM and PH evoked robust suppression of PS at short latency. The medial SUM carbachol injections, as whole, were ineffective in eliciting suppression. The greater potency of lateral injections in evoking suppression is consistent with anatomical evidence of a large projection from the region to MS-VLDBB.

Overall, the current study provides evidence that the SUM region mediates a decrease in excitatory synaptic transmission at the apical dendrites of CA1 pyramidal cells via neural mechanisms that are distinct, at least in part from those mediating CA1 theta activation. The neural elements in SUM that mediate suppression include cholinoceptive neurons in the lateral SUM region. The neural pathway from SUM involves the MS-VLDBB region in anatomical overlap with the neural components underlying theta generation. The finding that the medial SUM region is preferentially recruited on reticular stimulation, while a cholinergic agonist affects lateral SUM region with greater potency, suggests the possibility that the SUM is organized in a modular fashion in regulation of CA1 excitability. The activation of the ascending inhibitory pathway(s) from SUM together with theta generation may provide a neural basis for regulating hippocampal excitability during the theta functional state of the hippocampus.

CHAPTER I INTRODUCTION

1.1 General morphology

The hippocampus (cornu ammonis or CA) is a three-layer allocortex, which is a part of hippocampal formation (including hippocampus, dentate gyrus and subiculum). The three-dimensional position of the rat hippocampal formation in the brain is rather complex. It appears grossly as an elongated structure with its long axis extending in a C-shaped fashion from the septal nuclei of the basal forebrain rostrodorsally, over and behind the thalamus, to the incipient temporal lobe caudoventrally (Fig. 1.1A; Swanson et al., 1978; Amaral and Witter, 1995). The long axis and orthogonal axis are referred to as the septotemporal and transverse axis, respectively. The part of the hippocampus lying above the thalamus is often called the dorsal hippocampus and the temporal part the ventral hippocampus.

The pioneering work on the cytoarchitecture of the hippocampus was performed by Ramón y Cajal (1893) and Lorente de Nó (1934), and has been reviewed and updated in more recent review articles (Amaral and Witter, 1995; Freund and Buzsáki, 1996). The description of the hippocampal cytoarchitecture given below is based on the foregoing articles. It is notable that the cytoarchitecture has been derived using a variety of techniques, including Weigert-Pal, Golgi or Cox preparation, and intracellular labeling with dye.

The hippocampus has two major subfields, namely the fields CA1 and CA3 (Fig. 1.1B) that differ in terms of the size of the principal (pyramidal) neurons and connections (see below). Although Lorente de Nó (1934) also defined another hippocampal region, namely field CA2, this area has not received any extensive attention and is ignored here.

Fig. 1.1: The rat hippocampal formation: location, subdivision and cytoarchitecture. A. Three dimensional illustration of the hippocampal formation (hippocampus and the dentate gyrus). Note the C-shaped structure of the hippocampal formation and its position in the brain. The hippocampal formation extends from the basal forebrain, over and behind the diencephalon (not shown here), to the temporal lobe. B. Nissl stained coronal section through the dorsal hippocampus (rectangular panel in A), showing the subfields of hippocampal formation. The two major subfields illustrated are CA1 and CA3, while DG is the dentate gyrus. In the dorsal to ventral order in the coronal section, the layers of the hippocampus-DG are the: alveus (a), stratum oriens (o), stratum pyramidale (p), stratum radiatum (r), stratum lacunosum (l), stratum moleculare (m), stratum granulosum (g), and hilus (or stratum polymorphe; h).

A.

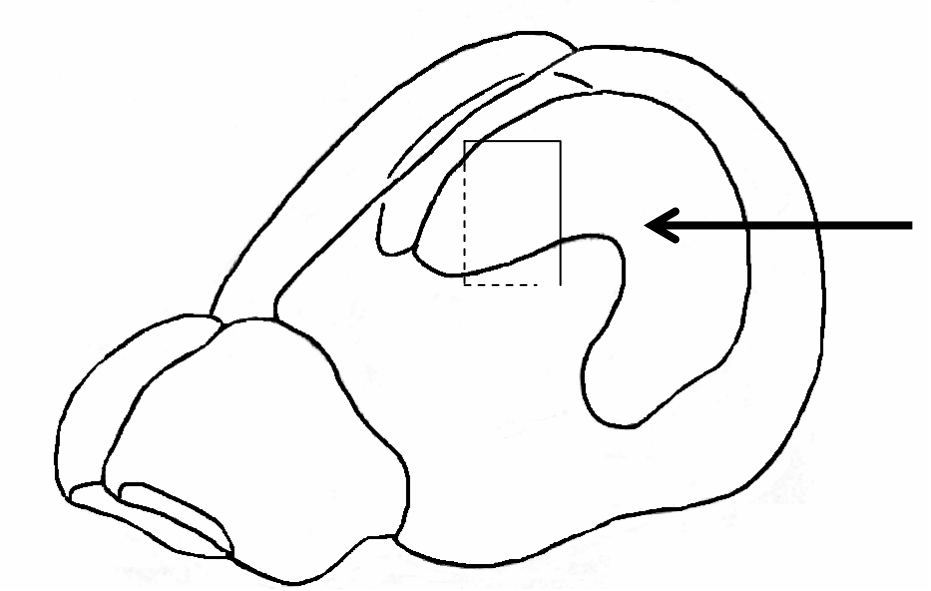

B.

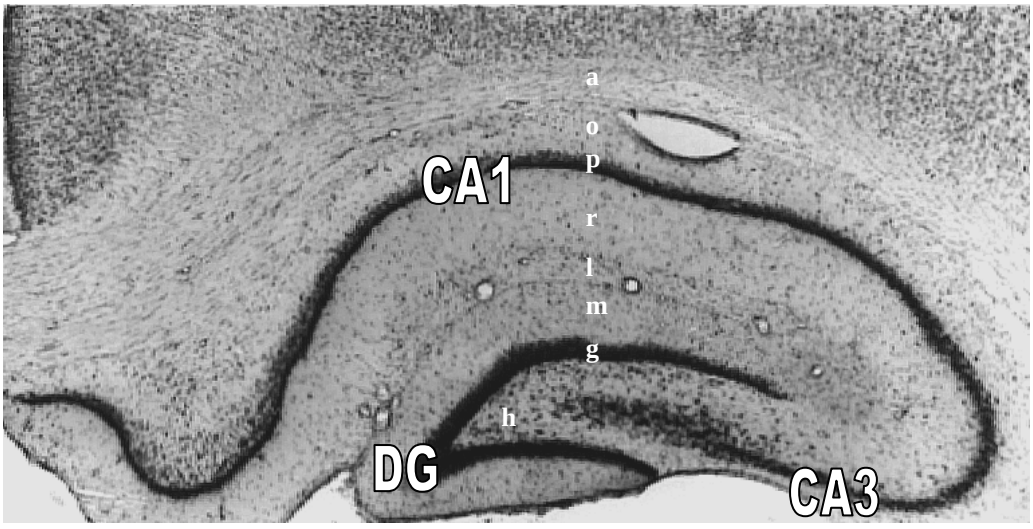

In a dorsal to ventral order in the transverse section, the layers of the hippocampus-dentate gyrus are the: alveus, stratum oriens, stratum pyramidale, stratum radiatum, stratum lacunosum, stratum moleculare, stratum granulosum and stratum polymorphe (Fig. 1.1B).

The alveus is a fiber bundle marking the outer boundary of the hippocampus. The stratum oriens has number of interneuron type near the border with alveus and, in addition, also contains basal dendrites and axon collateral from pyramidal cells. The interneurons include (a) O-LM cells (interneuron with soma and dendrites in stratum oriens, and axons in strata lacunosum-moleculare and oriens), which have an oval or pyramidal shaped soma. The dendrites of these cells are either largely confined to stratum oriens (in field CA1) or span all layers except stratum lacunosum-moleculare (in field CA3). The axons of these neurons arborize in stratum lacunosum-moleculare forming synapse with distal dendrites and spines of presumed pyramidal cells. Occasionally, axonal branches are also directed towards stratum oriens, (b) bistratified and horizontal trilaminar cells. The dendrites of bistratified cells are mostly radially oriented and extend up to stratum radiatum, while the axon arborizes in stratum oriens and in the proximal stratum radiatum forming synapse with proximal dendrites and dendritic spine of pyramidal cells. The trilaminar cells posses either horizontal dendrites running in stratum oriens or radial dendrites that can extend up to stratum lacunosum-moleculare. The axon arbor of trilaminar cells is observed in three layers, namely stratum oriens, stratum pyramidale and stratum radiatum, and (c) other types that include interneurons that project across subfield boundaries and interneurons specialized to innervate other interneurons. Basket cell interneurons that innervate the soma and proximal dendrites may also be observed in the region (Klausberger et al., 2003).

The stratum pyramidale has 3-4 rows of the principal (pyramidal) cells. The pyramidal cells of hippocampus along with the principal (granule) cells of the dentate gyrus make up the bulk (~90%) of the cell population in the two regions (Olbricht and Braak, 1985). The cell bodies of the pyramidal neurons are fusiform or ovoid. The soma of the pyramidal cells in field CA1 is smaller as compared to those in field CA3. In CA1 region the pyramidal cells have a single apical dendritic tree that extends into stratum radiatum. Several processes emit from apical dendrite in stratum radiatum. These dendritic processes finally terminate in a tuft of thin branches in stratum lacunosum-moleculare, and in most cases reach the hippocampal fissure. Basal dendrites from CA1 pyramidal cells are numerous. These arborize in stratum oriens and often reach the alveus. The axon of pyramidal cells usually emerges from the region of soma adjacent to the apical dendrite or occasionally from a basal dendrite before entering the alveus.

The pyramidal cells from CA3 give rise to one or two prominent apical dendrites usually from the soma and often branch into large-diameter segments with proximately equal size. The apical dendrites are radially oriented in strata radiatum and lacunosum-moleculare, where they give rise to additional thin side branches that reach the hippocampal fissure or the border of the hilus. The axons of CA3 pyramidal cells usually arise from a primary basal dendrite or the lower pole of the soma. In addition to pyramidal cells, population of interneurons is found with soma located within or adjacent to stratum pyramidale. The first class of interneuron is basket cells. The predominant dendritic morphology of basket cells in CA1 and CA3 is pyramidal-shaped or bitufted. One or three dendrites originate from the apical pole of triangular or fusiform soma and then branch and ascend through stratum radiatum, often penetrating

stratum lacunosum-moleculare. The primary basal dendrites also branch close to the soma and proceed toward the alveus in a fan-like fashion, spanning the entire depth of stratum oriens (Gulyás et al., 1993; Sik et al., 1995). The axon from the basket cell extends transversely from the cell body and forms a basket plexus innervating the cell body of pyramidal cells.

The second type of interneuron with cell body in stratum pyramidale or adjacent to it is the chandelier (or axo-axonic) cells. These cells possess radially oriented dendrites spanning all layers. The dendrites of chandelier cells rarely branch. Three to six main dendritic trunks extend toward the hippocampal fissure**.** The basal dendrites in stratum oriens extend up to, or occasionally penetrate the alveus. The axon of chandelier cells originates from the soma or primary dendrites and forms a dense arbor in stratum pyramidale and proximal oriens-usually 2 to 30 boutons arranged in rows parallel to the axon initial segments of pyramidal cells (CA1 and CA3). Electron microscopy demonstrated that these boutons selectively target axon initial segments of pyramidal cells. In addition to basket cells and chandelier interneurons, bistratified interneurons are also observed in this region (Bland et al., 2002).

Further ventral to stratum pyramidale is stratum radiatum. Stratum radiatum contains apical dendrites mainly from pyramidal cells and, to a less extent from interneurons in the stratum oriens and stratum pyramidale. Some interneurons with multipolar-stellate like cell body are also found located in the stratum radiatum. The dendrite of this type interneuron is smooth and varicose and forms a tree largely confined to stratum radiatum (Freund and Buzáki, 1996). The axon branches close to the soma and forms a rather

sparse arbor which extends throughout the entire width of stratum radiatum. Only a small number of collaterals enter stratum pyramidale or stratum oriens.

Stratum lacunosum consists of branches of apical dendrites of the pyramidal cells. Interneurons are also found in stratum lacunosum. The cell bodies of these interneurons are within stratum lacunosum or at the border of this layer with stratum radiatum. The dendritic tree of these cells is typically bitufted with a predominantly horizontal orientation as opposed to those from stratum pyramidale. Some branches extend into stratum pyramidale and others even cross the hippocampal fissure and reach stratum moleculare of DG. The axon from soma or proximal dendrites arborizes mainly in stratum lacunosum and the border with stratum radiatum.

The stratum moleculare of dentate gyrus is mainly occupied by the dendrites of granule cells, basket cells and various polymorphic cells as well as terminal axonal arbors from several sources such as entorhinal cortex. Using intracellular recording combined with dye injection in horizontal slice of the dentate gyrus of the rat, a type of neuron with its cell body located in the deep stratum moleculare was found by Han et al. (1993). The dendrite of this type of interneuron ascended to reach the hippocampal fissure and spanned an area over 800 μm in transverse length. The axon of this type of cell ran perpendicular to the granule cell dendrites and arborized in a terminal cloud. Since the axonal and dendritic trees of this cell type are mostly confined to the outer two-third of the dentate molecular layer, it was named molecular layer perforant path-associated cell (MOPP cell). Electron microscopy revealed that axon terminals of this cell type synapses with spiny distal dendrites of granule cells (Halasy and Somogyi, 1993).

Deeper to stratum moleculare is stratum granulosum. The granule cells (principal cells of dentate gyrus) in this layer have a small elliptical cell body and form a densely packed layer that is 4-8 soma in thickness. The granule cell has a characteristic cone-shaped tree of spiny dendrites with all branches directed towards the superficial portion of the molecular layer. The distal tips of the dendritic tree end just at the hippocampal fissure or at the ventricular surface. The axon of granule cells originates at the opposite pole of the soma and enters the adjacent polymorphic layer termed hilus. In the hilus the axon branches into several local collaterals that largely remain in the hilar region (Claiborne et al., 1986). Some collaterals course towards the granule cell layer, climb along the cell bodies and synapse on basket cells interneuron in the granule cell layer. The main axon of granule cell leaves the hilar region and courses towards CA3 pyramidal cell layer.

The principal cell of the hilus is the mossy cells. The cell bodies of the mossy cells are large (25-35 μm), triangular or multipolar in shape. The dendrites of mossy cells are typically confined to the hilar region, occasionally a dendrite also extends through the granule cell layer and into molecular layer. The most distinctive feature of the mossy cell is that all of the proximal dendrites are covered by very large and complex spines that are the sites of termination of the dentate granule cell axons. The axons of mossy cells terminate mainly on dendrites of granule cell at inner one-third of molecular layer. Some mossy fiber collaterals also terminate on unidentified dentritic shafts in the hilus and occasionally on dendrites of interneurons.

The cell body of chandelier and basket cells, with features similar to those described in CA1 and CA3 region, are also observed within or adjacent to granule cell layer. The

axon from chandelier cells terminates on the initial segment of granule cells. The axon from the basket cells emit a large number of collaterals, enter into the granule cell layer and form dense pericellular arrays of synaptic boutons. Other interneurons that are observed adjacent to the granule cell layer are the hilar perforant path associated cell (HIPP) and hilar commissural-associational pathway related cell (HICAP).

1.2 Intrahippocampal circuitry

The intrahippocampal connections consist of prominent serial connections that include those between the dentate granule cells and the hippocampal field CA3 as well as the projection from CA3 neurons to field CA1. These connect the different regions in a transverse and longitudinal plane. In addition, the neurons of the hippocampus and dentate gyrus are also networked by longitudinal associational and commissural fiber systems.

The axonal projection from the dentate granule cells to the field CA3 constitutes the mossy fiber bundle. These axons are called mossy fibers because of their varicose appearance that is similar to mossy fibers of the cerebellum (Ramon y Cajal). The details of the mossy fiber system has been investigated in rat using variety of techniques including (a) terminal and axonal degeneration following lesions in the dentate granule cell layer (Blackstad et al., 1970; Gaarskjaer, 1978), (b) anterograde transport of tritiated amino acids (Swanson et al., 1978), horseradish peroxidase (HRP; Claiborne et al., 1986) or Phaseolus vulgaris leucoagglutinin (PHA-L; Amaral and Witter, 1989) and (c) intracellular injection of HRP (Claiborne et al., 1986). The mossy fibers, which are unmyelinated, travel in CA3 in a narrow band between the pyramidale cell layer and

below stratum radiatum in the region called stratum lucidum. Studies using Timm's preparation (Swanson et al., 1978) or electron microscopy (Blackstad and Kjaerheim, 1961) indicate that the mossy fiber varicosities make synaptic contacts with thorn-line spine or dendritic shafts of the apical dendrites of pyramidal cells in field CA3. Interestingly, the mossy fibers extend throughout the transverse extent of CA3 in a lamellar fashion (Blackstad et al., 1970; Swanson et al., 1978; Amaral and Witter, 1989 and 1995). That is, the mossy fibers arising from granule cells at a septotemporal level innervate a restricted septotemporal level of field CA3, though at the septal level the mossy fibers near the field CA1 run caudally and parallel to the long axis of the hippocampal formation for as much as 2 mm (Swanson et al., 1978).

The hilar collaterals arising from mossy axon have a number of varicosities which make synaptic contacts upon dendrites of neurons in the polymorphic layer, including the proximal dendrites of the mossy cells. These cells contribute to both associational and commissural projection from the hilus to the inner third of the molecular layer of the dentate gyrus (Claiborne et al., 1986; Amaral and Witter, 1995). The associational and commissural projection from mossy cells is, at least in part, via collateral projections (Swanson et al., 1981). The associational fibers from the hilus, both at septal and middle levels, project to a considerable septotemporal extent of the dentate gyrus, though the temporal hilus has a relatively restricted projection to the temporal dentate gyrus (Fricke and Cowan, 1978; Swanson et al., 1978). Interestingly, the projection is relatively dense away from point of origin (Amaral and Witter, 1995).

The axonal projection from CA3 pyramidal neurons that is intrinsic to the hippocampus has been described using Golgi preparation, terminal degeneration, tracer transport and

intracellular labeling (Schaffer, 1892; Lorente de No, 1934; Hjorth-Simonsen, 1973; Swanson et al., 1978; Laurberg, 1979; Amaral and Witter, 1989; Li et al., 1994). These studies indicate that the CA3 projects both to stratum oriens and stratum radiatum of CA1, the projection being termed as 'Schaffer collateral'. In tracer studies, the termination of the projection from CA3 exhibits a pattern such that the fibers and terminals are located closer to CA3/CA1 border and in deeper portions of stratum radiatum and in stratum oriens near the septal pole, whereas the termination shifts progressively more towards CA1 border with subiculum and in the superficial region of stratum radiatum at progressively more temporal levels of the hippocampus.

A subiculodentate gradient in projection has also been defined with anterograde transport of PHA-L (Amaral and Witter, 1989). At septotemporal level of microinjection of the tracer, the projection from CA3 cells located close to the dentate gyrus distributes preferentially to the field CA1 near the subicular border where the fibers terminate in the superficial portion of stratum radiatum. CA3 neurons that are located progressively closer to field CA1 project preferentially to parts of CA1 that are progressively closer to CA3 and to deeper portions of stratum radiatum and stratum oriens. A septotemporal gradient was also observed such that the projection from CA3 cells localized near the dentate gyrus tends to project more heavily in the septal direction. Conversely, cells nearer to field CA1 tend to project more heavily in a temporal direction.

Unlike the lamellar organization of the mossy fiber projection, the CA3 projection from septal and middle CA3 to CA1 has an extensive septotemporal length (Hjorth-Simonsen, 1973; Swanson et al., 1978; Laurberg, 1979; Amaral and Witter, 1989); the projection

from the temporal field CA3 is restricted to the temporal field CA1 (Hjorth-Simonsen, 1973; Swanson et al., 1978; Laurberg, 1979; Amaral and Witter, 1989).

Axon collaterals of CA3 terminating in CA3 that contribute to longitudinal association bundle have been described (Li et al., 1994; see Amaral and Witter, 1995 for review). These terminate in both stratum oriens and stratum radiatum of field CA3. Like the Schaffer collateral projection, the associational projection is also divergently distributed along the septotemporal axis of CA3. Interestingly, the same pyramidal cells in CA3 may give rise to Schaffer collaterals, collateral in CA3 and commissural projection to contralateral fields CA1 and CA3 (Swanson et al., 1981; Li et al., 1994).

The CA1 pyramidal cells axons project outside the hippocampus; local axonal collaterals among CA1 pyramidal cells are relatively sparse (Lorente de Nó, 1934; Radpour and Thomson, 1992) compared with the CA3 region. These collaterals travel parallel to the alveus in stratum oriens and remain restricted to this layer.

In addition to the connections amongst the principal neurons, neuroanatomical techniques also suggest interconnections between the principal neurons and the local interneurons in the hippocampus, including field CA1 (also see the section above). In an extensive review, Freund and Buzsáki (1996) proposed a schema of the interaction between pyramidal cells in CA1 and interneurons that is partly based on the match between laminar distribution of dendrites and axonal arborization of interneurons, and the intrinsic afferent. The major features of the scheme include: (a) interneurons in stratum oriens, including O-LM and horizontal trilaminar cells are positioned to receive collateral input from pyramidal cells and, in turn, influence pyramidal cell responses at

synapse on distal dendrites in stratum lacunosum molecular, (b) the chandelier, basket and bistratified interneurons in the stratum pyramidale are influenced by recurrent collateral and Schaffer collaterals. In turn, the chandelier and basket cells influence perisomatic excitability of pyramidal cells, whereas bistratified cells influence synaptic transmission at basal and apical dendrites of pyramidal cells, and (c) interneurons in stratum radiatum and lacunosum-moleculare are influenced by Schaffer/commissural collaterals fibers and entorhinal afferents, respectively, and in turn affect the dendritic excitability of pyramidal cells. In addition, some interneurons are specialized to innervate other interneurons but not pyramidal cells and are named interneuron-selective (IS) cells (Freund and Buzsáki, 1996). Similar schemas have also been proposed for field CA3 and the dentate gyrus (Freund and Buzsáki, 1996).

1.3 Physiological characteristics of hippocampal neurons

In relation to the present study, the following section will focus mostly on field CA1 of the hippocampus. The electrophysiological characteristics of hippocampal pyramidal neurons, including those in field CA1, have been documented *in vivo* in a number of studies (e.g. Kandel et al., 1961; Spencer and Kandel, 1961; Fox and Ranck, 1975; Fox and Ranck, 1981; Finch et al., 1983; Fox, et al., 1986; Vertes et al., 1997). Pyramidal cells generally discharged at low spontaneous rates (usually about 2 Hz or less, and not greater than 30 Hz), had relatively longer duration of action potentials (0.4-1.2ms), and could be antidromically driven from hippocampal efferent pathways.

A characteristic feature of pyramidal cell discharge recorded *in vivo*, including in CA1 is the occurrence of burst firing. The burst firing can often be observed extracellularly *in*

vivo in form of 'complex-spike' that comprises of 2-10 action potentials of progressively decreasing amplitudes and short interspike intervals at 3-10 ms. Notably, simultaneous recording of behavior-dependent or somatic depolarization-evoked bursts from soma and dendrites of CA1 and CA3 pyramidal cells, *in vivo* and *in vitro,* indicated that the large progressive decrement of spikes is observed in dendrites as the burst back-propagate from the perisomatic region (Spruston et al., 1995; Buzsáki et al., 1996). Little or no spike reduction was observed in the perisomatic region, suggesting that the progressive decrement of spikes partly reflects dendritic processing of action potential discharge.

The burst firing of pyramidal cells is implicated in synaptic plasticity and information processing in the hippocampus. In context of the former, in slice experiments, pairing of bursts with synaptic stimulation led to long-term potentiation of synaptic transmission at the activated input (Thomas et al., 1998; Pike et al., 1999). Notably, Pike et al. (1999) reported that long-term potentiation of synaptic transmission across a synapse on single CA1 pyramidal cell was elicited with repeated stimulation of the synapse in temporally close relationship with intracellular depolarization-evoked burst. Such potentiation was not observed when synaptic stimulation was paired with depolarization-induced single postsynaptic action potential. Further, selective block of bursts with low concentration of tetrodotoxin without affecting baseline synaptic transmission blocked the induction of LTP to synaptic stimulation (Thomas et al. 1998). Based on these and other related findings, including from neocortical pyramidal cells, it has been proposed that the basis of synaptic plasticity as described above involves back-propagation of burst action potentials which acts as depolarizing signal that, when coincident with synaptic EPSP, affect synaptic plasticity by modulating the strength of the dendritic calcium signal(s) (Paulsen and Sejnowski, 2000). As regards the role of complex-spike burst in

information processing, such firing of CA1 pyramidal cells is suggested to be 'information-rich'; that is the mapping of animals position in environment, a feature encoded by hippocampus, is defined more accurately when only bursts are considered than when all spikes are counted (Otto et al., 1991; Lisman, 1997).

The basis of burst firing has also been investigated. In this context, Kandel et al. (1961) reported that single spike or burst firing of pyramidal neurons was associated with a depolarizing post-spike potential. These after-potentials were additive and the magnitude corresponded to the number of spikes in a burst. Similarly, in slice preparation such after potentials were observed following a spike (Schwartzkroin, 1975; Wong and Prince, 1978; Azouz et al, 1996; Jensen et al., 1996) and manipulation that enhanced the size of the after potential could trigger a second spike or a burst of spikes (Azouz et al., 1996). On the other hand, hyperpolarization or depolarization of the pyramidal cell beyond a narrow range attenuated both the depolarizing after potential and burst discharge (Wong and Prince, 1978; Jensen et al., 1996). Thus, it has been suggested that the burst firing of hippocampal pyramidal neurons is triggered from large depolarizing after potentials (Wong and Prince, 1978; Wong et al., In 'Neural mechanisms of conditioning', eds. DL Alkon, CD Woody, pp. 311-318, 1986; Azouz et al., 1996). In line with the idea that the depolarizing after potential summates, spontaneous or brief somatic-depolarization-induced burst firing of pyramidal cells was observed riding on a slow depolarization (Wong and Prince, 1978; Azouz et al, 1996). Further, treatment that decreased the slow depolarization also reduced the depolarizing after potential and burst firing (Wong and Prince, 1978; Wong et al., 1986; Azouz et al., 1996).

The ionic mechanisms underlying the depolarizing after potential have also been investigated and with varying results. For example, the slow depolarization in CA3 pyramids in slices taken from guinea pig was attenuated with manipulations that attenuated the cellular influx of calcium (Wong and Prince, 1978). Whereas, the depolarizing after potential and the somatic-depolarization-induced burst discharge of CA1 pyramidal cells in slices taken from rat was sensitive to block of the voltage-dependent sodium channels with tetrodotoxin (Azouz et al., 1996). Conversely, the depolarizing after potential and burst firing in CA1 pyramidal cells were undiminished following suppression of calcium currents.

The response of pyramidal cells to afferent stimulation has also been studied. Following single shock afferent stimulation, including stimulation of the field CA3 Schaffer collateral/commissural afferents, the complex-spike pyramidal cells, including those from CA1 generally responded with a single spike discharge (Andersen et al., 1964a, b; Schwartzkroin, 1975; Fox and Ranck, 1981; Rose and Pang, 1985; Spruston et al., 1995). Here it is notable that single CA3 pyramidal cell stimulation-evoked excitatory postsynaptic current (EPSC) recorded from the soma of a CA1 pyramidal cell exhibited a single Gaussian peak indicating the possibility that the given CA3 pyramidal cell made only a single synaptic contact with a given CA1 neuron (Bolshakov and Siegelbaum, 1995).

Importantly, from the viewpoint of the present study, afferent stimulation also evokes large extracellular potentials in the hippocampus and the dentate gyrus. For example, relatively high intensity Schaffer collateral/commissural afferent stimulation evokes a large negative potential in the apical dendrites. This potential reverses in the pyramidal

cell layer. When the apical dendritic field potential reached a certain magnitude, a negative population spike is superimposed on the positive field in the pyramidal cell layer. Further, after a population spike, a large positive wave is recorded. Based upon correlation between intracellular potentials, and the extracellular field in the dentate gyrus and hippocampus (Andersen et al., 1971; Richardson et al., 1984), it is accepted that (a) the negative wave in the dendrites is the extracellular sign of intracellular excitatory postsynaptic potential (EPSP) produced on afferent stimulation, and (b) the amplitude of the population spike reflects the number of principal neurons discharging in a synchronized fashion. The positive wave recorded after a population spike may reflect intracellular inhibitory postsynaptic potential.

The site of initiation of Schaffer collateral/commissural afferent stimulation-evoked population spike has also been investigated. *In vivo* investigations using near threshold and supra-threshold stimulation of afferents, especially in the stratum radiatum, consistently pointed to the proximal dendrites of the pyramidal cells as the trigger zone for generation of the CA1 population spike (Andersen, 1960; Herreras, 1990; Kloosterman et al., 2001). For example, in a current source density analysis of threshold population spike recorded simultaneously from different depths of CA1 in anaesthetized rat, Kloosterman et al. (2001) reported that the current sink of the shortest latency that was associated with the population spike was found in the proximal apical dendrites (50-100 μm from soma). Further, based on latency measures, it was found that the population spike propagated towards basal dendrites. Interestingly, similar measures indicated that population spike evoked on stimulation of afferents to basal dendrites was initiated near the cell body region (Kloosterman et al., 2001). In contrast to the *in vivo* observations, the threshold CA1 population spike evoked on stimulation of apical

afferents is triggered from cell body region in the hippocampal slices (Richardson et al., 1987; Turner et al., 1989; Turner et al., 1991). The site of initiation of the population spike shifts to proximal dendrites at higher intensity stimulation. The dendritic spike is blocked by local administration of tetrodotoxin, suggesting that active conductance through tetrodotoxin-sensitive sodium channels in proximal dendrites is instrumental in generating such spike (Turner et al., 1989 and 1991).

In addition to synaptic activation, ephaptic interactions may also contribute to the excitation of pyramidal neurons following afferent stimulation. In this context, intracellular trans-membrane depolarization in pyramidal neurons is observed simultaneously with the extracellular negative going phase of the antidromic or orthodromic population spike (Richardson et al., 1984; Taylor and Dudek, 1984). These authors suggested that such changes in pyramidal cell excitability due to extracellular field would aid in the synchronous activation of the population following afferent stimulation since the ephaptic depolarization of each neuron is restricted in time to the peak of the population spike. The electric field effect could also lead to the recruitment of otherwise subthreshold neurons and increase the size of population spike beyond that resulting from synaptic activation alone.

Analysis of afferent stimulation-evoked field potentials *in vivo* in rabbit and rat suggest that the flow of excitatory information from the dentate gyrus to CA3 and from CA3 to CA1 is in a plane approximately normal to the septotemporal axis of the hippocampal formation (Andersen et al., 1971; Rawlins and Green, 1977; Andersen et al., 2000). However, given that the CA3 to CA1 connections, unlike the dentate gyrus to CA3 connections are also longitudinally oriented (see the section on anatomical connections),

more recently Andersen et al. (2000) re-evaluated the Schaffer collateral/commissural afferent synapse with CA1 in horizontal slices of the hippocampus that covered the entire CA1 and also included a strip of CA3 to stimulate the Schaffer collateral/commissural afferents. In line with data obtained in vivo, point stimulation of CA3 evoked axon signal and population spike that were largest in a slightly oblique, transverse band across the CA1 with a progressive decrease in amplitude towards the either flanks. Such spatially restricted excitation may perhaps reflect (a) synaptic density of Schaffer collaterals on CA1 pyramidal cell dendrites, and (b) feed-forward and/or feedback (lateral) inhibition that spatially restrict the flow of excitation to pyramidal cells that are most densely innervated by the given afferents and are, therefore, more strongly activated on afferent stimulation.

In the feed-forward inhibition an excitatory input excites both principal cells and inhibitory interneurons; the excited interneurons in turn induce inhibitory postsynaptic potential and limit the discharge probability of principal cells. In the feed-back inhibition an excitatory input activates the principal cells, whose excitatory output is fed-back to the inhibitory cells through recurrent axon collaterals. The inhibitory interneuron excited by the recurrent axon collaterals discharges and inhibits the group of principal cells including those that initially activated the interneuron and also adjacent principal neurons (recurrent and lateral inhibition). Here it is notable that electrophysiological studies suggest that the local interneurons in the hippocampus and dentate gyrus that innervate the principal neurons exert an inhibitory influence on the excitability of the principal cells (Buzsáki, 1984; Freund and Buzsáki, 1996).

The feed-forward inhibition of hippocampal pyramidal cells (Buzsáki, 1984) via local interneurons has been suggested partly on the basis that (a) afferent stimulation threshold to activate some interneurons, including immunocytochemically identified basket cells and trilaminar interneuron, is lower than that required to evoke a population spike (Buzsáki and Eidelberg, 1982; Sik et al., 1995) and (b) interneurons, including identified basket cell, can respond to afferent stimulation at a shorter latency than that of the population spike (Fox and Ranck, 1981; Buzsáki and Eidelberg, 1982; Ashwood et al., 1984; Rose and Pang, 1985; Ylinen et al., 1995) and in some instances fire on the positive field potential preceding the population spike (Ashwood et al., 1984). Similarly, feedback inhibition of hippocampal pyramidal cells is postulated partly based on the *in vivo* evidence that (a) stimulation of pyramidal cell axons in fornix of hippocampal deafferentated cat resulted in antidromic invasion followed by inhibitory postsynaptic potential in intracellularly recorded pyramidal cells (Kandel and Spencer, 1961), (b) stimulation of afferents or deafferented fimbria evoked activity in stratum oriens presumed interneurons after antidromic invasion of pyramidal cells (Andersen et al., 1964b), and (c) putative interneurons, including identified basket cells fired on the post-population-spike positive field potential (Fox and Ranck, 1981; Buzsáki and Eidelberg, 1982; Ashwood et al., 1984; Ylinen et al., 1995). Evidence similar to the preceding are also reported from experiments in hippocampal slices which also indicate that identified interneurons that innervate the pyramidal cell perisomatic region (basket cells and chandelier interneurons) or the dendrites (bistratified interneurons and O-LM cells) were activated in a feedback fashion following excitation of hippocampal pyramidal cells (Knowles and Schwartzkroin, 1981; Lacaille et al., 1987; Gulyas et al., 1993; Buhl et al., 1994a; Buhl et al., 1994b; Sik et al., 1995; Blasco-Ibanez and Freund, 1995; Maccaferri and McBain, 1995; Ali et al. 1998). Interestingly, in some instances reciprocal

interaction between identified pyramidal cell-interneuron pair was also observed. Pharmacological evidence suggests that the afferent/efferent-evoked inhibition is mediated at least in part by release of GABA. For example, in hippocampal slice preparation both the alveus and stratum radiatum stimulation-evoked inhibitory postsynaptic potentials in CA1 pyramidal cells were antagonized by the GABAa-receptor antagonist bicuculline (Alger and Nicoll, 1982).

The recruitment of inhibitory processes upon afferent/efferent stimulation is also demonstrated with paired-pulse paradigm. In this paradigm paired stimulation pulses with same intensity are delivered at various interpulse intervals either orthodromically or antidromically (Albertson and Joy, 1987; Freund et al., 1990; Cao and Leung, 1991; Steffensen and Henriksen, 1991; Sayin et al., 2001). Delivered at appropriate inter-pulse interval the pyramidal cell response to the second stimulus is inhibited (paired-pulse suppression). The role of inhibition in paired-pulse suppression is suggested by different lines of evidence. For example, locally applied bicuculline antagonizes the paired-pulse depression of CA1 and dentate population spike (Freund, et al., 1990; Steffensen and Henriksen, 1991). Further, Martin and Sloviter (2001) reported that local microinjection of a neurotoxic conjugate of saporin and a peptidase-resistant analog of substance P, which specifically destroyed the interneurons without affecting principal cells at the site of injection, attenuated paired pulse suppression at the injection site in both CA1 and dentate gyrus. In addition, Sayin et al. (2003) demonstrated that perforant pathway stimulation induced paired pulse suppression in granule cell layer was reduced or lost following kindling-induced seizure. The loss of such paired-pulse inhibition was accompanied by loss of subclasses of interneurons, especially those that innervated the perisomatic region of granule cells.

1.4 CA1 neural network activity-theta rhythm

Several types of the extracellular field potentials have been described in field CA1 that reflect activity of network of local neurons. These include two relatively large field potentials, namely sharp waves and theta waves. The former are population field excitatory postsynaptic potentials associated with near synchronous depolarization of CA1 pyramidal cells due to synchronous activation of Schaffer collateral input impinging on these neurons (Buzsáki et al., 1983; Buzsáki, 1989; Moser and Paulsen, 2001). Such sharp wave field potentials are observed during slow-wave sleep and immobility. The theta waves are sinusoidal-like field potential of 3-12 Hz frequency and with several millivolts amplitude which, in rat, are generally observed during goal-directed movement and rapid eye-movement sleep (Vanderwolf, 1969; Bland, 1986). Theta can also be observed in anesthetized animals, spontaneously or in response to sensory stimuli, including noxious stimuli (Buszáki et al., 1983 and 1986; Bland, 1986; Khanna, 1997). The theta frequency in anesthetized rat usually ranges from 3 to 6 Hz compared with 3-12 Hz in behaving animals.

The depth distribution of theta wave (rhythmic slow activity, RSA) in the dorsal hippocampus, especially field CA1 has been investigated both in the behaving and anesthetized animals (Leung, 1984a; Buzsáki et al., 1986; Bland and Whishaw, 1976; Green and Rawlins, 1979; Holsheimer, et al., 1979; see Buzsáki, 2002 for a review). In the behaving rat, the amplitude of RSA increased gradually when the recording electrode penetrated from stratum alveus to hippocampal fissure. The first RSA maximum occurred near the border of stratum oriens and the pyramidal cell layer with the second

and larger maxima at hippocampal fissure (Buzsáki, 2002; Buzsáki et al., 1986). In addition, the phase of the theta wave shifted with depth from the pyramidal cell layer. The complete reversal (i.e. 180^{o} out-of phase with respect to theta recorded from stratum oriens/pyramidale) of RSA occurred at about the hippocampal fissure. The theta profile in anesthetized rat is different from that in the behaving rat. In this context, the amplitude of RSA in deeply anaesthetized rat is lower at all depths in CA1 and a null zone of RSA is found in the inner part of stratum radiatum of CA1 with phase-reversal below the null zone (Buszáki et al., 1986).

Leung (1984b) in a simulation study proposed that the gradual phase-shift of theta in behaving rat was a vector summation of two dipoles that were generated by perisomatic inhibition (dipole I) and a phase-shifted distal dendritic excitation (dipole II). On the other hand, perisomatic inhibition alone generated the pattern of phase-shift that mimicked that observed in urethane-anaesthetized animal.

A number of lines of evidence favor the above model. One, current source density (CSD) analysis of theta field potentials, especially in behaving animals, revealed a prominent inhibitory source at field CA1 stratum pyramidale, and a prominent excitatory sink at the hippocampal fissure with a phase lag between the two (Buzsáki et al., 1986; Mitzdorf, 1985; Brankack et al., 1993). Two, intracellular somatic theta in physiologically identified CA1 pyramidal cells reversed in phase with respect to the extracellular wave whenever the IPSP impinging on pyramidal cells was reversed by polarizing current or ion diffusion (Leung and Yim, 1984; Soltesz and Deschenes, 1993; Ylinen et al., 1995). Three, intracellularly or extracellularly recorded putative GABAergic interneurons, including identified chandelier cells and basket cells located in or around the pyramidal

cell layer or in stratum oriens exhibited a rhythmically modulated increased firing during theta (Ylinen et al., 1995; Klausberger et al., 2003). Four, the preferred phase of CA1 interneuronal discharge, especially chandelier cells and basket cells corresponded to the hyperpolarizing potentials of intra-soma membrane potential oscillation in pyramidal cells (Bland et al., 1980; Buzsáki and Eidelberg, 1983; Buzsáki, et al., 1983; Fox et al., 1986; Ylinen et al., 1995; Klausberger et al., 2003). Five, intracellular recording from dendrites of CA1 pyramidal cells indicate that these depolarize during theta and, furthermore, exhibit intra-dendritic theta-oscillations whose depolarizing phase correspond to the hyperpolarizing phase of intra-somatic theta (Kamondi et al., 1998). Interestingly, intra-dendritic putative calcium spike were occasionally observed during theta. These corresponded to the hyperpolarizing phase of intra-somatic theta.

Contrary to above (Leung and Yim, 1984; Soltesz and Deschenes, 1993; Ylinen et al., 1995), Bland et al. (2002) reported that in CA1 pyramidal cells the intra-somatic membrane potential oscillations did not show appreciable phase shift with respect to extracellular theta on large hyperpolarization or depolarization of the membrane. Interestingly, the CA1 pyramidal cells recorded by Bland et al. (2002) depolarized and increased their discharge rate with onset of theta, whereas others reported hyperpolarization of pyramidal cells in correlation with theta (Soltesz and Deschenes, 1993; Ylinen et al., 1995). Further, the background activity of pyramidal cells in the study by Bland et al. (2002) was high as compared to that reported by others (Soltesz and Deschenes, 1993; Ylinen et al., 1995). This raises a possibility that subset of pyramidal cells are differentially affected during theta.

In anaesthetized rat, the amplitude but not frequency of intra-somatic theta in pyramidal cells and basket cell interneurons in CA1 was dependent on the polarization state of the neurons (Ylinen et al., 1995; Bland et al., 2002). On the other hand, both the amplitude and frequency of intra-dendritic theta was influenced by large depolarization of the dendrites (Kamondi et al., 1998). Collectively this suggests that the intra-somatic theta, especially in pyramidal cells is largely paced by other neurons while interplay of intrinsic currents might contribute, at least in part, to intra-dendritic theta, especially during intense excitation.

During behavior-induced theta or spontaneous and/or sensory stimuli-induced theta in anaesthetized animals, extracellularly recorded discharge (Buzsáki et al., 1983; Fox et al., 1986; Csicsvari et al., 1999) and/or intracellularly recorded action potential (Ylinen et al., 1995; Bland et al., 2002) of majority of CA1 pyramidal cells, when present, tended to lock to the negative phase of the local extracellular theta waves. This corresponds with period of release from the rhythmic somatic inhibition impinging upon these neurons during theta, at least for a subset of pyramidal cells. However, the phase-relationship is not invariant and can alter. For example, during exploratory behavior as the animal moved through the environment, the putative pyramidal cells that encoded the animal's position in environment (place cell) fired progressively forward on each theta cycle (phase precession; O'Keefe and Recce, 1993). Intracellular recording from CA1 pyramidal cells in urethane anaesthetized rat indicated that the action potential evoked on somatic injection of sinusoidal current occurred progressively earlier on the depolarizing phase upon increasing the levels of somatic depolarization with injection of an additional DC current (Kamondi et al., 1998). The authors indicated that such progressive earlier firing was replicated in a neural model involving somatic theta

frequency oscillation combined with tonic dendritic excitatory drive that was coupled with activation of voltage-dependent potassium and sodium currents that, in part, played a role in eliciting dendritic oscillations. Indeed, in an *in vitro* experiment that mimicked synchronized, but 180^{o} out of phase theta rhythmic dendritic depolarization and somatic hyperpolarization via injection of sine wave current, an advancement of spike discharge was evoked by increasing the strength of depolarization (Magee, 2001). Further, theta patterned stimulation of excitatory afferents to apical dendrites when paired with somatic rhythmic hyperpolarization evoked phase precession whose degree depended upon the strength of the excitatory stimulation (Magee, 2001). Collectively, both the model based on *in vivo* findings and the result obtained from slice experiments predict that the phase precession of CA1 place cells (O'Keefe and Recce, 1993) correlates, at least in part, with the strength of rhythmic synaptic excitation as the animal moved through the environment (Kamondi et al., 1998; Magee, 2001).

In addition, the synaptic excitation of field CA1 pyramidal cells to stimulation of excitatory afferents is reduced during periods of theta activity evoked during animal locomotion, rapid eye-movement sleep and sensory stimulation, including noxious stimulation in anesthetized animals (Winson and Abzug, 1977; Leung, 1980 and 1985; Herreras et al., 1988; Khanna, 1997).

1.5 Ascending regulation of hippocampal field CA1 neural activity

Keeping with the focus of the present study, this section will cover the two major subcortical regions, namely the medial septum-vertical limb of diagonal band of Broca (MS-VLDBB) and the posterior hypothalamus (PH)-supramammillary (SUM) region

that project to the hippocampal formation and have been implicated in modulation of hippocampal neural activity.

1.5.1 Medial septum-vertical limb of diagonal band of Broca (MS-VLDBB) region

The septohippocampal projection from the medial septum-vertical limb of diagonal band of Broca (MS-VLDBB or the medial septal region) and the horizontal limb of the diagonal band of Broca has been described using retrograde and anterograde transport of tracer (Meibach and Siegel, 1977; Swanson and Cowan, 1979; Monmaur and Thomson, 1983; Nyakas et al., 1987; Gaykema et al., 1990; Yoshida and Oka, 1995; Dutar et al., 1995). Overall, these studies indicate that the septal afferent innervates the hippocampal formation through three main routes: the fimbria, the dorsal fornix and the supracallosal striae. A minor projection via a ventral route through the amygdala to the hippocampus has also been suggested (Milner and Amaral, 1984). Retrograde tracer transport studies indicate that the projection is mostly ipsilateral (Monmaur and Thomson, 1983; Woolf et al., 1984; Kiss et al., 1990; Kiss et al., 1997).

A relatively detailed medial-lateral organization of hippocampal projection from the MS-VLDBB region was described using the anterograde tracer PHA-L (Nyakas et al., 1987). These authors reported that the lateral region of the medial septum projected preferentially to the ventral hippocampus, while the medial regions projected along the length of the hippocampus. Most of the VLDBB projected to the hippocampus along its entire length, though some preference for dorsal and ventral hippocampus was observed from more rostral and ventral sites of VLDBB, respectively. The caudal vertical limb of

the diagonal band (caudal VLDBB; Nyakas et al., 1987) projected dominantly to dorsal hippocampus. Further, the axons from the MS-VLDBB region to the hippocampus, especially field CA1, were of variable thickness (Nyakas et al., 1987; Freund and Antal, 1988). The thinner axons (type 2 axons) had relatively small varicosities and occasional drumstick-like terminal and were observed in the proximal dendritic region of principal neurons and in stratum lacunosum-moleculare, while the thicker axons (type 1 axons) innervated mostly in stratum oriens and radiatum/lacunosum-moleculare, had large en passant boutons and often established basket-like formations around hippocampal neurons.

Immunocytochemical studies indicate that the septohippocampal neurons include cholinergic and GABAergic projection neurons. For example, Freund and Antal (1988) reported that the boutons of type 2, but not type 1 axons of septohippocampal neurons were immunoreactive for GABA. Further, most of the postsynaptic targets of these GABAergic boutons were either cell bodies or dendrites of hippocampal interneurons. It is notable that GABA positive type 2 septohippocampal axons are also immunoreactive for the calcium binding protein parvalbumin (Freund, 1989). Conversely, many neurons in medial septum that were labeled following microinjection of retrograde tracer into the dorsal hippocampus were parvalbumin positive and were mostly localized to the medial regions of the MS-VLDBB and the horizontal limb (Kiss et al., 1990). Many of other retrogradely labeled neurons in the medial septum that were parvalbumin negative were immunoreactive for the acetylcholine synthesizing enzyme choline acetyltransferase (CHAT), indicating that these were cholinergic in nature (Kiss et al., 1990). These neurons were mostly localized to the lateral regions of the MS-VLDBB and the horizontal limb. In addition to above, others have also reported retrograde labeling of

CHAT-positive septohippocampal neurons following injection of the tracer into the hippocampus (Woolf et al., 1984; Amaral and Kurz, 1985). Interestingly, within the hippocampus, especially field CA1, the cholinergic varicosities may synapse with both pyramidal cell and interneurons (Frotscher and Lernath, 1985), be juxtaposed to other axonal varicosities or be non-synaptic in nature (Umbriaco et al., 1995).

The effects of GABAergic and cholinergic septohippocampal afferents on hippocampal excitability have also been studied. For example, in a combined septum-hippocampal slice preparation stimulation of the septum evoked inhibition of CA3 inhibitory interneurons that was observed in presence of antagonists that suppressed cholinergic and glutamatergic transmission, thereby raising the possibility that the stimulation-evoked inhibition involved excitation of GABAergic septohippocampal neurons (Toth et al., 1997). In line with the inhibitory effect on interneurons, the septal stimulation also blocked spontaneous inhibitory postsynaptic potentials in the CA3 pyramidal cells. The pyramidal cells depolarized and the septal stimulation-evoked depolarization increased in amplitude as the pyramidal cell membrane was depolarized away from the reversal potential of the inhibitory postsynaptic potentials. Overall the findings suggest that activation of septohippocampal afferents evoked disinhibition of hippocampal pyramidal neurons (Toth et al., 1997). The cholinergic mediated effects of septal stimulation and the effects of acetylcholine have also been investigated, sometimes with paradoxical results. In this context, stimulation of the MS-VLDBB region *in vivo* evoked an increase in field CA1 population spike, an effect which was also observed with iontophoretic acetylcholine applied in the pyramidal cell body region (Krnjevic and Ropert, 1982). Both the septal and acetylcholine facilitation of CA1 population spike was antagonized by a systemic or locally applied muscarinic antagonist, suggesting that

the facilitation was mediated by release of acetylcholine in hippocampus on activation of the septohippocampal afferents (Krnjevic and Ropert, 1982; Rovira et al., 1983). The foregoing facilitatory effect was linked to disinhibition. In this regards, iontophoretic acetylcholine, applied near the pyramidal cell body recording site, reduced inhibitory postsynaptic potential due to fimbrial or entorhinal cortical stimulation without affecting the hyperpolarization due to direct application of GABA (Ben-Ari et al., 1981). Furthermore, acetylcholine might also excite hippocampal pyramidal cells, by postsynaptically decreasing several of potassium conductances in pyramidal cells (Madison et al., 1987) or by enhancing NMDA receptor currents (Auerbach and Segal, 1996).

On the other hand, both MS-VLDBB stimulation and local application of acetylcholine in vivo decreased apical dendritic synaptic field excitatory postsynaptic potential that was blocked by systemic or local administration of cholinergic-muscarinic antagonists (Rovira et al., 1983). Likewise, in slice preparation conditioning stimulation of afferents in oriens evoked an inhibition of Schaffer collateral stimulation-evoked excitatory postsynaptic current in CA1 pyramidal cells that was blocked by administration of atropine, suggesting that cholinergic afferents are activated on oriens stimulation (Fernandez de Sevilla and Buno, 2003). The authors also indicate that the inhibition was accompanied by enhancement of paired-pulse facilitation of Schaffer collateral elicited excitatory postsynaptic current. This and the pattern of normalized variance of the excitatory postsynaptic current amplitude suggested that the cholinergic afferent-mediated inhibition of Schaffer collateral response was presynaptically mediated (Fernandez de Sevilla and Buno, 2003). Correspondingly, the effect of acetylcholine on Schaffer collateral evoked excitatory postsynaptic potential recorded from pyramidal

cells is suggested to be due to presynaptic inhibition of transmitter release (Valentino and Dingledine, 1981).

The MS-VLDBB region is also crucial for the theta wave rhythm (Bland, 1986; Stewart and Fox, 1990; Vertes and Kocsis, 1997; Buzsáki, 2002). In this context, iontophoretic application of atropine attenuated theta-rhythmic discharge of putative interneuron in CA1 of anaesthetized rat, suggesting that septohippocampal cholinergic neurons influence theta-linked discharge in hippocampus (Stewart et al., 1992). More recent findings indicate a role of septum cholinergic neurons in the modulating the amplitude of hippocampal theta. In this regard, selective destruction of septal cholinergic neurons with intraseptal microinjection of the immunotoxin 192 immunoglobulin G-saporin attenuated the theta peak power, but not theta peak frequency of running-induced theta (Lee et al., 1994). Further, the power of theta, but not its frequency, elicited upon direct activation of medial septum via intraseptal carbachol or by indirect activation upon reticular stimulation was attenuated in 192 immunoglobulin G-saporin pretreated rats (Zheng and Khanna, 2001). Presumably the effect on amplitude reflects an influence of septum cholinergic neurons on the number of CA1 neurons recruited into theta oscillations and/or the size of intracellular theta induced in pyramidal cells.

A role for GABAergic septohippocampal neurons has also been proposed. For example, in the combined septum-hippocampal slice (see above) theta-patterned stimulation of presumed septohippocampal GABAergic neurons induced theta-rhythmic oscillations in CA3 pyramidal cells that were as result of disinhibition (Toth et al., 1997; also see above). Further, it has been proposed that the generation of theta rhythm may involve septohippocampal GABAergic neurons, since spontaneous or direct septal stimulation-

induced theta in anaesthetized animal, and running-induced theta in behaving animals was present, although reduced in power, following destruction of the MS-VLDBB cholinergic neurons (Lee et al., 1994; Zheng and Khanna, 2001). Indeed, both in the urethane-anesthetized and behaving rat, intracellularly and extracellularly recorded putative cholinergic and GABAergic neurons in MS-VLDBB region displayed rhythmic discharge that was phase-locked to the positive and negative peak of dentate theta wave, respectively (Brazhnik and Fox, 1997 and 1999). Interestingly, the rhythmicity of the putative cholinergic, but not GABAergic MS-VLDBB neurons, was abolished with intraseptal administration of the GABAa –receptor antagonist, bicuculline (Brazhnik and Fox, 1999), suggesting that rhythmic GABAergic mechanisms in MS-VLDBB synchronized the rhythmic activity of neurons in the MS-VLDBB region.

The finding that putative cholinergic and GABAergic in MS-VLDBB discharged rhythmically at opposite phase of hippocampal theta fits with the model of hippocampal theta generation proposed earlier by Stewart and Fox (1990). In the proposed model, the CA1 interneurons were rhythmically excited by septohippocampal cholinergic input that was coupled with rhythmic inhibition of the same interneurons by septohippocampal GABAergic neurons. The preferred firing phase of interneurons during the theta rhythm was determined by the strength of the two rhythmic septal inputs and their phase-relation to hippocampal theta rhythm. The rhythmic excitation of hippocampal interneurons in turn influenced the activity of their target pyramidal cells and synchronized the activity of pyramidal cells leading to generation of theta. In line with this (1) CA1 interneurons were excited by cholingergic agents (Reece and Schwartzkroin, 1991), (2) during theta, extracellularly recorded CA1 interneurons exhibited increased firing rate and rhythmic activity phase-locked to local theta in anaesthetized rat (Buzsaki et. al., 1983), (3) in

hippocampal slice preparation, stimulation of an intracellularly recorded basket cell resulted in a hyperpolarization followed by rebound of discharge in its target pyramidal cell and synchronous entrainment of simultaneously recorded pyramidal cells (Cobb et al., 1995).

Evidence also suggests that at least the septohippocampal cholinergic neurons mediate, at least in part, the behavior- and sensory stimuli-induced pyramidal cell inhibition. For example, systemically administered cholinergic-muscarinic antagonist attenuated the inhibition of Schaffer collateral stimulation-evoked field excitatory postsynaptic potential and population spike observed in correlation with theta during movement (Leung and Vanderwolf, 1980). Moreover, intrahippocampal administration of atropine attenuated both the noxious and non-noxious sensory stimulation-induced suppression of CA1 pyramidal cell synaptic excitability (Herreras et al., 1988; Khanna and Sinclair, 1992). More recent evidence indicates that intraseptal carbachol elicited suppression of CA1 population spike was blocked following 192 immunoglobulin G-saporin-induced destruction of the medial septum cholinergic neurons with (Zheng and Khanna, 2001). Such destruction also attenuated noxious stimulus-induced suppression of CA1 pyramidal cell discharge or the excitation of local inhibitory interneurons in anaesthetized rat (Zheng and Khanna, 2001).

1.5.2 Posterior hypothalamus-supramammillary (PH-SUM) region

The posterior hypothalamus connects directly or indirectly via MS-VLDBB to the hippocampus and dentate gyrus. In context of the former, anterograde tracing with PHA-L indicated relatively dense projection from the supramammillary (SUM) region to

the granule cell layer and the immediately adjoining molecular layer throughout septotemporal extent of the dentate gyrus (Haglund et al., 1984; Vertes, 1992; Magloczky et al., 1994). The projections were denser in dorsal and suprapyramidal blade than in ventral and infrapyramidal blade. Compared with dense projections to dentate gyrus, SUM projected relatively less densely to the hippocampus. PHA-L labeled fibers in hippocampus were mainly restricted to stratum oriens and stratum pyramidale in CA3 along its septotemporal axis and CA2 of the rostral pole of the dorsal hippocampus. As regards the septum, labeled axons were found distributed densely throughout the rostral-caudal extent of both the medial and lateral septum (Vertes, 1992). A medial-lateral gradient in projection from SUM was observed. In this context, the lateral SUM region, as compared to the medial region of SUM, projects more heavily to both the hippocampal formation and the MS-VLDBB region (Vertes, 1992).

Consistent with the findings based on the anterograde tracer, retrograde tracer techniques also indicate a denser projection from lateral region of SUM which is dominantly ipsilateral (Haglund et al., 1984; Vertes, 1988; Magloczky et al., 1994; Leranth and Kiss, 1996; Borhegyi and Leranth, 1997; Borhegyi et al., 1998; Kiss et al., 2000). Interestingly, retrograde tracer combined with double labeling techniques indicates that population of SUM neurons project both to the hippocampus/dentate gyrus and the MS-VLDBB region via collaterals (Borhegyi et al., 1998; Vertes and Mckenna 2000).

In the hippocampus and dentate gyrus, the SUM axons were observed to form a dense network around the principal cell proximal dendrites and soma, forming asymmetric, presumably excitatory synapse (Magloczky et al., 1994). Synapses on local interneurons

were not observed. Within the MS-VLDBB region, SUM glutamtergic axons formed asymmetric synapse mainly on distal dendrites of cholinergic and parvalbumin-containing GABAergic neurons (Leranth and Kiss, 1996; Borhegyi et al., 1998).

The neurochemical identity of SUM projection to MS-VLDBB and hippocampus/dentate gyrus has also been investigated using immunocytochemistry. For instance, Borhegyi and Leranth (1997) reported that a large population of SUM-hippocampal neurons from the lateral region of SUM was immunopositive for the calcium binding protein calretinin. The SUM-hippocampal neurons from more medial region were also immunopositive for calretinin or substance P. Colocalization of calretinin with substance P was not found in the projecting neurons (Borhegyi and Leranth, 1997). Population of calretinin positive neurons also project to the MS-VLDBB (Kiss et al., 2000), although the overlap between the calretinin positive neural projection to dentate gyrus/hippocampus and MS-VLDBB remains unclear. Interestingly, the great majority of calretinin positive SUM neurons were back-labeled with [^{3}H]D-aspartate microinjected into the dentate gyrus or the MS-VLDBB/lateral septum region, suggesting that the calretinin positive SUM projection neurons utilize aspartate/glutamate as neurotransmitter (Kiss et al., 2000). Some SUM-hippocampus/dentate gyrus neurons are also immunopositive for cholecystokinin and vasoactive intestinal polypeptide (Haglund et al., 1984).

Similar to SUM, PHA-L anterograde tracer technique indicates that the posterior hypothalamic (PH) nucleus also projects to medial and lateral septum, although a projection to the hippocampus is not described (Vertes et al., 1995). Interestingly, PH was found to project directly to the SUM.

The physiology of PH-SUM region has been investigated extensively in anaesthetized animals with the main focus on the involvement of the region in the induction of hippocampal theta activity. Indeed, evidence supports that the PH-SUM region mediates, at least partly, the generation of theta rhythmic oscillation recorded from the hippocampus/dentate gyrus (Kirk and McNaughton, 1993; Vertes and Kocsis, 1997; Kirk, 1998; Bland and Oddie, 1998) and a model has been proposed whereby ascending pathway from PH-SUM send both frequency coded (from SUM) and tonic output (from PH nucleus) to the MS-VLDBB region which in turn influence hippocampal generation of theta (Kirk, 1998). The following evidence favors this view. One, infusion of relatively large volume of the local anesthetic procaine in the region of PH-SUM nuclei abolished spontaneous, tail pinch and the reticular pontis oralis (RPO) nucleus (or reticularly) stimulation-evoked theta (Oddie et al., 1994). Conversely, electrical stimulation in the region of PH nucleus evoked hippocampal theta (Smythe et al., 1991; Oddie et al., 1994). Both the frequency of theta and its amplitude was stimulus intensity-dependent, although the frequency exhibited a much tighter relationship than amplitude. Chemical excitation with infusion of the muscarinic-cholinergic agonist, carbachol, in the PH-SUM region also evoked a prolonged increase in theta activity. With such infusion, the evoked theta exhibited relatively higher amplitude than spontaneous theta. The increase in amplitude was attenuated by local infusion of procaine (Oddie et al., 1994) while the generation of theta by carbachol was blocked by local infusion of atropine (Bland et al., 1994). The infusion of atropine also blocked the induction of theta on reticular stimulation (Bland et al, 1994).

Two, discrete microinjection into the medial SUM of relatively lower volumes of procaine or the benzodiazepine chlordiazepoxide that enhances effects of endogenous GABA also strongly attenuated the reticular pontis oralis (RPO) nucleus (or reticularly) elicited hippocampal theta in anaesthetized rat (Kirk and McNaughton, 1993; McNaughton et al., 1995; Thinschmidt et al., 1995). Both the frequency and the amplitude of theta were affected in parallel. Spontaneous theta was abolished with such microinjection. Interestingly, procaine microinjection into the medial forebrain bundle (that carries afferents from PH-SUM to the MS-VLDBB region) and in the MS-VLDBB region attenuated the amplitude but not the frequency of RPO elicited hippocampal theta (Kirk and McNaughton, 1993). Based on the differences in the effect of inactivation of medial SUM versus MS-VLDBB region, the authors (Kirk and McNaughton, 1993; McNaughton et al., 1995) proposed that in anaesthetized rat synapses, including GABAergic synapses in medial SUM, but not MS-VLDBB region, are important for transduction of reticularly input into hippocampal theta frequency while the recruitment of MS-VLDBB neurons by the output from medial SUM contributes to the size of theta.

Three, PH-SUM region neurons especially SUM neurons discharge in a theta rhythmic fashion in correlation with hippocampal theta (Kirk and McNaughton, 1991; Kocsis and Vertes, 1994; Bland et al., 1995; Kirk et al., 1996; Kirk, 1997; Vertes and Kocsis, 1997). Importantly, the rhythmic discharge was at the frequency of reticularly elicited hippocampal theta and was not attenuated by bilateral transactions made rostral to SUM or by inactivation of MS-VLDBB region (Kirk et al., 1996; Kirk, 1997). Neurons in the region of PH nuclei also increased their discharge during theta, though the discharge was tonic in fashion (Bland et al., 1995; Kirk et al, 1996). The theta-related discharge of PH neurons was also not inactivated by MS-VLDBB inactivation (Kirk et al., 1996).

Four, electrical or chemical stimulation in the region of PH nucleus evoke a theta-related discharge of MS-VLDBB and CA1 neurons in anaesthetized rat (Smythe et al., 1991; Bland et al., 1994). Similarly, reticular stimulation also excited MS-VLDBB neurons in a theta-related fashion (Bland et al., 1994). The block of PH region with procaine or atropine prevented the reticularly elicited rhythmic discharge of MS-VLDBB neurons (Bland et al, 1994), while infusion of procaine in MS-VLDBB blocked PH stimulation evoked changes in cell activity in CA1 (Smythe et al, 1991).

The PH-SUM region also influences hippocampal synaptic responses to afferent stimulation. For example, electrical or chemical stimulation of the lateral SUM enhanced granule cell synaptic excitability (Mizumori et al., 1989; Carre and Harley, 1991; Nakanishi et al., 2001). The effect was probably via a direct projection from lateral SUM to the dentate gyrus since it was blocked by transaction of ipsilateral fornix, through which fibers enter hippocampus, but not following lesion of the MS-VLDBB region (Mizumori et al., 1989). In addition to the above, inactivation of the SUM region by local microinjection of the GABAA-receptor agonist muscimol attenuated epileptic discharges and induction of Fos protein in hippocampal neurons (Saji et al., 2000), Fos being a transcription protein that is induced in neurons on their synaptic excitation.

1.6 Functional significance of theta in field CA1

A possibility is that theta-linked signaling in CA1 may lead, at least partly, to behavioral adaptation. In this context, evidence suggests that neural changes in hippocampus, especially in field CA1, that occur in parallel with theta or in relation to particular phase

of theta facilitate and/or promote long-term potentiation (LTP) of synaptic transmission that is proposed to be a neural mechanism of learning and memory. In context of the former, Leung et al. (2003) reported that the LTP of synaptic transmission at basal dendrites of pyramidal cells was facilitated during walking as compared to that observed during immobility, slow wave sleep and rapid eye-movement sleep. The facilitation was blocked by pretreatment with the muscarinic antagonist or by destruction of medial septum cholinergic neurons raising a possibility that the septohippocampal cholinergic neurons are involved in the observed facilitation (Leung et al., 2003).

In context of theta phase-linked promotion of LTP, high intensity burst stimulation of Schaffer collaterals at the peak, but not the trough of local theta wave in stratum radiatum of anaesthetized and behaving animal evoked a potentiation of the apical dendritic field excitatory postsynaptic potential (Holscher et al., 1997; Hyman et al., 2003). The physiological mechanism(s) underlying the selective potentiation remain unclear. However, the stimulation coincides with phasic changes in excitability of the somatic and the dendritic compartments of pyramidal cells. For example, stimulation at peak of theta in stratum radiatum coincides in time with decreased perisomatic inhibition, especially in anaesthetized rat, with increased probability of pyramidal cell discharge (see the section 'Physiological characteristics of hippocampal neurons'). On the other hand, stimulation at the trough of local theta wave in stratum radiatum is close in time to increasing perisomatic inhibition and decreased probability of discharge (Bland et al., 1980; Buzsáki and Eidelberg, 1983; Buzsáki, et al., 1983; Fox et al., 1986; Ylinen et al., 1995; Klausberger et al., 2003; see the section on CA1 neural network activity-theta rhythm). In addition to above-mentioned phase-linked changes, the apical dendritic field excitatory postsynaptic potential evoked unrelated to theta phase are also suppressed in

correlation with theta in behaving and anaesthetized animal (Leung and Vanderwolf, 1980; Herreras et al., 1988; Khanna and Sinclair, 1992; Zheng and Khanna, 2001). Overall, the preferential facilitation of apical signals that are linked to particular phase of theta perhaps reflects a form of 'signal-to-noise' processing.

1.7 Rationale and purpose of study

As reviewed above, the PH-SUM region has gained prominence as a crucial interface for ascending information from lower structures to the septohippocampal region. In this regard, it has been proposed that PH-medial SUM sends, at least in part, frequency-coded information to the MS-VLDBB region which in turn rhythmically paces the MS-VLDBB neurons that evoke theta rhythm in the hippocampus (Kirk and McNaughton, 1991, 1993; Kirk et al., 1996; Vertes and Kocsis, 1997; Kirk, 1998; Bland and Oddie, 1998).

Interestingly, while increased granule cell excitability is observed in correlation with theta in behaving rats, the excitability of CA1 pyramidal cells is suppressed during periods of theta activity evoked during animal locomotion, REM sleep and sensory stimulation, including noxious stimulation in anaesthetized animals (Winson and Abzug, 1977; Leung, 1980; Leung, 1985; Herreras et al., 1988; Khanna, 1997; Leung, 1998; Zheng and Khanna, 2001). It has been proposed, based on physiological and pharmacological observations, that activation of brainstem inputs produces the change in excitability of CA1 pyramidal cell responses that accompanies changes in the electroencephalogram (EEG; Leung, 1985, 1998). However, at present it is not clear

whether RPO stimulation also affects synaptic responses in CA1 and whether SUM mediates such an effect.

Given the links between theta activity and synaptic responses in CA1, it was hypothesized that the theta generating stimulation of RPO will evoke a suppression of CA1 synaptic excitability that is mediated via a neural relay involving the SUM and the MS-VLDBB regions. The following experiments were performed to test the hypotheses: (1) the effect of RPO stimulation on the amplitude of CA1 pyramidal cell population spike and the slope and/or amplitude of the somatic and dendritic field excitatory postsynaptic potential, (2) the effect of reversible inactivation of SUM and MS-VLDBB regions on RPO stimulation-induced changes in CA1 synaptic excitability, and (3) the effect of direct stimulation of PH-SUM region with carbachol on CA1 pyramidal cell excitability and its' sensitivity to reversible inactivation of the MS-VLDBB region. The sensitivity of carbachol-induced changes to antagonism by the muscarinic antagonist, atropine, was also investigated and compared with that evoked upon tail pinch. A previous report has shown that large dose of atropine (50 mg/kg, i.p.) abolished spontaneous theta and theta induced by tail pinch and electrical stimulation in PH (Colom et al., 1987).

CHAPTER II MATERIALS AND METHODS

2.1 Animals and general surgical procedure

Experiments were performed on male Sprague-Dawley rats (derived from Charles River stock) obtained from Animal Holding Unit, National University of Singapore. The local animal committee of the National Medical Research Council, Singapore, approved the experimental procedures. The animals were anaesthetized with urethane (1.0 g/kg, i.p.; Sigma, Singapore). Deep anesthesia during surgery was produced by supplementation with halothane. After anesthesia the rat was secured on a stereotaxic apparatus and the skin over the skull was cut along the midline and retracted. To permit the positioning of stimulating and recording electrodes and microinjection cannula, burrholes were drilled in the cranium at appropriates coordinates (see the following sections). The body (rectal) temperature was maintained around 36^{o}C by a homeothermic blanket control unit (Harvard Apparatus Ltd).

2.2 Electrophysiological recordings, electrical stimulation and drug microinjection

A carbon fiber microelectrode (filled with 0.9% saline) was used for recording extracellular potentials from the pyramidal cell layer of the left dorsal field CA1 (P 3.8-4.5 mm, L 1.5-2.0 mm, V 2.0-3.5 mm; Paxinos and Watson, 1982). The microelectrode was fashioned from glass capillary into which a carbon fiber of suitable length was inserted. The microelectrode was pulled using microelectrode puller (Stoelting Co., USA). The electrode formed had carbon fiber protruding from the tip. The protruding carbon fiber was etched with diluted silver nitrate solution (0.05 M) so that the length of

the carbon fiber was about 10 μm beyond the glass micropipette.

Signals from the carbon fiber microelectrode were amplified and filtered at (a) 1 Hz-100 Hz, to record local hippocampal EEG, and (b) 0.1 Hz-3 KHz to record population spike (PS) or field excitatory postsynaptic potential (fEPSP) from pyramidal cell layer or the region of apical dendrites in CA1, respectively. The PS and dendritic fEPSP (dfEPSP) were generated by electrical stimulation through stimulus isolation units in ipsilateral field CA3 (0.1 Hz, 0.01 ms; P 2.30 mm, L 1.5 mm, V 3.5 mm; Paxinos and Watson, 1982) via a concentric bipolar electrode (Model NE-100; tip diameter: 200 μm,, Rhodes; David Kopf, U.S.A.). The RPO region (P 8.0 mm, L 1.2 mm, V 8.0 mm; Paxinos and Watson, 1982) ipsilateral to CA1 recording was stimulated in the same way at 100 Hz, and pulse duration of 0.01 ms. Drugs were microinjected using a 33-gauge steel needle coupled to an Exmire microsyringe (Ito Corporation, Japan) mounted on a stereotaxic carrier inclined at an angle of 4^{o} or 10^{o} from the vertical. The microinjection of the various drugs (drug solutions were generally prepared in 0.01% alcian blue dye-saline solution) was directed towards the PH-SUM (P 4.2 mm, L 1.5 mm, V 8.0 mm) and/or the MS-VLDBB (A 0.5 mm; L 0.5 mm, V 6 mm) regions.

For later verification of RPO stimulation site, anode current was passed through stimulating electrode at the end of experiment. The microinjection site was marked by the presence of dye spot.

2.3 Experimental protocols

The experimental protocol followed is illustrated in Fig. 2.1.

Fig. 2.1: A. The protocol used to investigate the effect of theta generating electrical stimulation of the ipsilateral region of reticular pontis oralis nucleus (RPO; reticular stimulation) on CA1 field potentials. The reticular (0.01 ms pulse duration) and CA3 stimulation were paired as shown in A. Such paired stimulation was repeated every 10 sec (0.1 Hz). The reticular stimulation voltage was adjusted to T volt that evoked theta between 4-5 Hz frequencies. The CA3 stimulation (0.01 ms pulse duration) was adjusted to evoke a control (i.e. before reticular stimulation) population spike that was ~70% of maximal amplitude and control dendritic field excitatory postsynaptic potential (dfEPSP) that corresponded to population spike of ~25% of maximal amplitude. B. The effect of reticular stimulation on dorsal hippocampus field CA1 pyramidal cell somatic population spike (B, left) and the dfEPSP (B, right) recorded from the region of the apical dendrites. The field potential traces in B represent the average field potentials in the 1-min period immediately before, during and immediately after stopping RPO stimulation. The population spike amplitude was calculated as the average of the peak negative (lower arrowhead on the left in B) from the adjacent positive peaks (the upper arrowheads on the left in B). The slope of the somatic field excitatory postsynaptic potential (sfEPSP) and dfEPSP was calculated over a 2-ms interval on the rising phase of the somatic field potential (between arrows in B, left) and dfEPSP (between arrows in B, right). Reticular stimulation decreased both the population spike and dfEPSP that recovered towards control once reticular stimulation was stopped. C. The protocol used to investigate the effect of carbachol (carbamylcholine chloride; molecular weight 182.65; Sigma; 0.1μl, in 0.01% alcian blue dye solution in saline), microinjected into the posterior hypothalamus (PH)-supramammillary (SUM) region. Carbachol was microinjected after stable population spike was recorded from field CA1 for 2 min during a period of local irregular electroencephalogram (EEG). Generally, the effect of carbachol was monitored on population spike and the local EEG at time points as indicated in the figure (C, upper panel). In some experiments the microinjection of carbachol was repeated 5 minutes and around 1 hour after microinjection of the local anaesthetic procaine (0.5 μl, 20% w/v in 0.01% alcian blue dye solution in saline; C, lower panel) in the medial septum-vertical limb of diagonal band of Broca (MS-VLDBB) region. The effect of carbachol was continually monitored for 10 min after microinjection and an additional 1 min from 19-20 min post injection. The amplitude of CA1 population spike and the slope of the somatic field excitatory postsynaptic potential (sfEPSP), evoked upon ipsilateral CA3 stimulation, were monitored as indices of CA1 pyramidal cell synaptic excitability. The strength of CA3 stimulation was adjusted to evoke a control (i.e. before carbachol microinjection) population spike that was ~70% or ~25% of maximal. The population spike amplitude and the slope of the sfEPSP were measured using the same protocol as explained in B.

A.

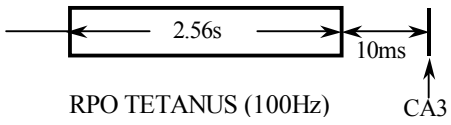
2.56s
10ms
RPO TETANUS (100Hz)
CA3

B.

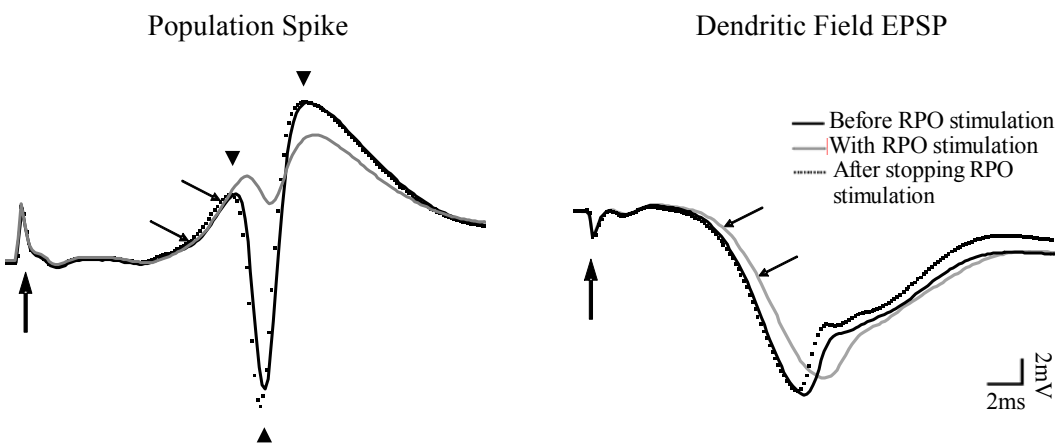
Population Spike
Dendritic Field EPSP
Before RPO stimulation
With RPO stimulation
After stopping RPO stimulation
2mV
2ms

C.

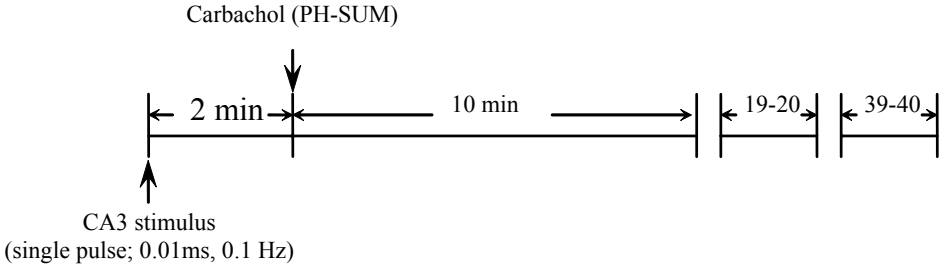
Carbachol (PH-SUM)
2 min
10 min
19-20
39-40
CA3 stimulus
(single pulse; 0.01ms, 0.1 Hz)

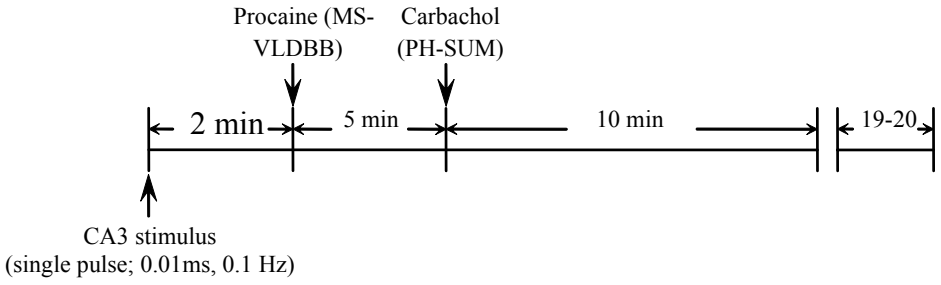
Procaine (MS-VLDBB)
Carbachol (PH-SUM)
2 min
5 min
10 min
19-20
CA3 stimulus
(single pulse; 0.01ms, 0.1 Hz)

2.3.1 Effect of electrical stimulation of the region of reticular pontis oralis nucleus (RPO)

To evaluate the effect of RPO stimulation on the CA1 population spike, both the RPO stimulation intensity and duration were varied during experiments. Initially, the duration of RPO stimulation was adjusted to 2.56 s followed by CA3 stimulation (10 ms from last RPO pulse; Fig. 2.1A). A prolonged RPO stimulation was applied so as to facilitate the induction and measurement of theta waves in line with that reported in the literature (e.g. Kirk and McNaughton, 1993). The CA3 stimulation was adjusted to evoke a control response of ~70% of the maximal population spike amplitude. This allowed both increases and decreases in size to be observed. To determine the change in PS amplitude with changes in frequency and amplitude of RPO elicited theta, RPO stimulation voltage was varied in steps of T-1, T and T+1 volts, where T volt was the threshold stimulation voltage that evoked theta waves between 4-5 Hz frequency. Stimulation at T-1 volt was sub-threshold to evoke theta waves while stimulation at T+1 volt evoked theta waves of 5-6 Hz frequencies.

Following investigations into the effect of prolonged RPO stimulation on CA1 population spike, the duration of RPO stimulation was reduced to 3 pulses followed by CA3 stimulation (10 ms from last RPO pulse) while maintaining the RPO stimulation intensity at T volt (i.e. the threshold for previously producing theta with a 2.56 s train). The effect of such RPO stimulation was investigated on control CA1 population spike with control CA1 population spikes set to an amplitude of ~70% or ~25% of maximal.

2.3.2 Effect of microinjection of procaine and gamma aminobutyric acid (GABA) in the PH-SUM region

To evoke reversible local neural inactivation, procaine (0.1 µl of 20% w/v, Sigma, Singapore), was microinjected into the PH-SUM region over a period of 10-20 s. The concentration of procaine and the rate at which it was injected into posterior hypothalamic regions were based on a previous report (Kirk and McNaughton, 1993). Experiments were initiated with injections of 0.1 µl into the SUM region. This volume is low compared to the volume injected (0.2-0.5 µl) in some related studies (Kirk and McNaughton, 1993; Thinschmidt et al., 1995). However, minimizing volume allows greater accuracy of localization. Crucially, injection of 0.1 µl into the SUM region evoked robust and reproducible effects on reticularly elicited responses in the hippocampus, and was therefore clearly delivering an adequate dose. It was therefore used for all related experiments.

To enable selective block of synaptic transmission without affecting the fibers of passage, gamma aminobutyric acid (GABA; 0.5 µl of 0.8 M in the dye solution; Sigma) was microinjected into the PH-SUM region in the same way as procaine. The concentration and volume of GABA was based on a pilot study in which a number of different concentrations and volumes of GABA solution were microinjected into the SUM region.

The effect of SUM region microinjection of procaine or GABA was investigated on CA1 responses elicited on 2.56 s RPO stimulation (100 Hz) at T volt. Prior to microinjection, the effect of regular RPO tetanic stimulation (every 10 s) was followed

for at least 10 minutes. Subsequent to microinjection the RPO elicited responses were monitored for 10 min for all cases and an additional 1 min from 19-20 min after procaine microinjection.

In 7 experiments following the foregoing investigation, the recording electrode was lowered to the apical dendrites to record the effect of RPO stimulation at an intensity of T volts on the dfEPSP followed by investigation into the influence of microinjection of procaine on the RPO elicited change in the dfEPSP.

In addition to the above investigations, the effect of microinjection of both procaine and GABA on control population spikes and on paired-pulse suppression of CA1 population spike was also recorded. For the latter, paired stimulation was applied to CA3 to evoke a pair of population spikes in CA1. The inter-pulse interval (~60-200 ms) of the paired stimuli was adjusted to evoke the second population spike in CA1 that was around 50% of the first population spike, the first being about 70% of maximal. The suppression of the second population spike relative to the first spike is suggested to be due to recruitment of CA1 inhibitory mechanisms with the first spike (see introduction).

As control for microinjection 0.01% alcian blue dye solution in saline (0.5 μl) was injected into the PH-SUM region.

2.3.3 Effect of microinjection of carbachol (carbamylcholine chloride) into the PH-SUM region

To investigate the effect of direct neural activation of the PH-SUM region on CA1 pyramidal cell excitability, the cholinergic-muscarinic agonist carbachol (carbamylcholine chloride; molecular weight 182.65; Sigma) was microinjected into the region. The concentrations of carbachol used were based on a pilot study in which a number of different concentrations of the drug were microinjected into the SUM region. In this pilot study, the initial concentration tested was 0.0547 M (0.1 μl, microinjected over 10-20 s) that however evoked very prolonged effects (greater than 1 hr; also see Oddie et al., 1994). In order to evoke relatively brief changes (less than hour), the concentration of carbachol was titrated downwards leading to selection of three widely separated concentrations (0.0285 mM, 0.854 mM and 3.42 mM; dissolved in alcian blue dye solution in saline) that enabled an analyses of carbachol concentration-dependant effect of PH-SUM activation on CA1 excitability and the evaluation of the differential sensitivity of the region, especially SUM along its medial-lateral axis (see results). The volume of 0.1 μl was injected over 10-20 s for all three different concentrations.

In the experiments, one of the selected concentrations of carbachol was microinjected into the PH-SUM region following 2-min recording of stable CA1 PS (~70% of maximal) during irregular EEG. The CA1 PS and EEG were followed for at least 10 min and additional 1 min from 19-20 min and 39-40 min after microinjection (Fig. 2.1C). In some cases, the effect of carbachol (0.854 mM) was monitored on the amplitude of ~25% maximal PS.

In 4 experiments, the sensitivity of carbachol-induced changes to antagonism by the muscarinic antagonist, atropine, was investigated and compared with that evoked upon tail pinch. In this protocol atropine was administered intraperitoneally (i.p.) at dose of 5 mg/kg. Light pinch was applied to the distal 1-cm end of the tail either before, 15 min or 30 min following atropine. The tail was pinched using forceps for 5 s at similar intensity each time. Such light pinch induced a suppression of PS accompanied by theta activation, both of which usually recovered within 5 min following pinch. Carbachol (0.1 μl, 0.854 mM) was microinjected 5 min later following each pinch. Recording was followed up to 10 min after carbachol.

As control, 0.01% alcian blue dye-solution in saline (0.1μl) was injected into the PH-SUM region in five animals.

2.3.4 Effect of microinjection of procaine into the MS-VLDBB region

The effect of reversible inactivation of the MS-VLDBB region with procaine (0.2 or 0.5 μl of 20% w/v solution microinjected over 10-20 s) was investigated on RPO- (stimulated at T volt) and PH-SUM carbachol- (0.854 mM) elicited changes in CA1 synaptic excitability. The lower volume, when microinjected into the MS-VLDBB region, was effective in modulating RPO-elicited responses (see the result section). However, preliminary investigation indicated that such volume did not reliably modulate carbachol-elicited responses. But the larger volume of procaine, selected based on a previous report (Kirk and McNaughton, 1993), was effective (see the result section) presumably due to inactivation of greater volume of the MS-VLDBB region. Indeed, the cumulative weight of the evidence suggests that microinjection of 0.1 μl of 0.854

mM carbachol into the PH-SUM region evoked a significantly greater effect on CA1 excitability than electrical stimulation of the RPO region (see the result and discussion section: 3.2.4 and 4.4).

During the experiments, procaine was microinjected into the MS-VLDBB region 10 min into the investigation on the effect of regular RPO tetanic stimulation (every 10 s) or 5 min prior to a carbachol microinjection into the PH-SUM region. The effect of RPO stimulation or carbachol microinjection was monitored up to 20 min following microinjection of procaine. To investigate the effectiveness of PH-SUM carbachol before microinjection of procaine and to demonstrate the recovery of carbachol effect from MS-VLDBB inactivation, carbachol was also microinjected into the PH-SUM site around 1 hr before and after MS-VLDBB procaine microinjection.

2.4 Histology

To facilitate the histological verification of stimulating and microinjection sites, the animal, at the end of experiment, was perfused transcardially with 200 ml saline followed by 200 ml of 4% formaldehyde fixative solution. The brain was then removed and post-fixed for at least 24 hrs in the same fixative at 4^{o}C. Coronal 100-µm (60-µm in some cases) sections were taken through the regions extending from MS-VLDBB up to the RPO on vibratome (Campden Instruments) and collected in 0.05 M Tris-buffered saline (Fisher Scientific). Later, the sections were mounted onto gelatin-coated slides and air-dried. Subsequently, the sections were stained with 1% cresyl violet (5-10 min), and then dehydrated by immersing them in alcohol with an ascending order of concentration (80% x 1→ 90% x 2 → 100% x 2) and then immersed in 100% xylene (x

1). Finally the sections were coverslipped with DePex. The identification of stimulation and microinjection sites was performed under a light microscope.

2.5 Data analysis

Data were digitized (PS and dfEPSP were digitized at 10 KHz, and EEG at 500 Hz) and were collected using Spike 2 software (Cambridge Electronic Design, UK) and analyzed off-line for the following measures: (a) amplitude of the CA1 population spike (mV), (b) peak suppression of CA1 population spike (expressed as % suppression relative to control), (c) latency (s) to suppression of population spike following microinjection of carbachol, (d) slope (mV/ms) of the somatic field EPSP (sfEPSP), (e) slope and amplitude of the dfEPSP, (f) latency to onset of theta (s) and the duration of theta (s/min) following microinjection of carbachol, (g) the frequency at the peak fast Fourier Transform (FFT) power (FFT peak frequency; Hz), and FFT peak power (mV^2) in the 3.42-6.35 Hz theta frequency range of field activity recorded with RPO stimulation, and (h) FFT peak frequency and peak power of theta waves recorded following microinjection of carbachol or tail pinch.

The amplitude of population spikes was calculated as the average of the negative peak from the two positive peaks around it (Fig. 2.1B). The population spike amplitude reflects the nearly synchronous discharge of a population of CA1 pyramidal cells and an increase in the amplitude of the spike reflects an increase in the number of cells firing. The peak suppression of CA1 PS for different experimental condition was calculated from the minimum amplitude (i.e. maximal suppression) of the population spike in 1-min block observed (a) following RPO stimulation, (b) within 5 min following carbachol

injection, and (c) 1 min following tail pinch. The minimum amplitude was expressed as % suppression which is the reduction in the amplitude of the population spike at maximal suppression from the control amplitude (the average amplitude in the 2 min before carbachol injection) expressed as percentage of control (taken as 100%). The latency to suppression of CA1 population spike was the time (s) measured from onset of carbachol injection to the initiation of sustained suppression of population spike by ≥ 20% from the average PS in 2 min before injection. The minimum latency was 10 s which is the interval between 2 successive stimulation applied to CA3 to evoke CA1 PS. The slope of the sfEPSP and dfEPSP was calculated over a 2-ms interval on the rising phase of the somatic field potential and the dfEPSP, respectively (Fig. 2.1B). The slope of the fEPSP corresponds to the intracellular EPSP in these neurons. As such, increases in the slope of fEPSP can reflect increased intracellular EPSP, increased number of contributing cells, or both. We measured the slope of the sfEPSP for both ~70% and ~25% population spike. We specifically targeted the ~25% sfEPSP and also the ~25% dfEPSP for measurement of slope because of *in vitro* evidence that the recruitment of CA1 pyramidal cells corresponds more closely to the size of fEPSP at lower levels of CA3 stimulation (Leung and Au, 1994).

The population spike and fEPSP were averaged in one minute blocks (6 sweeps per minute). An increase or decrease of the population spike was defined as > 20% change from the average value in the 2 min prior to, RPO stimulation, carbachol microinjection or tail pinch. The criterion of 20% change from baseline was not applied to the fEPSP for the following reasons. One, the dfEPSP was recorded in experiments following the investigations into the effect of RPO on CA1 population spike. The effect of RPO stimulation on the population spike was consistent (see results). So, the dfEPSP were

grouped together, irrespective of the size of change in the slope or the amplitude, in order to determine whether in these selected experiments the change in the dfEPSP corresponded in direction to the effect of experimental manipulations on population spike. Two, previous work from our laboratory indicates that the changes in fEPSP slope and amplitude that accompany changes in population spike amplitude are markedly smaller (Zheng and Khanna, 2001; also see the results section in the present study).

Duration of theta was calculated by counting time period (in second per 1-min block) for which hippocampal field activity displayed rhythmic slow wave activity at 3-6 cycles/s in the EEG trace. Latency to theta was defined by measuring the time (s) of onset of sustained theta following carbachol microinjection.

FFT analyses (frequency resolution of 0.488 Hz) of RPO induced theta was performed on 2.048-s blocks of EEG trace (low pass filtered at 10 Hz) immediately before the last pulse of RPO stimulation. The values of the FFT parameters were obtained from the average of six, 2.048-s EEG segments in blocks of one minute. The effect of RPO stimulation intensity on power was determined on raw, non-normalized data. However, to plot and evaluate the time course of effects of microinjection, the power was expressed as a fraction of the control. The control, equated as 1 (or 100%), was the average of the power in the 10 min preceding microinjection of the drugs. Normalizing the data in this way reduced the variance between animals and facilitated comparison. A change in peak frequency or power with drug microinjection was defined as > 0.488 Hz or > 20% change, respectively for two consecutive 1-min blocks within 5-min following microinjection from the 2 min preceding drug injection. FFT on carbachol-induced field

activity was performed only on theta waves taken from 9-s block of EEG (low pass filtered at 10 Hz) between consecutive CA3 stimulation and averaged for six such blocks to give the value of theta peak power and theta peak frequency for the minute corresponding to maximal suppression of the population spike. FFT analysis on pinch-induced field activity was performed on theta waves taken from EEG in first 1-min block following pinch.

The data are expressed as mean ± S.E.M. Statistical comparisons were made using (i) one way, repeated-measure ANOVA followed by Newman-Keul's test for multiple comparisons, (ii) two-tail paired T-test, (iii) two-tail unpaired T-test or (iv) one-tail paired T-test. Significant differences between compared values were accepted at $P < 0.05$.

CHAPTER III RESULTS

3.1 RPO (reticular) stimulation

3.1.1 Effect of RPO stimulation on CA1 pyramidal cell excitability

In these experiments changes in the amplitude of CA1 population spike and the slope and/or amplitude of the somatic field EPSP (sfEPSP) or the dendritic field EPSP (dfEPSP) were monitored as indices of CA1 pyramidal cell excitability.

Relatively prolonged (2.56 s) stimulation of the RPO region evoked a stimulation intensity-dependent decrease in the amplitude of the CA1 population spike (Stimulation intensity, $F_{4, 30} = 38.33$, $p < 0.0001$; Figs. 2.1B and 3.1). The population spike amplitudes corresponding to T-1, T and T+ 1 volts RPO stimulation were 61 ± 6%, 37 ± 5% and 39 ± 5%, respectively, relative to the average spike amplitudes recorded during periods of irregular EEG in the two minutes prior to RPO stimulation. In addition to the relatively prolonged RPO stimulation, investigations were carried out to determine the effect of relatively brief RPO stimulation (3 pulses) at T volt on the CA1 population spike at ~25% (mean amplitude of 2.60 ± 0.24 mV, n = 9) and ~70% (mean amplitude of 7.55 ± 0.50 mV, n = 9) of maximal amplitude. The brief RPO stimulation (three pulses) was much more efficacious in suppressing the amplitude of the ~25% population spike. The mean peak suppression of the ~25% and ~70% population spike was 48 ± 7% (one-tail paired T-test, $p < 0.0005$) and 14 ± 6% (one-tail paired T-test, $p < 0.05$), respectively.

In context of suppression of the ~70% population spike, it is notable that with prolonged reticular stimulation at T volt the mean peak suppression of the ~70% population spike was 63 ± 5% as compared to a suppression of 14 ± 6% with 3 pulse T volt stimulation.

Fig. 3.1: Reticular stimulation intensity-dependent effects on hippocampal electroencephalogram (EEG; A and B) and CA1 pyramidal cell excitability (C). The FFT on the right of each EEG trace in A is the associated fast Fourier Transform (FFT; frequency resolution of 0.488 Hz) of the 2.56 s during reticular stimulation. The broken line drawn from the FFT peaks to the scale at the bottom of the FFT traces indicates the frequency at the peak FFT power. Note that reticular stimulation at T and T±1 volt, but not at T-1 volt, induced clear theta waves in the EEG with the corresponding FFT peak frequencies in the theta range. The peak FFT power (mV^2) with reticular stimulation is indicated on the right of the corresponding FFT. The group data for the effect of reticular stimulation on the FFT parameters is drawn in B where each bar represents mean ± SEM. The effect of reticular stimulation on pyramidal cell excitability was measured by investigating the influence of such stimulation on CA3 stimulation evoked CA1 population spike amplitude (C, left) and the slope of the dendritic field excitatory postsynaptic potential (dfEPSP; C, right). The CA3 stimulation intensity and the protocol for paired stimulation of the reticular region and CA3 was as explained in Fig. 2.1. Each bar in the histogram in C represents mean ± SEM. The histogram values in the two minutes prior to reticular stimulation are represented by 'control', while the values at different intensities (volt) of reticular stimulation are represented by T-1, T and T+1. The population spike amplitude and the slope of dfEPSP were analyzed as explained in Fig. 2.1. Notice that a robust suppression of population spike was evoked at T-1 volt that reached a maximal at T volt reticular stimulation (C), whereas the frequency and amplitude of theta waves were increased further by increasing the reticular stimulation voltage to T+1 volt (B). Further, the slope of dfEPSP was decreased by reticular stimulation at T volts (T-1 and T+1 volt were not tested for effect on fEPSP). Significant difference: $p < 0.05$, * vs. control pretest values prior to reticular stimulation; # vs. value at T-1; & vs. value at T.

A.

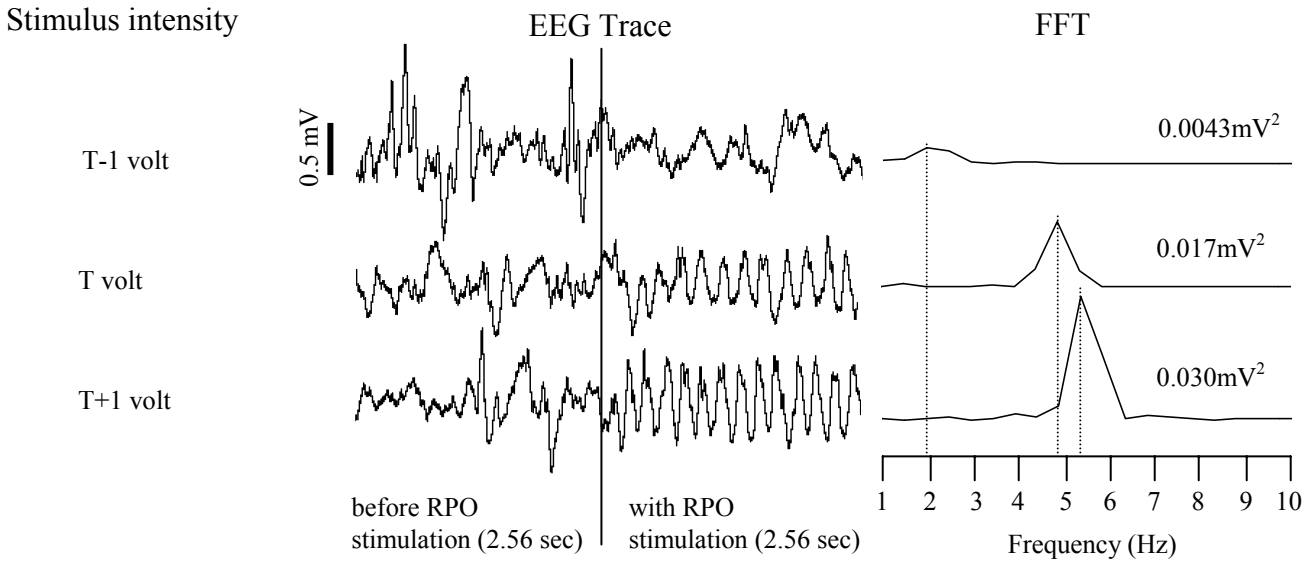
Stimulus intensity
EEG Trace
FFT
T-1 volt
T volt
T+1 volt
0.5 mV
0.0043mV2
0.017mV2
0.030mV2
1 2 3 4 5 6 7 8 9 10
Frequency (Hz)
before RPO stimulation (2.56 sec)
with RPO stimulation (2.56 sec)

B.

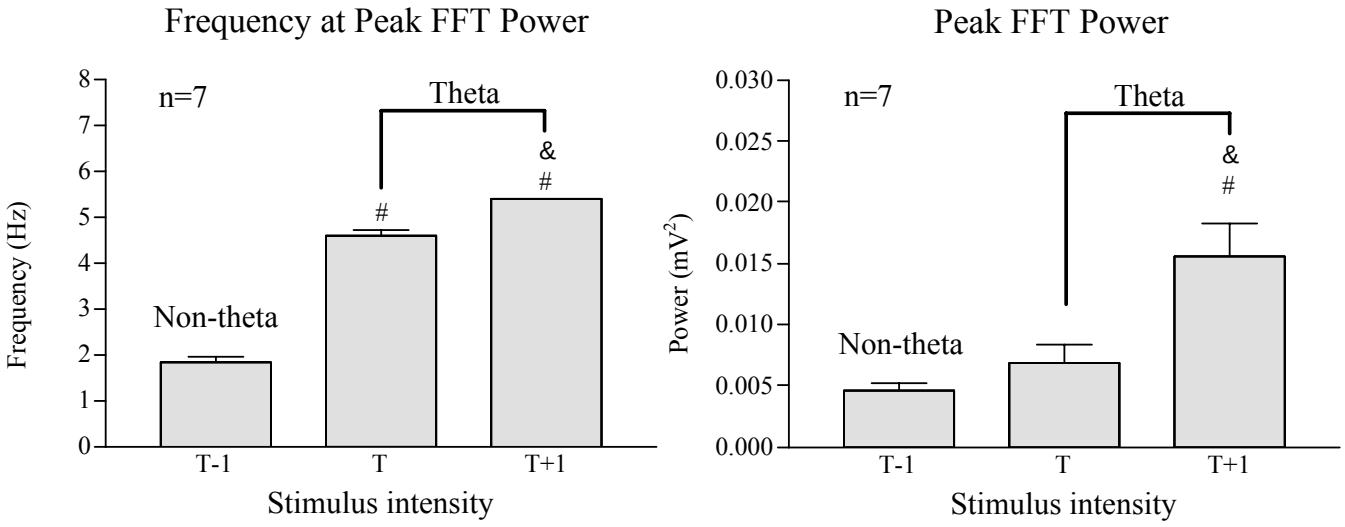
Frequency at Peak FFT Power
n=7
Theta
&
#
#
Non-theta
Frequency (Hz)
0 1 2 3 4 5 6 7 8
T-1 T T+1
Stimulus intensity
Peak FFT Power
n=7
Theta
&
#
Non-theta
Power (mV2)
0.000 0.005 0.010 0.015 0.020 0.025 0.030
T-1 T T+1
Stimulus intensity

C.

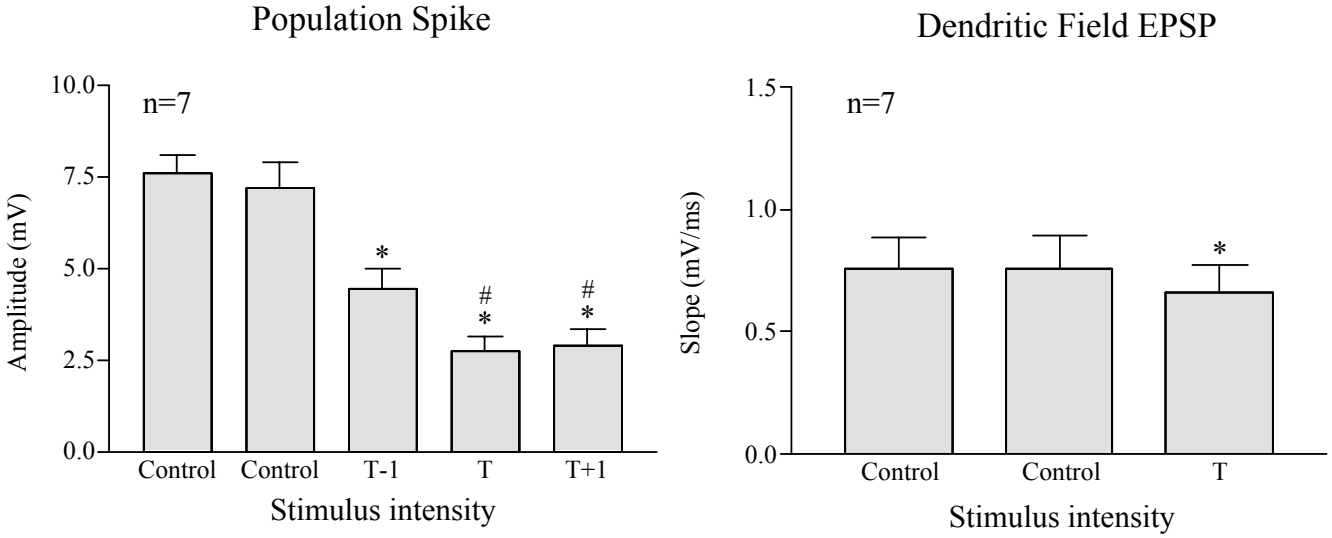
Population Spike
n=7
Amplitude (mV)
0.0 2.5 5.0 7.5 10.0
*
*
*
Control Control T-1 T T+1
Stimulus intensity
Dendritic Field EPSP
n=7
Slope (mV/ms)
0.0 0.5 1.0 1.5
*
Control Control T
Stimulus intensity

In line with this, the population spike amplitude with prolonged T volt reticular stimulation (2.74 ± 0.41 mV, n = 7) was significantly smaller (two-tail unpaired T-test, $p < 0.0001$) than the amplitude recorded with brief RPO stimulation (6.35 ± 0.43 mV, n = 9). The control population spike amplitudes prior to prolonged vs. brief reticular stimulation were not different from each other (7.38 ± 0.61 mV, n = 7 vs. 7.55 ± 0.50 mV, n =9; two-tail unpaired T-test, $p > 0.8$).

The effect of RPO stimulation on the slope of sfEPSP was dependent upon the amplitude of the control population spike. Thus, the sfEPSP slope of the ~70% population spike was not significantly altered with prolonged (2.56 s) RPO stimulation at T-1, T and T+1 volts (Stimulation intensity, $F_{4, 30} = 2.45$, $p > 0.07$; the value of slope before reticular stimulation vs. value with T-1, T and T+1 volt stimulation was 1.42 ± 0.16 mV/ms vs. 1.46 ± 0.15 mV/ms, 1.33 ± 0.18 mV/ms and 1.33 ± 0.18 mV/ms, n=7). Similarly, the sfEPSP slope of ~70% population spike was unaffected with relatively brief (3 pulse) RPO stimulation at T volt (Stimulation intensity, $F_{2, 24} = 0.14$, $p > 0.8$, n = 9; the value of slope before reticular stimulation vs. value with T volt stimulation was 1.05 ± 0.13 mV/ms vs. 1.05 ± 0.13 mV/ms). By contrast, the sfEPSP slope of the ~25% population spike was significantly reduced with brief RPO stimulation at T volt (Stimulation intensity, $F_{2, 24} = 61.53$, $p < 0.0001$, n = 9). The control slope of sfEPSP in the two minutes prior to RPO stimulation was 1.01 ± 0.11 mV/ms and 1.01 ± 0.10 mV/ms (n = 7), while the slope with RPO stimulation was 0.76 ± 0.09 mV/ms. Expressed as percentage the slope at T volt RPO stimulation was 74.1 ± 3.1% relative to the average slope recorded during period of irregular EEG in the two minutes prior to RPO stimulation (reduction of slope by 25.9 ± 3.1% with T volt stimulation). The effect of T-1 and T+1 volt stimulation on ~25% population spike was not tested.

As with the sfEPSP slope of ~25% population spike, the slope of the ~25% dfEPSP, monitored from experiments separate from sfEPSP, was also reduced with RPO stimulation (Stimulation intensity, $F_{2, 18} = 9.32$, $p < 0.004$; Figs. 2.1B and 3.1). In these experiments the effect of relatively prolonged (2.56 s) RPO stimulation at T volt was evaluated. The dfEPSP slope at T volt stimulation was 87 ± 3% relative to the average slope recorded during the period of irregular EEG in the two minutes prior to RPO stimulation (reduction of slope by 12.6 ± 2.8% with T volt stimulation). Similarly, the amplitude of dfEPSP, measured from the baseline to the peak negative, was significantly decreased compared to control (Stimulation intensity, $F_{2, 18} = 26.51$, $p < 0.0001$). The control amplitude in the two minutes prior to RPO stimulation was 7.39 ± 0.59 mV (n = 7) and 7.37 ± 0.53 mV (n = 7), while the amplitude with RPO stimulation was 6.27 ± 0.47 mV (n = 7). The effect of T-1 and T+1 volts stimulation on dfEPSP was not tested.

In 7 rats, in which the PS and dfEPSP were monitored before onset and after RPO stimulation, the amplitude of population spike or the slope of the dfEPSP recovered towards control in the minute after stopping stimulation (Fig. 2.1B).

3.1.2 Relationship of reticularly-elicited suppression to generation of theta

The relatively prolonged (2.56 s) reticular stimulation at T and T+1 volts also generated theta waves concomitant with the suppression of the CA1 population spike (Fig. 3.1). However, the suppression of the CA1 population spike appeared independent of theta generation since (a) clear population spike suppression was evoked at T-1 volt without

any evocation of theta waves and (b) increasing the stimulus strength from T to T+1 volts (increasing the frequency of theta by ~1 Hz) did not increase suppression. Both the peak FFT power and frequency at peak FFT power were increased significantly with increasing the strength of stimulation (Stimulation intensity, $F_{2, 18} = 24$, $p < 0.004$ and Stimulation intensity, $F_{2, 18} = 292.9$, $p < 0.001$; Fig. 3.1). In line with the dissociation noted above, theta waves were not observed with brief stimulation (3 pulses at 100 Hz) at T volts that, nevertheless, clearly evoked a suppression of the CA1 population spike (see the section above). FFT analyses could not be performed on EEG data corresponding to the period of brief stimulation since the number of EEG data points for this period was too few. However, we analyzed 2.56 s of EEG following RPO stimulation. In all cases the FFT peak frequency following brief RPO stimulation was below the theta frequency range (average FFT peak frequency of 1.57 ± 0.07 Hz, n = 9).

3.1.3 Effect of procaine microinjection in PH-SUM or MS-VLDBB region on reticularly-elicited suppression vs. theta generation

A paired stimulation of RPO with stimulation of CA3 was used to concomitantly evaluate the effect of drug microinjection on suppression of CA1 pyramidal cell excitability and the EEG state (Fig. 2.1A). In this protocol 2.56 s of RPO stimulation at T volt was followed 10 ms later by CA3 stimulation. Such paired stimulation was repeated every 10 sec for 10 min prior to and 10 min after microinjection for all cases and an additional 1 min from 19-20 min after procaine microinjection. The reticularly elicited suppression of CA1 PS (~70% of maximal amplitude) and the EEG theta state monitored prior to drug manipulation were both stable (Figs. 3.3, 3.5 and 3.6). Procaine

Fig. 3.2: Diagrammatic representation of procaine microinjection (0.1 µl-0.2 µl, 20% w/v in 0.01% alcian blue dye solution in saline) sites in the posterior hypothalamus (PH)-supramammillary (SUM) and medial septum-vertical limb of diagonal band of Broca (MS-VLDBB) regions. The coronal sections represented are adapted from Paxinos and Watson (1982). The vertical lines in A subdivide the PH-SUM region into area medial or lateral to fasciculus retroflexus (Fr). Filled circles in A and B indicate sites where procaine attenuated FFT peak power and the suppression of CA1 population spike. In the PH-SUM region (A) these sites were localized in the region ipsilateral to the stimulation site and mostly encompassed SUM, the medial forebrain bundle (MFB), and the supramammillary decussation (SUMX). The open circles in A represent sites where procaine was ineffective on the parameters studied. These sites were ipsilateral and dorsal to SUM-MFB region (around Fr or lateral to PH) or contralateral and in the SUM-MFB region. Squares in A indicate sites where both dye solution (0.5 µl) and procaine were injected, but only procaine attenuated the parameters studied. Triangles in A indicate where only dye solution was injected. Such microinjections had no effect. The inverted triangles in B represent sites where procaine attenuated reticular stimulation-evoked suppression of population spike amplitude and the generation of theta power but not theta frequency. Notice that these sites were in the lateral part of the MS-VLDBB region.

A. Posterior Hypothalamus (PH) - Supramammillary (SUM) Region

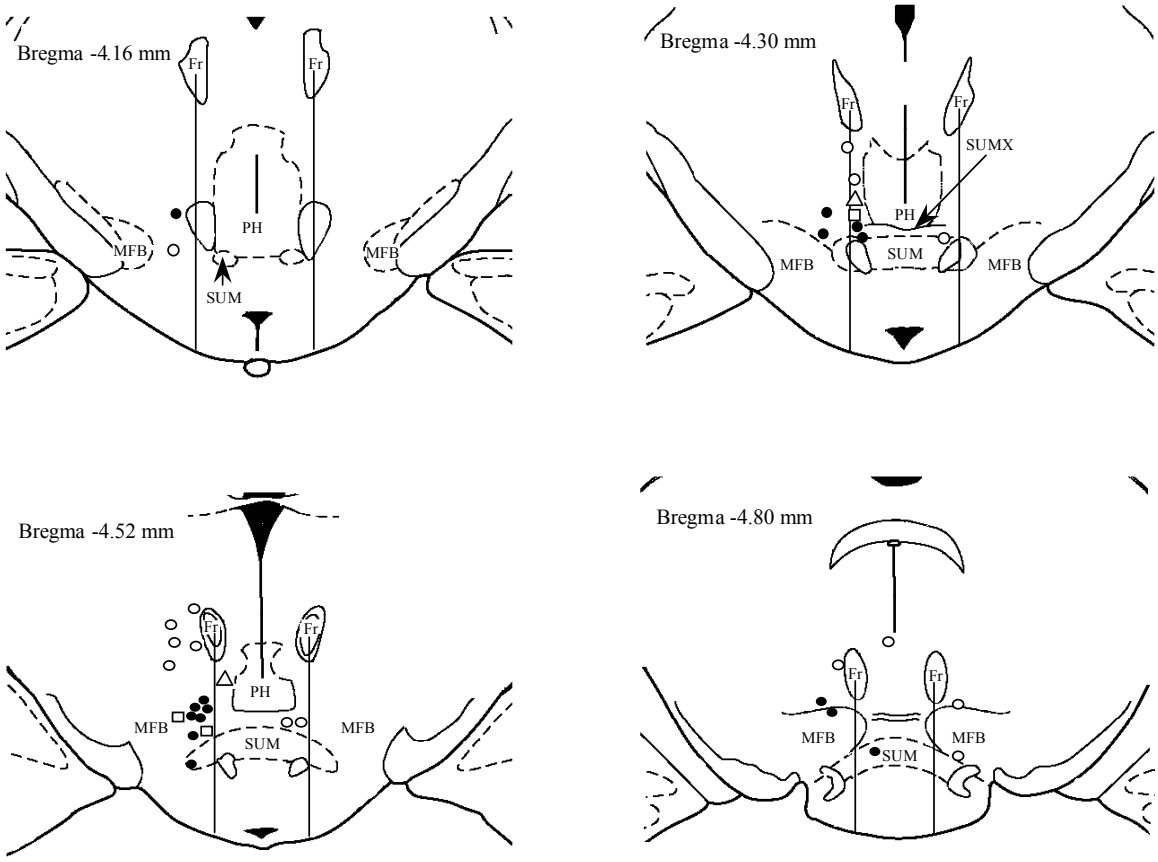

B. Medial Septum-Vertical Limb of the Diagonal Band of Broca (MS-VLDBB)

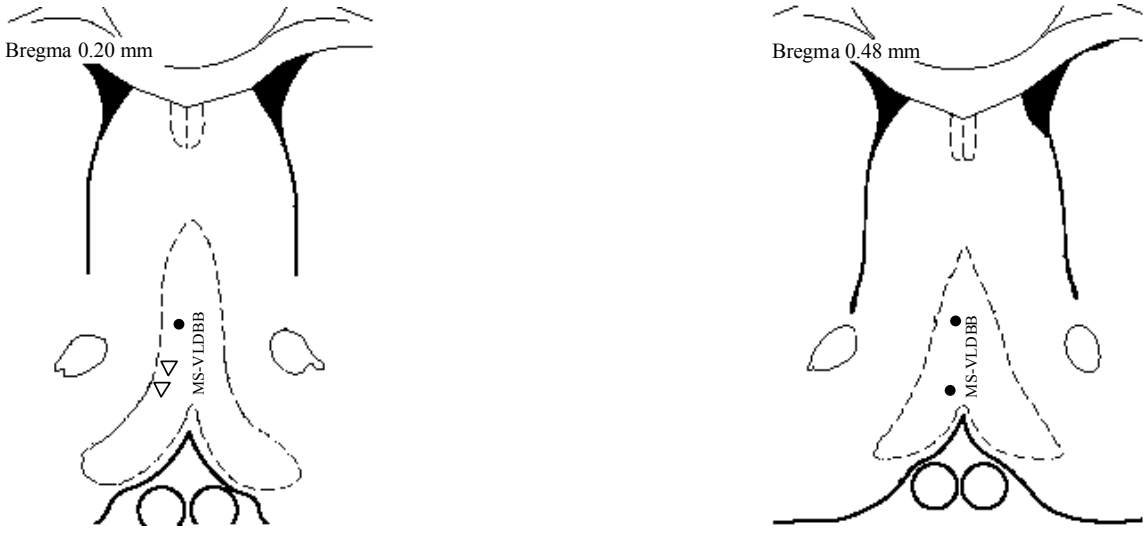

Fig. 3.3: The time course of the effect of procaine microinjected in the ipsilateral medial forebrain bundle (MFB)-supramammillary (SUM) region (sites illustrated in Fig. 3.2A) on reticular stimulation-elicited suppression of CA1 pyramidal cell population spike and FFT peak power. Reticular stimulation (0.1 Hz, 0.01 ms pulse duration, 2.56 s tetanus at 100 Hz) at threshold intensity (T volt) induced theta of ~4-5 Hz frequency when recorded from the pyramidal cell layer of dorsal hippocampus field CA1. The reticular stimulation was applied paired with CA3 stimulation (as explained in Fig. 2.1) so as to enable a concomitant investigation into the effect of procaine on suppression of pyramidal cell excitability and theta generation. The control population spike prior to onset of reticular stimulation was ~70% of maximal. The paired stimulation was applied repeatedly every 10 sec for 10 min prior to microinjection of procaine and 10 min after drug microinjection. An additional 1-min period from 19-20 min post microinjection was also monitored. The time period represented in the x-y plot corresponds to the effect of reticular stimulation on CA1 population responses in 10 min before (i.e. -10 to -1 min) and twenty minute following the drug microinjection. The time of procaine microinjection corresponds to 0-min on the plots (given by the arrow on the x-axis). The amplitude of the population spike was calculated as explained in Fig. 2.1. The FFT peak power was calculated using fast Fourier Transform (as described in Fig. 3.1) and expressed as fraction of the control. The control was the average of the power in the 10 min preceding procaine microinjection. A stable effect of reticular stimulation on CA1 pyramidal cell population spike and theta generation was observed prior to microinjection of procaine. Microinjection of procaine into MFB-SUM region decreased both the suppression of CA1 population spike and the FFT peak power. Significant difference: $p < 0.05$, # vs. -2 and -1 min prior to procaine microinjection.

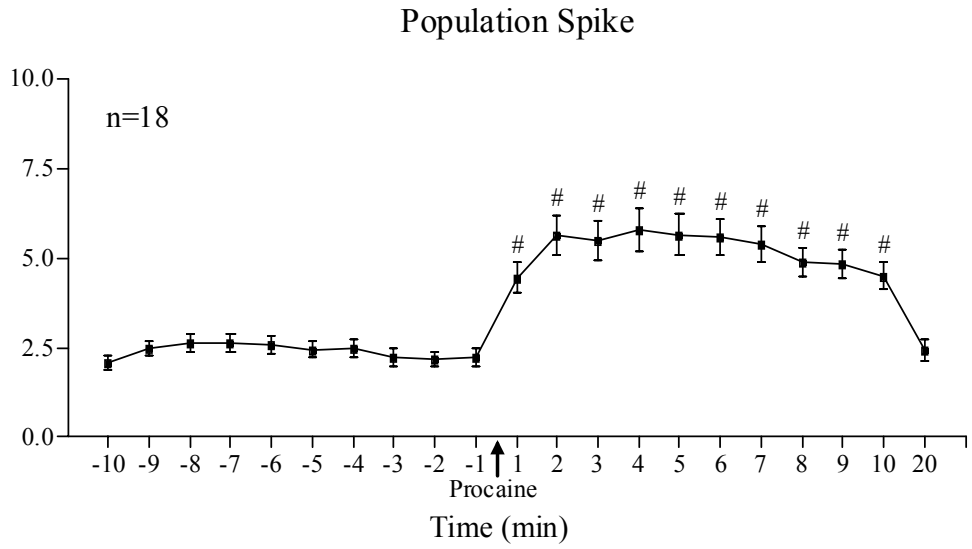
Population Spike
n=18
10.0
7.5
5.0
2.5
0.0
-10 -9 -8 -7 -6 -5 -4 -3 -2 -1 1 2 3 4 5 6 7 8 9 10 20
Procaine
Time (min)

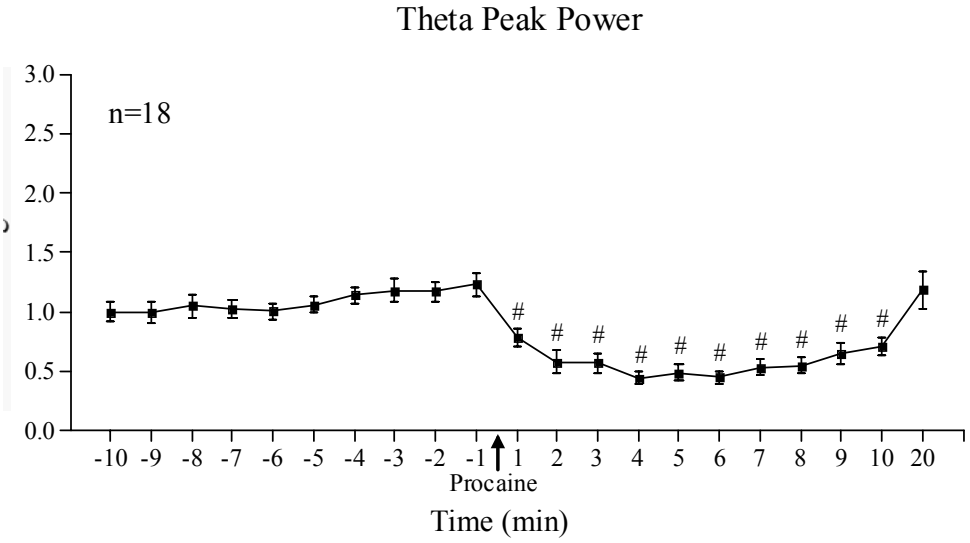
Theta Peak Power
n=18
3.0
2.5
2.0
1.5
1.0
0.5
0.0
-10 -9 -8 -7 -6 -5 -4 -3 -2 -1 1 2 3 4 5 6 7 8 9 10 20
Procaine
Time (min)

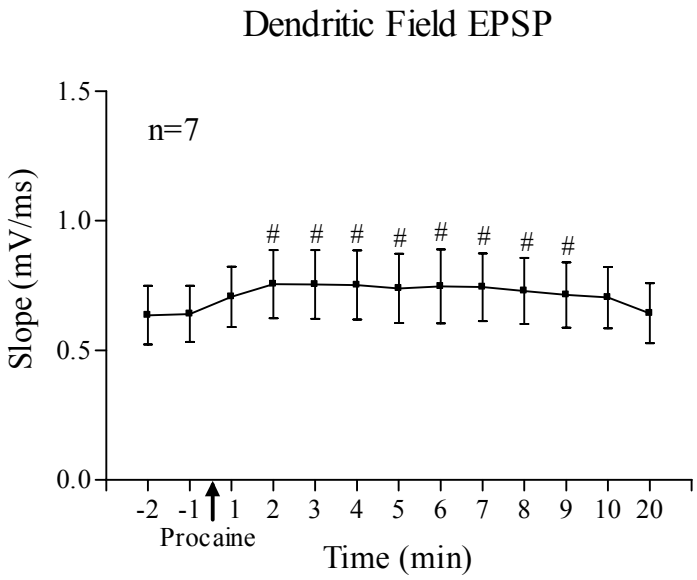

Fig. 3.4: Procaine microinjected into the posterior hypothalamus-supramammillary region attenuated the reticularly-elicited suppression of dendritic field excitatory postsynaptic potential (dfEPSP). In these experiments, following the investigations into the effect of the drug microinjection on PS suppression (Fig. 3.3), the recording electrode was lowered to the apical dendrites to investigate the effect of such microinjection on the RPO elicited change in the slope of dfEPSP. Details as for Fig. 3.3. The control dfEPSP was ~25% prior to onset of reticular stimulation. The time period represented in the x-y plot corresponds to the effect of reticular stimulation on CA1 population response in two minute before (i.e. -2 and -1 min) and 10 min following the drug microinjection. Additional 1-min record was obtained for the 19-20 min period after microinjection. Notice that the slope of the dfEPSP was increased following procaine microinjection. Significant difference: $p < 0.05$, # vs. -2 and -1 min prior to procaine microinjection.

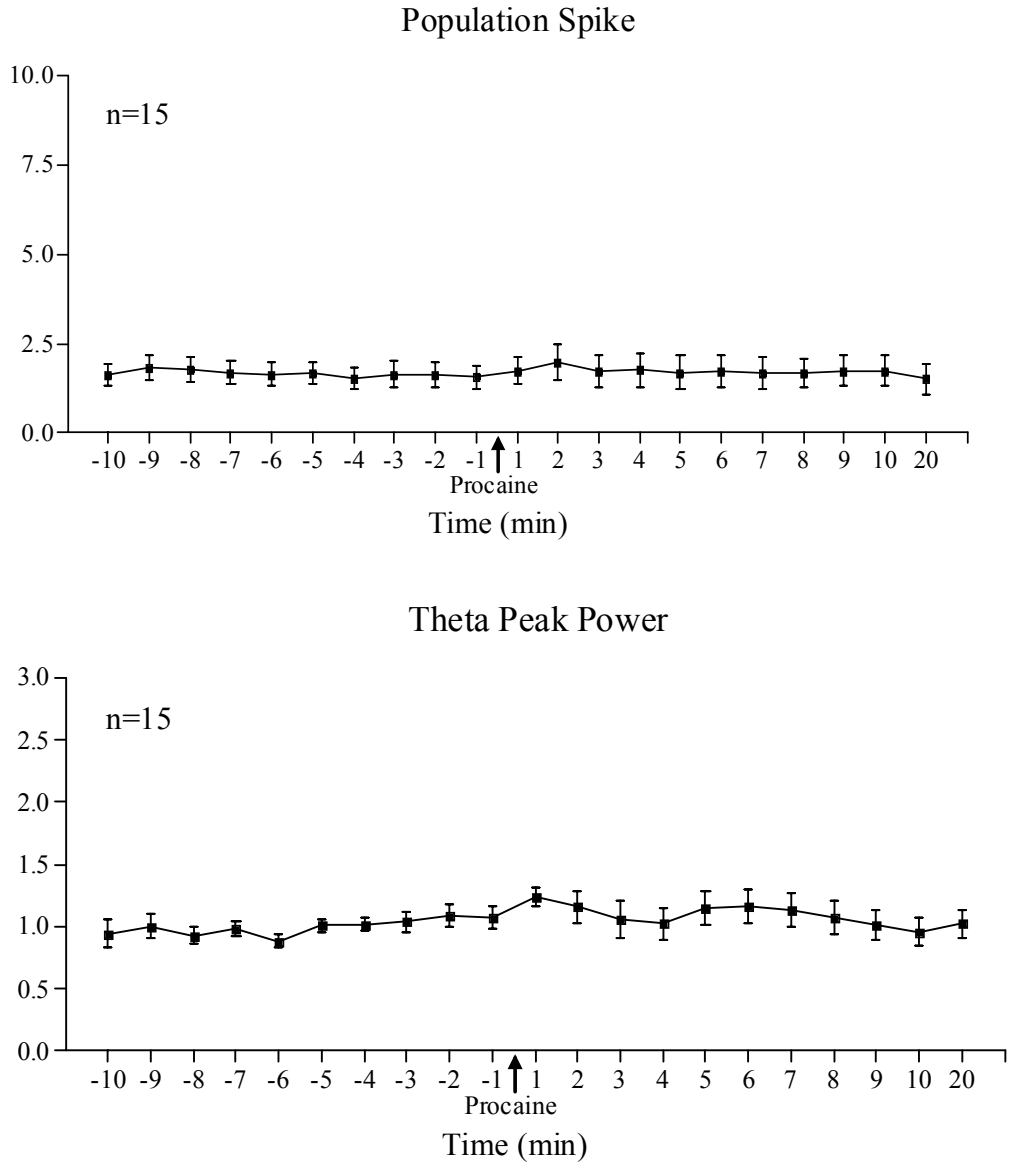

Fig. 3.5: The lack of effect of procaine microinjected in dorsal/contralateral regions on reticular stimulation-elicited suppression of CA1 pyramidal cell population spike and FFT peak power. Details as for Fig. 3.3. The microinjection sites were lateral and ventral to the fasciculus retroflexus (dorsal to ipsilateral medial forebrain bundle (MFB) -supramammillary (SUM) region) or in contralateral MFB-SUM (see Fig. 3.2A). Such microinjections did not attenuate reticularly elicited responses.

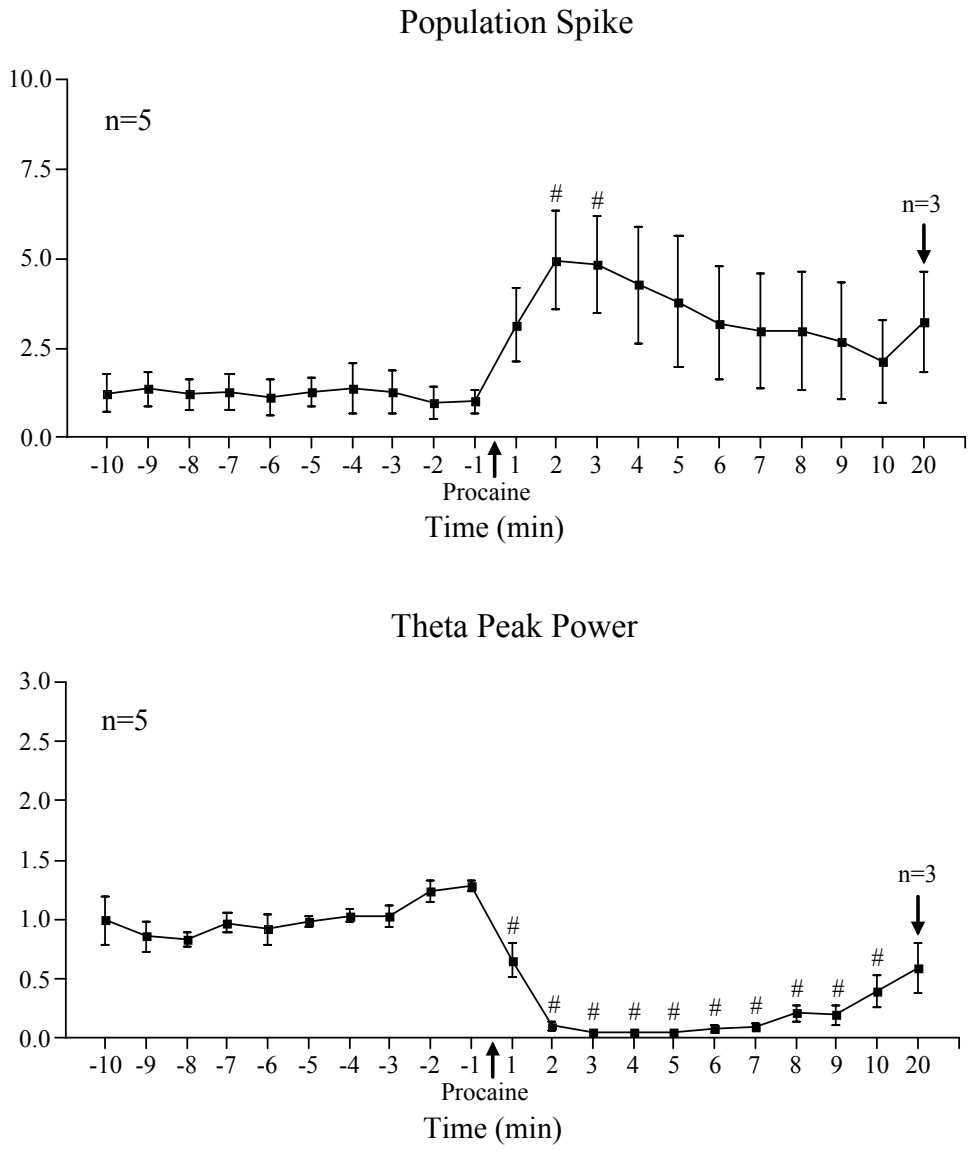

Fig. 3.6: The time course of the effect of procaine microinjected in the medial septum-vertical limb of the diagonal band of Broca (MS-VLDBB) region (see Fig. 3.2B) on reticular stimulation-elicited suppression of CA1 pyramidal cell population spike and FFT peak power. Details as in Fig. 3.3. All 5 sites in the MS-VLDBB region attenuated suppression of CA1 population spike amplitude and FFT peak power. Significant difference: $p < 0.05$, # vs. -2 and -1 min prior to procaine microinjection.

or GABA (see the subsection below) was microinjected against the background of stable responses.

Microinjection of procaine (0.1 μl, over 10-20 s) into the medial forebrain bundle (MFB), and SUM region (Fig. 3.2A) attenuated RPO elicited PS suppression (Time, $F_{12, 221} = 19.57$, $p < 0.0001$; Fig. 3.3) in the minute after injection and at the same time decreased the FFT peak power (Time, $F_{12, 221} = 13.38$, $p < 0.0001$; Fig. 3.3). For the group as a whole, a delayed loss of theta was observed in the 2nd minute after microinjection marked by a shift in RPO elicited FFT peak frequency from theta range to lower frequencies (Time, $F_{12, 221} = 16.47$, $p < 0.0001$, n =18; the value of the FFT peak frequency at -2 and -1 min before vs. the value in the 1st, 2nd, 3rd, 5th, 10th and 20th min after procaine microinjection was 4.88 ± 0.097 Hz and 4.85 ± 0.092 Hz vs. 4.37 ± 0.27 Hz, 2.85 ± 0.32 Hz, 2.85 ± 0.34 Hz, 2.33 ± 0.30 Hz, 3.31 ± 0.35 Hz and 4.64 ± 0.11 Hz). Examination of individual records indicated that in most instances a gradual shift in FFT peak frequency in the theta frequency range was not observed. However, in two instances the FFT peak frequency exhibited a decrease (average FFT peak frequency before and in the 2nd minute after microinjection of procaine being 4.40 Hz and 3.67 Hz, respectively) before a loss of theta. The suppression, FFT peak amplitude and peak frequency recovered to control by the 20th minute post microinjection. Since the period between 10-19 min post procaine was not monitored, a comparison of recovery of PS suppression and FFT parameters post procaine is not delineated.

The effective procaine injection sites that evoked an effect on both RPO-elicited suppression and EEG were ipsilateral to the RPO stimulation site, and were generally localized in and around SUM or the MFB (Fig. 3.2A). Medial-laterally, most of the

effective sites explored in the study were localized lateral to fasciculus retroflexus (Fr; Fig. 3.2A, n = 14) with only a few medial to it (Fig. 3.2A; n = 4). The sites from where procaine evoked a decrease in FFT peak frequency in the theta range were localized in the SUM medial to Fr (medial SUM or mSUM).

In 7 of the above experiments, following the investigations into the effect of the drug microinjection on PS suppression, the recording electrode was lowered to the apical dendrites to investigate the effect of such microinjection on the RPO elicited change in the slope and amplitude of dfEPSP. In these experiments procaine microinjection also attenuated the RPO elicited decrease in the slope of the dfEPSP (Time, $F_{12, 78} = 6.04$, $p < 0.0001$, n = 7; Fig. 3.4) and the amplitude (Time, $F_{12, 78} = 9.601$, $p < 0.0001$; data not illustrated). In these 7 experiments, theta was not monitored while recording dfEPSP; however these experiments comprised part of the above group for which the effect of microinjection on theta is described in the preceding paragraphs of this section. The procaine injection sites in the above 7 experiments were localized in and around MFB (n = 5), in SUM lateral to Fr (lateral SUM or lSUM, n =1) and mSUM (n = 2).

Procaine microinjection into the region dorso-lateral to ipsilateral SUM and into the contralateral SUM region (Fig. 3.2A) had little or no effect on RPO-elicited PS suppression (Time, $F_{12, 182} = 0.80$, $p > 0.6$, n = 15; Fig. 3.5), FFT peak power (Time, $F_{12, 182} = 0.70$, $p > 0.7$, n = 15; Fig. 3.5) and FFT peak frequency (Time, $F_{12, 182} = 1.57$, $p > 0.1$, n = 15; the value of the FFT peak frequency at -2 and -1 min before vs. value in the 1^{st}, 2^{nd}, 3^{rd}, 5^{th} , 10^{th} and 20^{th} minute after procaine microinjection was 4.99 ± 0.13 Hz, 4.89 ± 0.11 Hz vs. 4.86 ± 0.13 Hz, 4.73 ± 0.19 Hz, 4.60 ± 0.22 Hz, 4.60 ± 0.25 Hz, 4.50 ± 0.17 Hz and 4.96 ± 0.10 Hz). The dorsal sites were generally lateral and ventral

to Fr. The contralateral injection sites were localized dorsal to SUM and medial to Fr (Fig. 3.2A). Similar ipsilateral microinjections evoked a loss of theta (Fig. 3.2A; see above).

Microinjection into the MS-VLDBB region (Fig. 3.2B) also attenuated population spike suppression (Time, $F_{11, 48} = 3.37$, $p < 0.002$, $n = 5$; Fig. 3.6), and FFT peak power (Time, $F_{11, 48} = 49.71$, $p < 0.0001$, $n = 5$; Fig. 3.6). However, the effect with MS-VLDBB procaine on PS suppression was not as robust as on RPO elicited FFT peak power. A statistically significant effect of MS-VLDBB procaine on RPO elicited PS suppression was observed only to 2 min post injection and individually the suppression was attenuated for 3-8 min post injection; whereas individually and for the group the FFT peak power was attenuated for at least 10 min (Fig. 3.6). Individually, the effect of procaine on suppression and FFT peak power was observed in all 5 experiments and was marked by loss of theta in 3 out of 5 cases. The microinjection sites from these three experiments were more medial (filled circles in Fig. 3.2B) than the other two, which were in the lateral regions of the MS-VLDBB (inverted triangles in Fig. 3.2B).

3.1.4 Effect of PH-SUM region GABA on RPO-elicited suppression vs. theta generation

GABA microinjections (0.5 μl over 10-20 s) into the mSUM (Figs. 3.7 and 3.8) attenuated the suppression of the CA1 population spike evoked by T volt stimulation of the RPO region (Time, $F_{11, 72} = 5.57$, $p < 0.0001$, $n = 7$; Figs. 3.8A and 3.9A). The attenuation of suppression was observed in the minute after microinjection (Fig. 3.9A)

Fig. 3.7: Representation of the gamma aminobutyric acid (GABA) microinjection (0.5 µl, 0.8 M in 0.01% alcian blue dye solution in saline) sites in posterior hypothalamus (PH)-supramammillary (SUM) region. A. Illustration of a dye spot in the SUM region medial to (medial SUM or mSUM; left in A) or lateral to (lateral SUM or lSUM; right in A) fasciculus retroflexus (Fr). The contours of SUM are superimposed in white on the digital images. B. Injection sites represented on coronal sections adapted from Paxinos and Watson (1982) as in Fig. 3.2. Filled circles indicate sites where GABA both abolished reticularly elicited theta and attenuated the suppression of the CA1 population spike. These sites were localized in the mSUM region ipsilateral to the reticular stimulation site. The inverted triangles represent sites where GABA selectively attenuated the amplitude of reticular stimulation-evoked theta without affecting the other parameters studied. These sites were in the lSUM region, and in PH. The open circles represent sites where GABA was ineffective on the parameters studied. These sites were in the ipsilateral medial forebrain bundle (MFB), PH, supramammillary decussation (SUMX) and contralateral SUM. Microinjection sites from where GABA evoked effects were much more restricted than with microinjection of procaine (Fig. 3.2).

Posterior Hypothalamus (PH) – Supramammillary (SUM) Region

A.

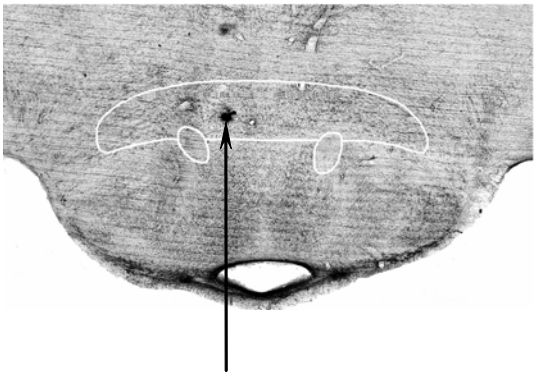

Dye spot (mSUM)

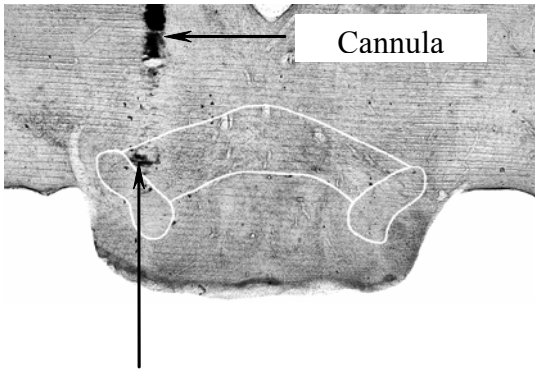

Dye spot (lSUM)

B.

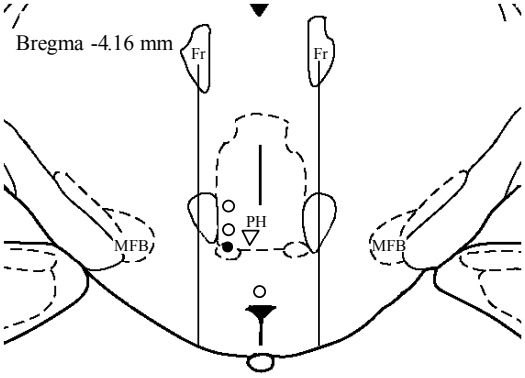

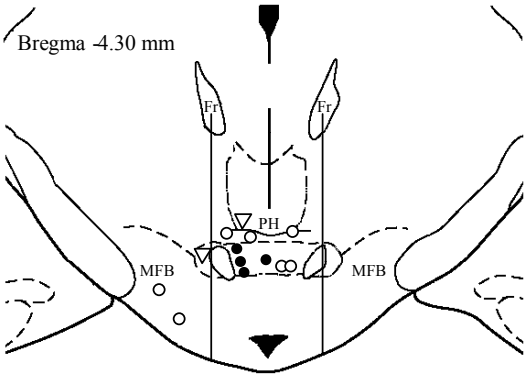

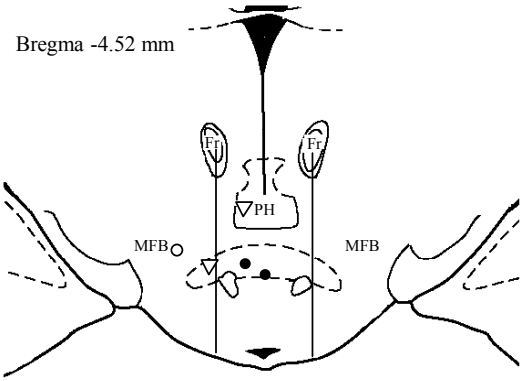

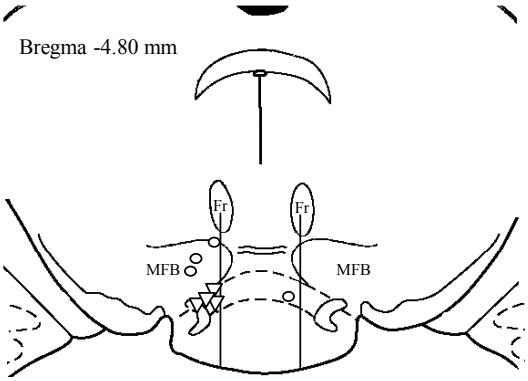

Fig. 3.8: The effect of microinjection of gamma aminobutyric acid (GABA; 0.5 μl, 0.8 M) on reticular nucleus pontis oralis (RPO) stimulation-elicited theta and suppression of CA1 population spike (PS). RPO was stimulated at T volts, and GABA was microinjected into the supramammillary nucleus either medial to (medial GABA, A) or lateral to (lateral GABA, B) fasciculus retroflexus. The PS traces represent the average PS size in one-minute blocks at times before (-1 min) or after (1 min to 10 min) GABA microinjection. The electroencephalogram (EEG) and fast Fourier Transform (FFT) traces are built as indicated in Fig. 3.1. The EEG traces and the corresponding FFT are at the times indicated on the right of each FFT. The FFT peak prior to microinjection of GABA was in the theta frequency range and is indicated by the dotted line drawn from the peak to the scale at the bottom of FFT traces. The FFT peak power prior to GABA microinjection is illustrated on the left of the corresponding FFT and corresponds to the FFT peak in the trace. Note that medial microinjection attenuated FFT peak power, shifted the FFT peak frequency from theta range to a lower frequency (less than 2 Hz) and reduced the suppression of CA1 PS amplitude. Lateral GABA did not affect suppression of CA1 population spike amplitude.

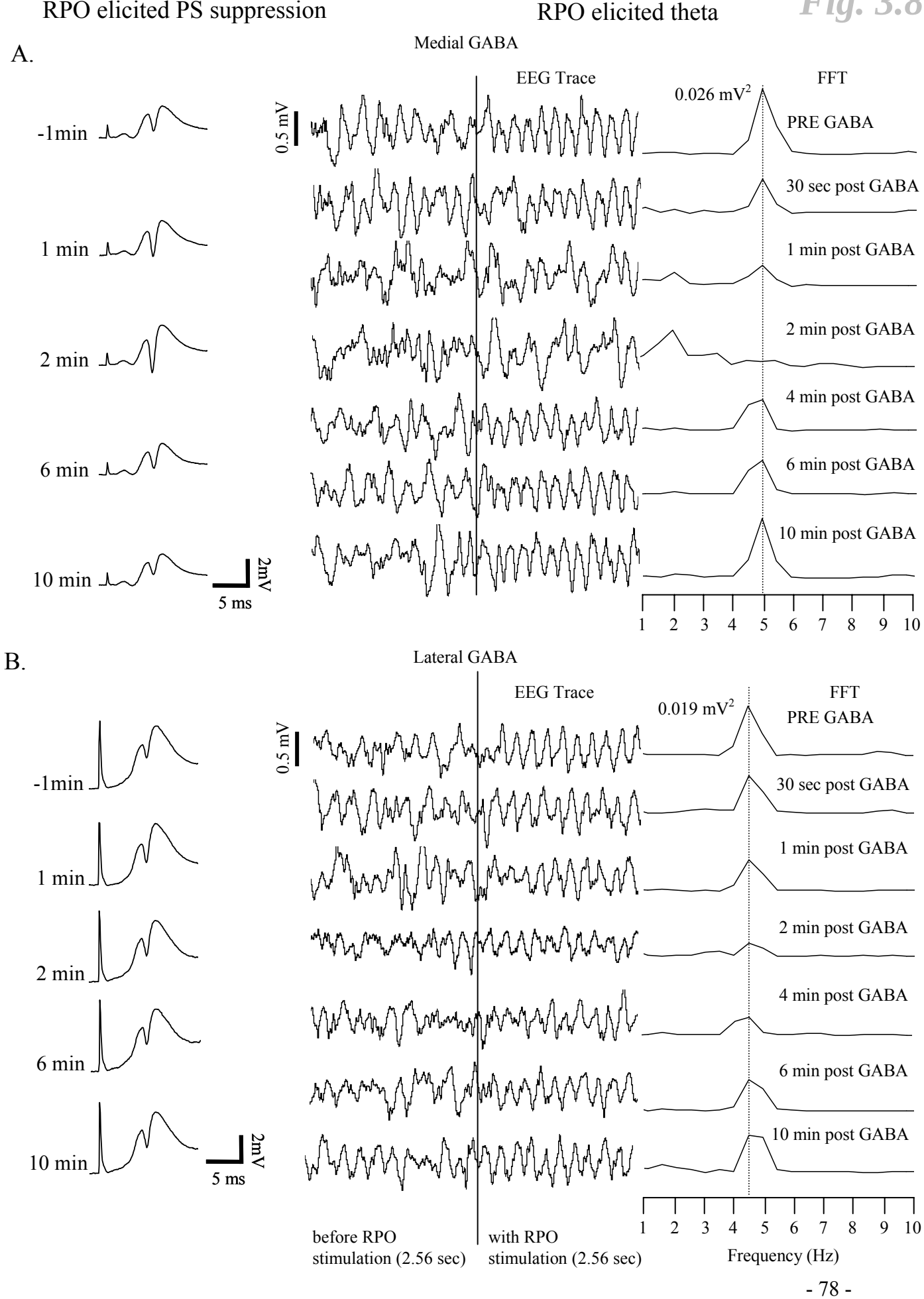
RPO elicited PS suppression
RPO elicited theta
A.
Medial GABA
EEG Trace
FFT
0.026 mV²
PRE GABA
30 sec post GABA
1 min post GABA
2 min post GABA
4 min post GABA
6 min post GABA
10 min post GABA
-1min
1 min
2 min
6 min
10 min
0.5 mV
2mV
5 ms
1 2 3 4 5 6 7 8 9 10
B.
Lateral GABA
EEG Trace
FFT
0.019 mV²
PRE GABA
30 sec post GABA
1 min post GABA
2 min post GABA
4 min post GABA
6 min post GABA
10 min post GABA
-1min
1 min
2 min
6 min
10 min
0.5 mV
2mV
5 ms
1 2 3 4 5 6 7 8 9 10
before RPO stimulation (2.56 sec)
with RPO stimulation (2.56 sec)
Frequency (Hz)

Fig. 3.9: The time course of the effect of microinjection of gamma aminobutyric acid (GABA; 0.5 µl, 0.8 M) into the supramammillary (SUM) region on suppression of the CA1 population spike and FFT peak power. This figure is built as explained for Fig. 3.3, except that the time period represented in the x-y plots in A, B, and C corresponds to the effect of reticular stimulation on CA1 population responses in two minute before (i.e. -2 and -1 min) and 10 min following the drug microinjection. Note that while microinjection of GABA in medial SUM (mSUM; A) ipsilateral to the reticular stimulation sites attenuated the RPO stimulation-evoked suppression of CA1 population spike, little or no effect on suppression was observed with microinjection into the ipsilateral lateral SUM (lSUM; B), contralateral mSUM (C), medial forebrain bundle (MFB; C) or the SUM decussation (SUMX; C). Whereas the FFT peak power was attenuated by microinjection in the mSUM (A) and the lSUM (B). The injection sites are as illustrated in Fig. 3.7. Significant difference: $p < 0.05$, # vs. -2 and -1 min prior to GABA microinjection.

A. Effect of Ipsilateral mSUM Region GABA on RPO Suppression and Theta

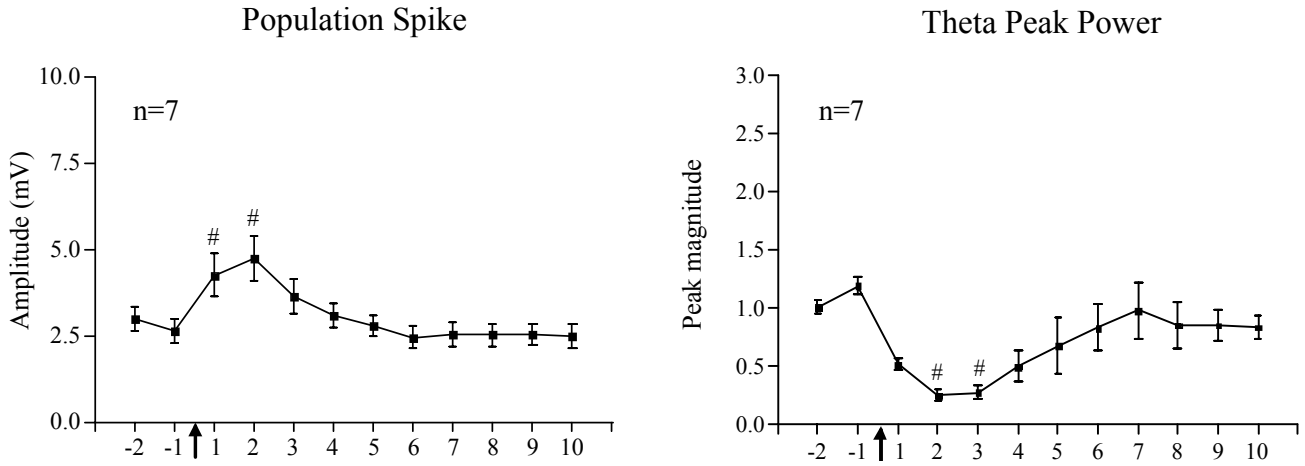

B. Effect of Ipsilateral lSUM Region GABA on RPO Suppression and Theta

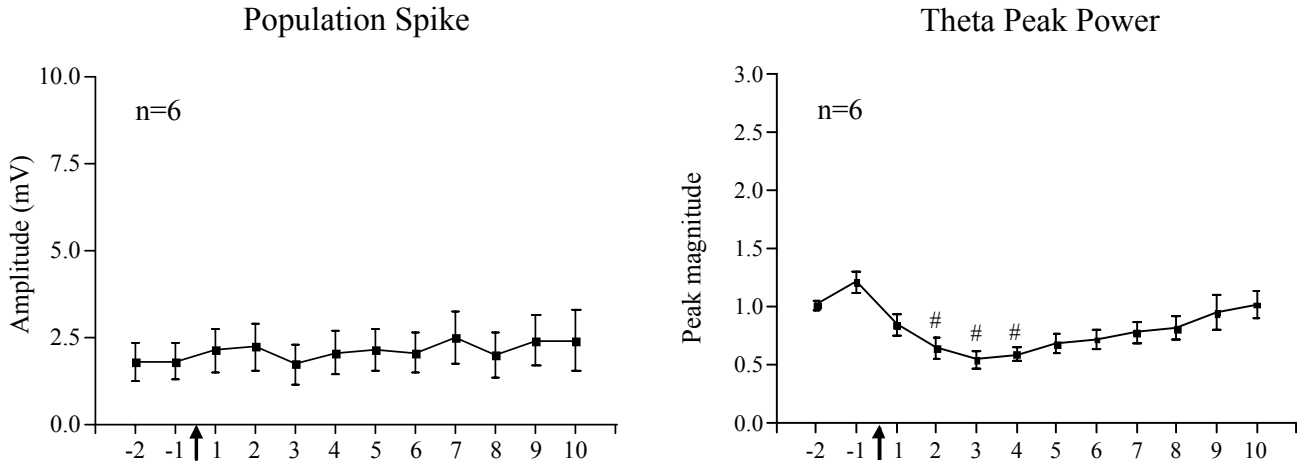

C. Lack of Effect of MFB/SUMX/contralateral Region GABA on Suppression and Theta

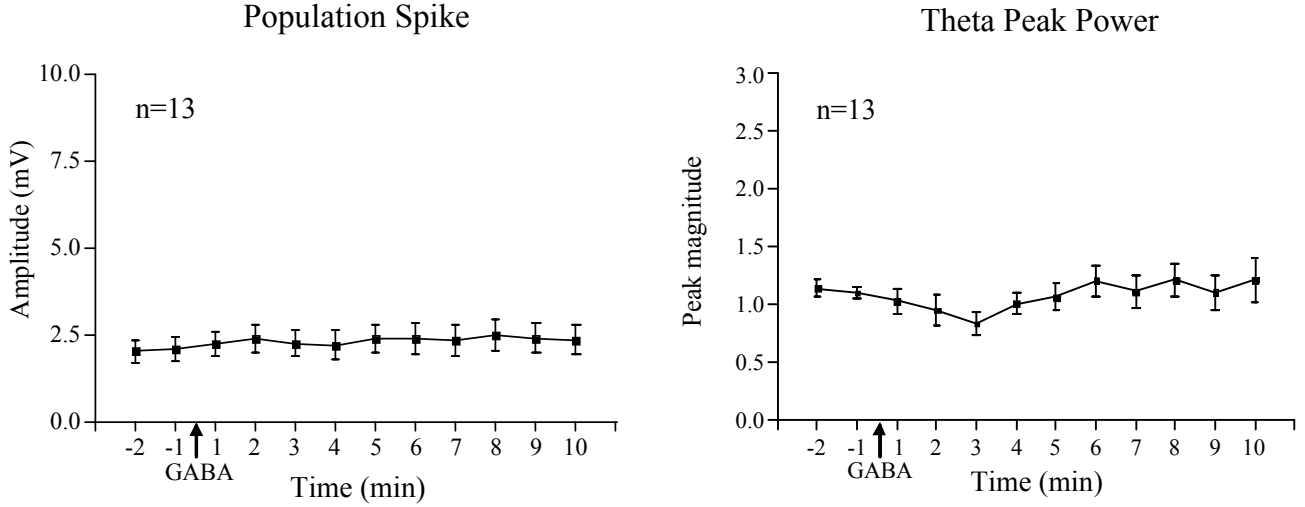

and the onset was in parallel with an effect on RPO elicited FFT peak power (Time, $F_{11, 72} = 6.19$, $p < 0.0001$, n =7; Figs. 3.8A and 3.9A). A delayed loss of theta was observed in the 2nd minute following microinjection marked by shift in FFT peak frequency from the theta range to lower frequencies (Time, $F_{11, 72} = 8.91$, $p < 0.0001$, n = 7; the value of the FFT peak frequency at -2 min and -1 min before vs. the value in the 1st, 2nd, 3rd, 5th and 10th min after GABA microinjection was 4.54 ± 0.09 Hz and 4.61 ± 0.10 Hz vs. 3.70 ± 0.49 Hz, 1.82 ± 0.09 Hz, 3.57 ± 0.54 Hz, 3.88 ± 0.53 Hz and 4.40 ± 0.10 Hz). The recovery from the effect of mSUM GABA was marked by an early recovery of PS suppression (in the 3rd minute following microinjection; Fig. 3.9A). A recovery of theta was also observed in the 3rd min which was marked by return of FFT peak frequency to theta range (see the foregoing paragraph). Generally, the FFT peak frequency recovered to pre-GABA values. However, the recovery of FFT peak power was more gradual (Fig. 3.9A). Indeed, at the 3rd min post GABA when RPO elicited suppression had recovered to pre-microinjection levels (Fig. 3.9A on left), the peak power was strongly suppressed (Fig. 3.9A on right). Similarly, at the 4th min post GABA the peak power was also suppressed, although statistically the value was not different from control. Individually, the suppression of peak power at 4th min was observed in 6 out of 7 experiments. In these 6 experiments the peak power at 4th min post GABA was 35.4 ± 9.5% relative to the average of control peak power in the two minutes prior to GABA microinjection.

Microinjection of GABA into lSUM (Figs. 3.7 and 3.8) did not attenuate PS suppression elicited by T volt RPO stimulation (Time, $F_{11, 60} = 1.65$, $p > 0.1$, n = 6; Figs. 3.8B and 3.9B). By contrast a reduction of FFT peak power was observed (Time, $F_{11, 60} = 6.84$, $p < 0.0001$, n = 6; Figs. 3.8B and 3.9B). This reduction was not as immediate or large as at more medial sites and so did not produce a total elimination of theta when the effect

was maximal. The FFT peak frequency and FFT peak power in the lSUM group (4.68 ± 0.18 Hz and 0.0083 ± 0.0013 mV^2) vs. the mSUM group (4.58 ± 0.09 Hz and 0.011 ± 0.002 mV^2) were not different from each other ($p > 0.244$; two-tail unpaired T-test). This suggests that the intensity of RPO elicited drive was similar in both the groups.

In some of the above experiments (n = 4) we examined the possibility that the effect of lSUM GABA was obscured due to the strong, maximal suppression of PS that is observed on RPO stimulation at T volt. In these experiments, the effect of GABA was monitored on suppression at both T volt and T-1 volt, the suppression of amplitude at latter voltage being about 50% (see subsection 3.1.1). In these experiments, while mSUM GABA also attenuated suppression evoked on T-1 volt stimulation (Time, $F_{11, 36} = 5.78$, $p < 0.0001$; significant reduction was seen in the 2nd minute following microinjection; the value of the population spike amplitude at -2 and -1 min before vs. value in the 1st, 2nd, 3rd, 5th and 10th minute after GABA microinjection was 4.42 ± 0.75 mV and 3.95 ± 0.42 mV vs. 4.35 ± 0.85 mV, 6.16 ± 0. 55 mV, 5.50 ± 0.66 mV, 4.30 ± 0.77 mV and 3.38 ± 0.69 mV), lSUM GABA was without a significant effect (Time, $F_{11, 24} = 0.80$, $p > 0.64$; the value of the population spike amplitude at -2 and -1 min before vs. value in the 1st, 2nd, 3rd, 5th and 10th minute after GABA microinjection was 5.01 ± 0.94 mV and 4.48 ± 0.17 mV vs. 4.69 ± 0.53 mV, 5.30 ± 0.38 mV, 5.27 ± 0.39 mV, 5.22 ± 0.55 mV and 4.96 ± 0.30 mV).

GABA microinjection into the MFB, the region of the supramammillary decussation (SUMX) and contralateral mSUM (Fig. 3.7) did not evoke a significant effect on T volt RPO stimulation-evoked PS suppression, and FFT peak power (Time, $F_{11, 144} = 1.80$, $p > 0.05$ and Time, $F_{11, 144} = 1.37$, $p > 0.1$, n = 13; Fig. 3.9C). The FFT peak frequency

that was in the theta range was also not affected (Time, $F_{11, 144} = 0.71$, $p > 0.7$, n = 13; the value of the FFT peak frequency at -2 and -1 min before vs. value in the 1st, 2nd, 3rd, 5th and 10th minute after GABA microinjection was 4.93 ± 0.14 Hz and 4.96 ± 0.14 Hz vs. 4.93 ± 0.14 Hz, 4.81 ± 0.24 Hz, 5.00 ± 0.18 Hz, 4.93 ± 0.14 Hz and 4.93 ± 0.16 Hz). The FFT peak frequency and amplitude for this group was not different from the above two GABA groups [4.94 ± 0.14 Hz and 1.12 ± 0.05 mV^2 vs. 4.58 ± 0.09 Hz and 1.10 ± 0.07 mV^2 (mSUM) and 4.68 ± 0.18 Hz and 1.12 ± 0.05 mV^2 (lSUM)].

In addition, in 5 experiments microinjection sites were localized to lateral-ventral PH area (medial to Fr; Fig. 3.7). Such injections did not affect PS suppression (Time, $F_{11, 48} = 1.27$, $p > 0.05$, n = 5; the amplitude at -2 and -1 min before vs. amplitude in the 1st, 2nd, 3rd, 5th and 10th minute after GABA microinjection was 2.60 ± 0.88 mV and 2.22 ± 0.71 mV vs. 2.36 ± 0.58 mV, 2.22 ± 0.66 mV, 2.32 ± 0.73 mV, 1.77 ± 0.61 mV and 2.46 ± 0.71 mV) or the FFT peak frequency (Time, $F_{11, 48} = 1.18$, $p > 0.05$, n = 5; the value of the FFT peak frequency at -2 and -1 min before vs. value in the 1st, 2nd, 3rd, 5th and 10th minute after GABA microinjection was 5.09 ± 0.39 Hz and 4.89 ± 0.34 Hz vs. 4.89 ± 0.34 Hz, 5.28 ± 0.28 Hz, 4.59 ± 0.81 Hz, 5.09 ± 0.24 Hz and 4.89 ± 0.34 Hz), but in three cases reduced the peak power (the value of the FFT peak power at -2 and -1 min before vs. value in the 1st, 2nd, 3rd, 5th and 10th minute after GABA microinjection was 1.05 ± 0.04 mV^2 and 1.00 ± 0.24 mV^2 vs. 0.92 ± 0.21 mV^2, 0.36 ± 0.04 mV^2, 0.36 ± 0.04 mV^2, 0.78 ± 0.10 mV^2 and 0.82 ± 0.08 mV^2) with no effect in the other two (the value of the FFT peak power at -2 and -1 min before vs. value in the 1st, 2nd, 3rd, 5th and 10th minute after GABA microinjection was 1.35 ± 0.13 mV^2 and 0.88 ± 0.10 mV^2 vs. 1.13 ± 0.19 mV^2, 1.38 ± 0.18 mV^2, 1.01 ± 0.02 mV^2, 1.19 ± 0.08 mV^2 and 1.02 ± 0.03 mV^2).

3.1.5 Control experiments

In 5 experiments, the dye solution was microinjected into the SUM region (Fig. 3.2A). In 3 of these experiments the dye solution was injected via one of the cannulae of a double cannula assembly, the other cannula being used to microinject procaine. In the other 2 experiments, only dye solution was injected. In none of the 5 experiments did the dye solution have an effect on RPO elicited PS suppression (Time, $F_{11, 58} = 0.71$, $p > 0.7$; Fig. 3.10A) or FFT parameters (Time, $F_{11, 58} = 1.22$, $p > 0.3$ for theta peak power, Fig. 3.10B; Time, $F_{11, 58} = 0.92$, $p > 0.5$ for FFT peak frequency; the value of the FFT peak frequency at -2 and -1 min before vs. value in the 1st, 2nd, 3rd, 5th and 10th minute after dye microinjection was 5.08 ± 0.20 Hz and 5.08 ± 0.29 Hz vs. 5.08 ± 0.20 Hz, 5.08 ± 0.20 Hz, 5.08 ± 0.20 Hz, 5.08 ± 0.20 Hz and 5.08 ± 0.20 Hz). The injection sites in these experiments were in the region around SUM where procaine microinjections, including the 3 experiments above where it was injected at same sites as saline injections, were effective in attenuating RPO theta (Fig. 3.2A).

In 12 experiments the effect of SUM region microinjection of procaine (n = 3; microinjected into the ipsilateral SUM-MFB region) or GABA (n = 9; microinjected into ipsilateral lSUM and mSUM regions) was also monitored on paired-pulse suppression. In this paradigm, under irregular EEG the first population spike was ~70% of maximal (6.69 ± 0.46 mV) while the second spike evoked at inter-pulse intervals of ~60-200 ms was 3.66 ± 0.48 mV in the two minutes before microinjection . The average decrease in the second population spike amplitude compared with the first population spike was 47 ± 4% (two-tail paired T-test, $p < 0.0001$). Microinjection of procaine or GABA did not affect the amplitude of the first (Time, $F_{11, 132} = 0.63$, $p > 0.8$; data not illustrated) or the

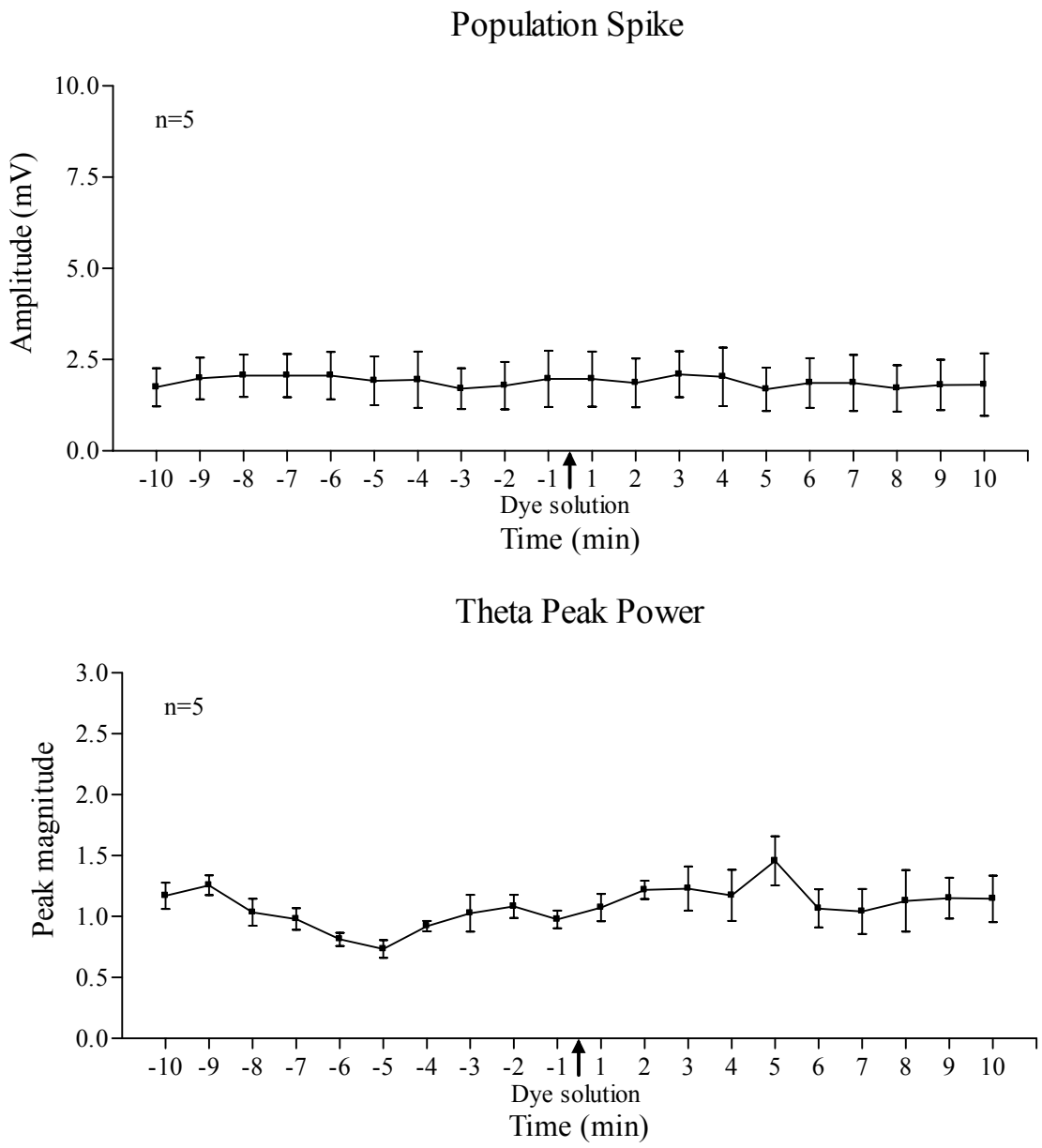

Fig. 3.10: The time course of population spike amplitude (panel A) and theta activation (panel B) from experiments where microinjection of dye solution (0.5 µl) was ineffective in attenuating RPO-elicited PS suppression and FFT parameters. The injection sites are as illustrated in Fig. 3.2. The plot is built as explained for Fig. 3.3. Data are mean ± SEM.

second (Time, $F_{11, 132} = 0.56$, $p > 0.8$; data not illustrated) population spikes. The lack of effect of microinjected procaine and GABA on the first/basal population spike amplitude and paired-pulse suppression suggests that such microinjection did not alter the basal properties of CA1.

3.2 Chemical stimulation with carbachol microinjection

3.2.1 Effects of carbachol microinjection on CA1 pyramidal cell excitability

As with RPO stimulation, microinjection (0.1 μl) of the cholinergic agonist, carbachol, into the SUM region (Fig. 3.11) evoked a suppression of the CA1 PS that was ~70% of maximal amplitude (Figs. 3.13 and 3.14). An immediate and robust suppression of ~70% population spike was observed that was significant for at least 10 min post carbachol at concentration of 0.0285- (Time, $F_{13, 117} = 4.63$, $p < 0.0001$, $n = 10$), 0.854- (Time, $F_{13, 117} = 9.68$, $p < 0.0001$, $n = 10$) and 3.42-mM (Time, $F_{13, 117} = 15.71$, $p < 0.0001$, $n = 10$), respectively (Fig. 3.14). The average amplitude of the population spike in the two minutes before carbachol microinjection (control amplitude) at concentrations of 0.0285-, 0.854- and 3.42-mM was 7.63 ± 0.34 mV, 6.84 ± 0.38 mV, 6.62 ± 0.49 mV, respectively. The control amplitudes were not different from each other (Concentration, $F_{2, 27} = 1.7$, $p > 0.2$, One-way ANOVA). The strength of suppression was carbachol concentration-dependent. In this regard, the mean peak suppression of the ~70% population spike observed with carbachol concentrations of 0.854- and 3.42-mM (72.06 ± 7.38% and 83.76 ± 5.43%, respectively) was significantly greater than that observed with the lower concentration of 0.0285 mM (51.41 ± 6.15%; Concentration, $F_{2, 27} = 5.78$,

Fig. 3.11: Diagrammatic representation of carbachol microinjection sites in the posterior hypothalamus (PH)-supramammillary (SUM) region associated with suppression of CA1 population spike. The coronal sections represented are adapted from Paxinos and Watson (1982). The vertical lines from fasciculus retroflexus (Fr; middle and lower panels) subdivide the SUM region into area medial (medial SUM or mSUM) or lateral (lateral SUM or lSUM) to Fr. Filled circles (n=16; only 15 are shown, the remaining is not shown on the figure due to overlap), triangles (n=10) and diamonds (n=10) in the figures correspond to sites where carbachol (0.1 μl) was microinjected at concentration (mM) of 0.0285, 0.854 or 3.42. Twenty-three microinjection sites (3 sites for concentration of 0.0285 mM and all the sites for concentration of 0.854- and 3.42-mM) were in the mSUM region, ipsilateral or contralateral to the recording site. Seven injection sites were located in the ipsilateral lSUM, although due to overlap one site is not shown on the figure. Three microinjection sites (carbachol at concentration of 0.0285 mM) were localized to the ipsilateral PH spread out along its anterior-posterior extent. Effective sites (at carbachol concentration of 0.0285 mM) were also observed in the supramammillary decussation (SUMX, n = 1) just dorsal to mSUM, medial forebrain bundle (MFB, n = 1) and in the mammillary body (n = 1).

Posterior Hypothalamus (PH)-Supramammillary (SUM) Region

● Carbachol (0.0285 mM) ▲ Carbachol (0.854 mM) ◆ Carbachol (3.42 mM)

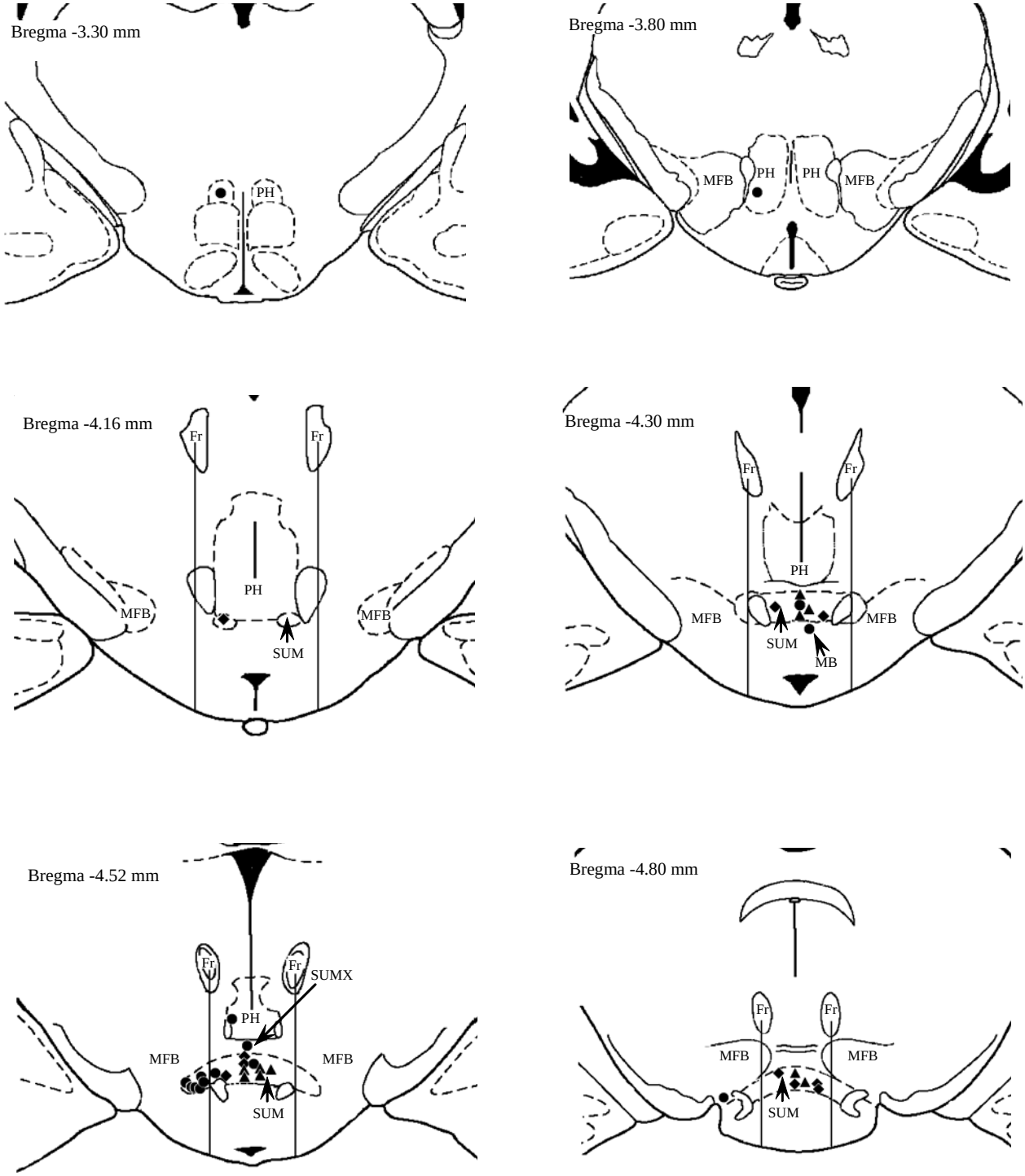

Fig. 3.12: Diagrammatic representation of sites in the posterior hypothalamus (PH)-supramammillary (SUM) region where microinjection of carbachol (0.1µl, 0.0285 mM; open circles) or dye solution (0.1µl of 0.01% alcian blue dye solution in saline; circles with cross in the centre) was ineffective in inducing a suppression of the population spike. The figure was built as explained for Fig. 3.11. The carbachol sites were mostly in the posterior hypothalamus (PH; n = 8) along its anterior-posterior and dorsal-ventral axis, ipsilateral (5 out of 8) or contralateral (3 out of 8) to CA1 recording site, medial forebrain bundle (MFB, n = 1), supramammillary decussation (SUMX, n = 1) or the mammillary body (MB, n = 1). In two cases, carbachol microinjected into the medial SUM was also ineffective. The sites corresponding to dye microinjections (n=5) were all within medial SUM.

Posterior Hypothalamus (PH)-Supramammillary (SUM) Region

⊕ Dye solution ○ Carbachol (0.0285 mM)

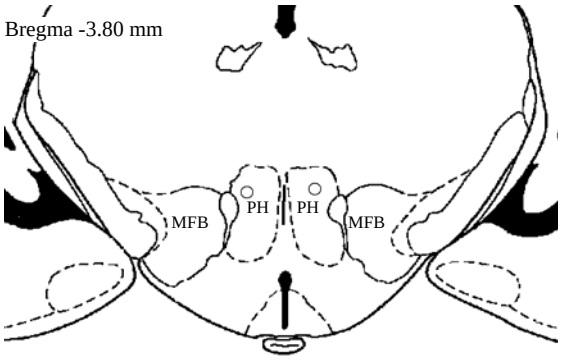

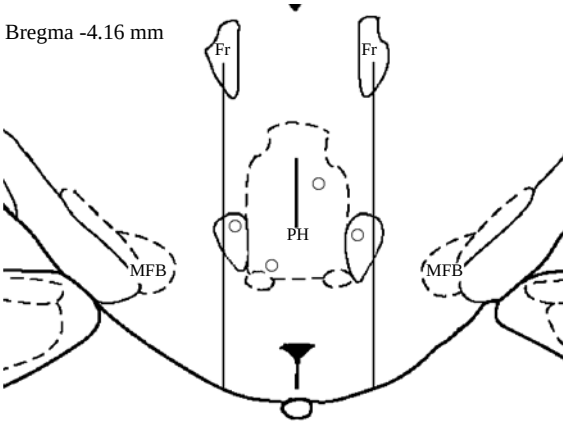

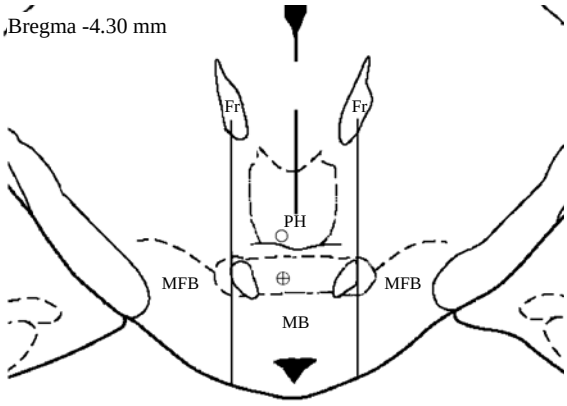

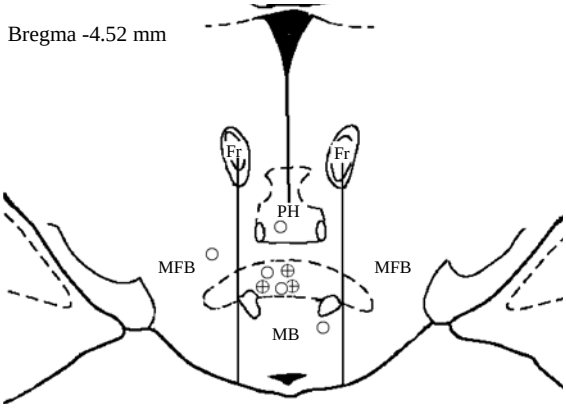

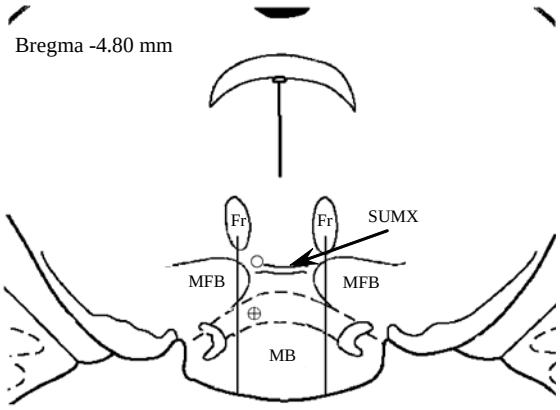

Carbachol Alone

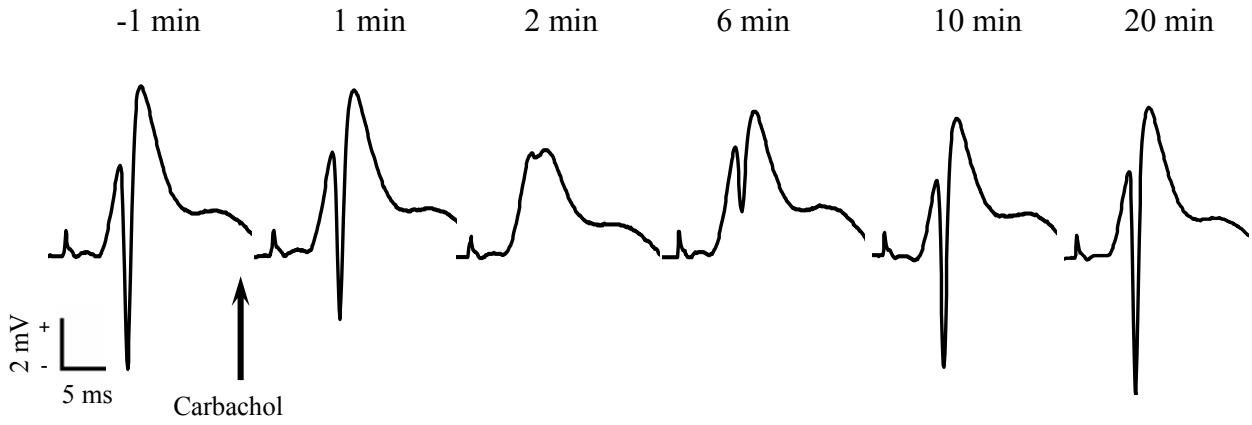

Carbachol and Procaine

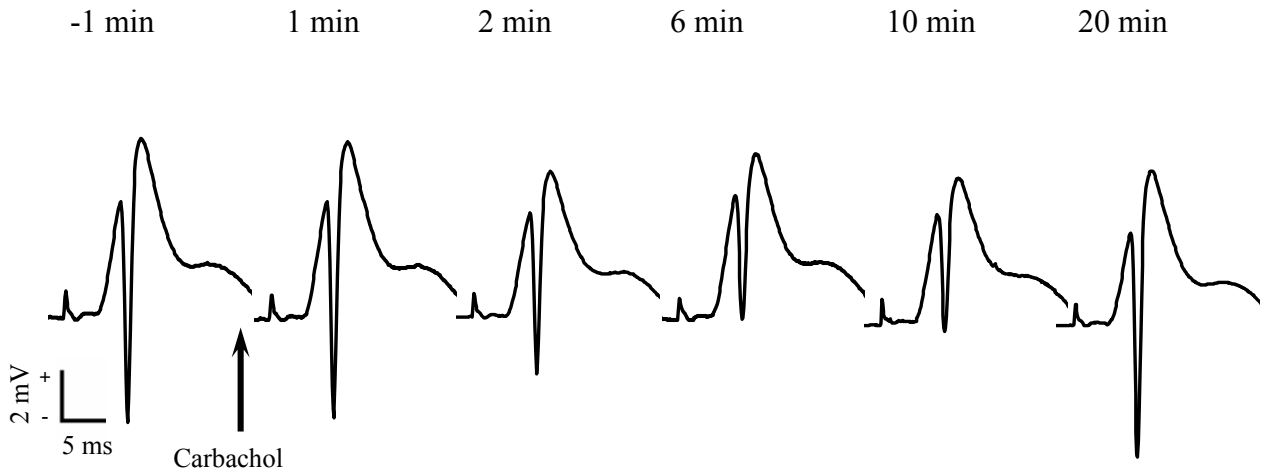

Fig. 3.13: Population spike traces illustrating the carbachol-induced suppression of CA1 pyramidal cell population spike (upper panel) that is attenuated with procaine microinjection (0.5 μl, 20% w/v in 0.01% alcian blue dye solution in saline) into the medial septum-vertical limb of diagonal brand of Broca (MS-VLDBB; see Fig. 3.22) region (lower panel). Carbachol (0.854 mM) microinjection site was localized to the supramammillary region (SUM) medial to fasciculus retroflexus or medial SUM (mSUM; see Fig. 3.11). The agent was microinjected before (top panel) and after procaine (lower panel) in accordance with the protocol described in the legend to Fig. 2.1C. The field CA3 stimulation intensity was adjusted to evoke population spike that was ~70% of maximal. The population spike traces illustrated represent the average population spike size in one-minute blocks at times before (-1 min) or after (1 min to 20 min) carbachol microinjection.

Fig. 3.14: The time course of suppression of CA1 population spike amplitude (upper panel) and theta activation (lower panel) following microinjection of carbachol (0.1µl, 0.0285-, 0.854- or 0.62-mM) into the supramammillary region (SUM; sites illustrated in Fig. 3.11). Carbachol was injected at time 0-min given by the arrow on the x-axis. The protocol followed was illustrated in Fig. 2.1C (upper panel). Control experiments involved microinjection of the dye solution (0.1µl of 0.01% alcian blue dye solution in saline) into the medial SUM (sites illustrated in Fig. 3.12). The control population spike prior to onset of injection was ~70% of maximal. The amplitude of population spike was calculated as explained in Fig. 2.1 and averaged in 1-min blocks. The duration of theta was calculated as time in seconds per 1-min block of electroencephalogram (EEG) for which the EEG displayed rhythmic slow activity at frequency between 3-6 Hz. Each data point in the figure represents mean ± SEM. The error bar is shown one-sided for clear presentation. Notice the robust suppression and theta activation following microinjection of carbachol. A theta activation and delayed suppression of PS (at time points 20 and 40 min after microinjection) was also observed following control microinjection of the dye solution. The theta activation and concomitant population spike suppression following microinjection of saline was observed in 2 of 5 experiments and may reflect 'spontaneous' activation that is observed in urethane anaesthetized and surgically manipulated rat. Significant difference: $p < 0.05$, * vs. -2 and -1 min prior to microinjection of carbachol at concentration of 0.854- or 3.42-mM, @ vs. -2 and -1 min prior to microinjection of carbachol at concentration of 0.0285 mM, # vs. -2 and -1 min prior to microinjection of dye solution.

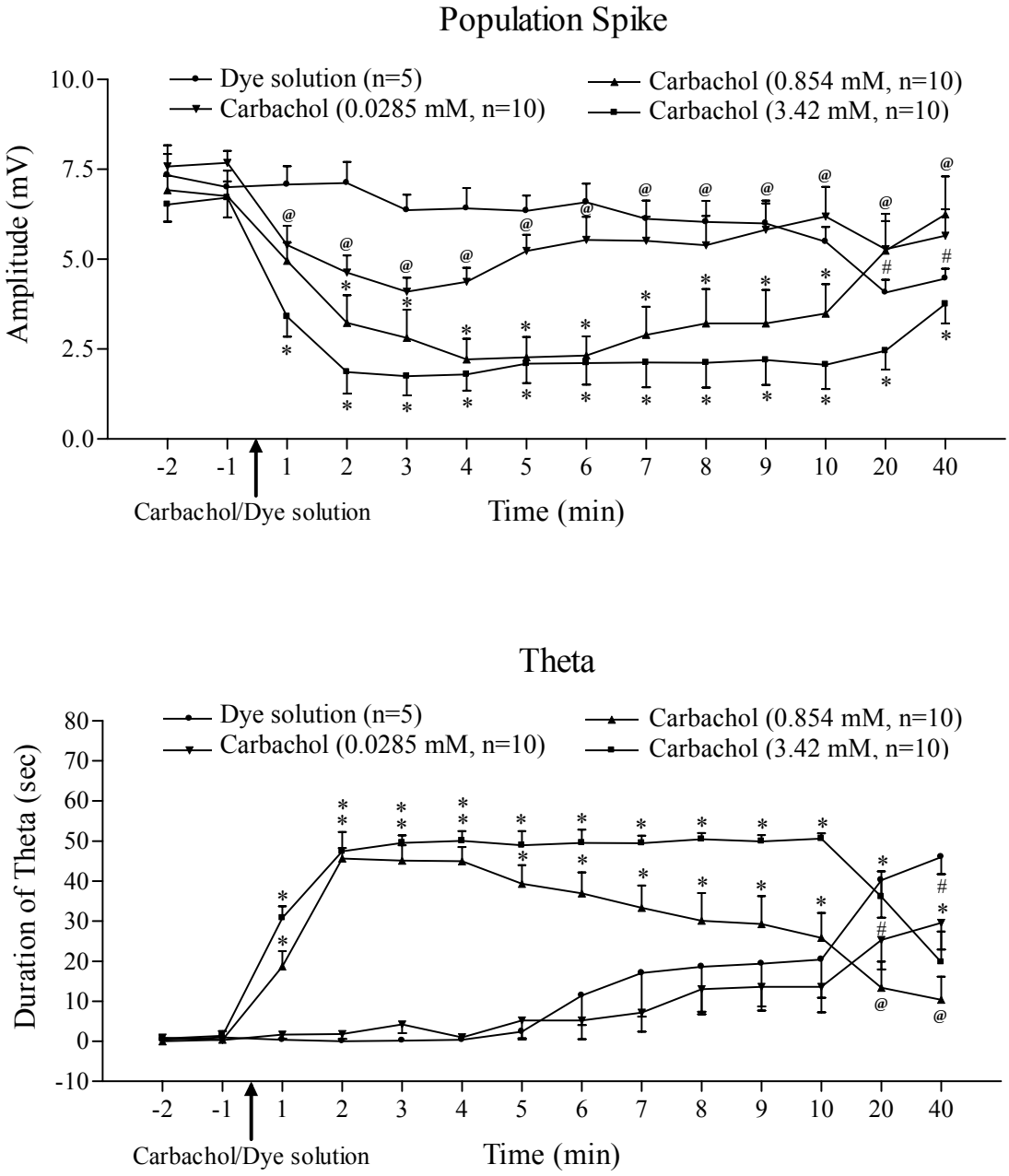
Population Spike
Dye solution (n=5)
Carbachol (0.0285 mM, n=10)
Carbachol (0.854 mM, n=10)
Carbachol (3.42 mM, n=10)
Amplitude (mV)
10.0
7.5
5.0
2.5
0.0
-2
-1
1
2
3
4
5
6
7
8
9
10
20
40
Carbachol/Dye solution
Time (min)
Theta
Dye solution (n=5)
Carbachol (0.0285 mM, n=10)
Carbachol (0.854 mM, n=10)
Carbachol (3.42 mM, n=10)
Duration of Theta (sec)
80
70
60
50
40
30
20
10
0
-10
-2
-1
1
2
3
4
5
6
7
8
9
10
20
40
Carbachol/Dye solution
Time (min)

Fig. 3.15: The peak suppression of population spike (A, left), latency to population spike suppression (A, right), the fast Fourier Transform (FFT) theta peak power (B, left upper panel), theta peak frequency (B, right upper panel) and latency to theta activation (B, lower panel) following microinjection of carbachol (either 0.0285-, 0.854- or 3.42-mM) into the supramammillary (SUM) region (see Fig. 3.11). The peak suppression of CA1 population spike (PS) was calculated using the minimum amplitude of the population spike (i.e. maximal suppression) in 1-min block observed within 5 min after carbachol injection. The maximal suppression was then expressed as % suppression which is the reduction in the amplitude of the population spike at maximal suppression from the control amplitude (the average amplitude in the 2 min before carbachol injection) expressed as percentage of control (control amplitude taken as 100%). The latency to suppression of CA1 population spike was the time (s) measured from onset of carbachol injection to the initiation of sustained suppression of population spike by $\geq$ 20% from the average PS in 2 min before injection. The minimum latency was 10 s which is the interval between 2 successive stimulation applied to CA3 to evoke CA1 PS. The theta peak power (mV^2) and theta peak frequency of electroencephalogram (EEG) was calculated using FFT (frequency resolution: 0.488Hz; frequency range: 3.42-6.35 Hz) performed on theta waves taken from 9-s block of EEG (low pass filtered at 10 Hz) between consecutive CA3 stimulation and averaged for six such blocks to give the value for the minute corresponding to maximal suppression of the population spike. Latency to theta was defined by measuring the time (s) of onset of sustained theta following carbachol microinjection. FFT calculations were not performed for carbachol at concentration of 0.0285-mM, since theta activation was not observed during peak suppression. Each bar in histogram represents mean ± SEM. Notice the carbachol concentration-dependent effect on the peak suppression. The latency to suppression did not differ. Further, theta activation (theta peak power, theta peak frequency and latency to theta, B) induced by the two higher concentrations of carbachol were similar. Significant difference: $p < 0.05$, * vs. peak suppression with carbachol concentration of 0.0285-mM.

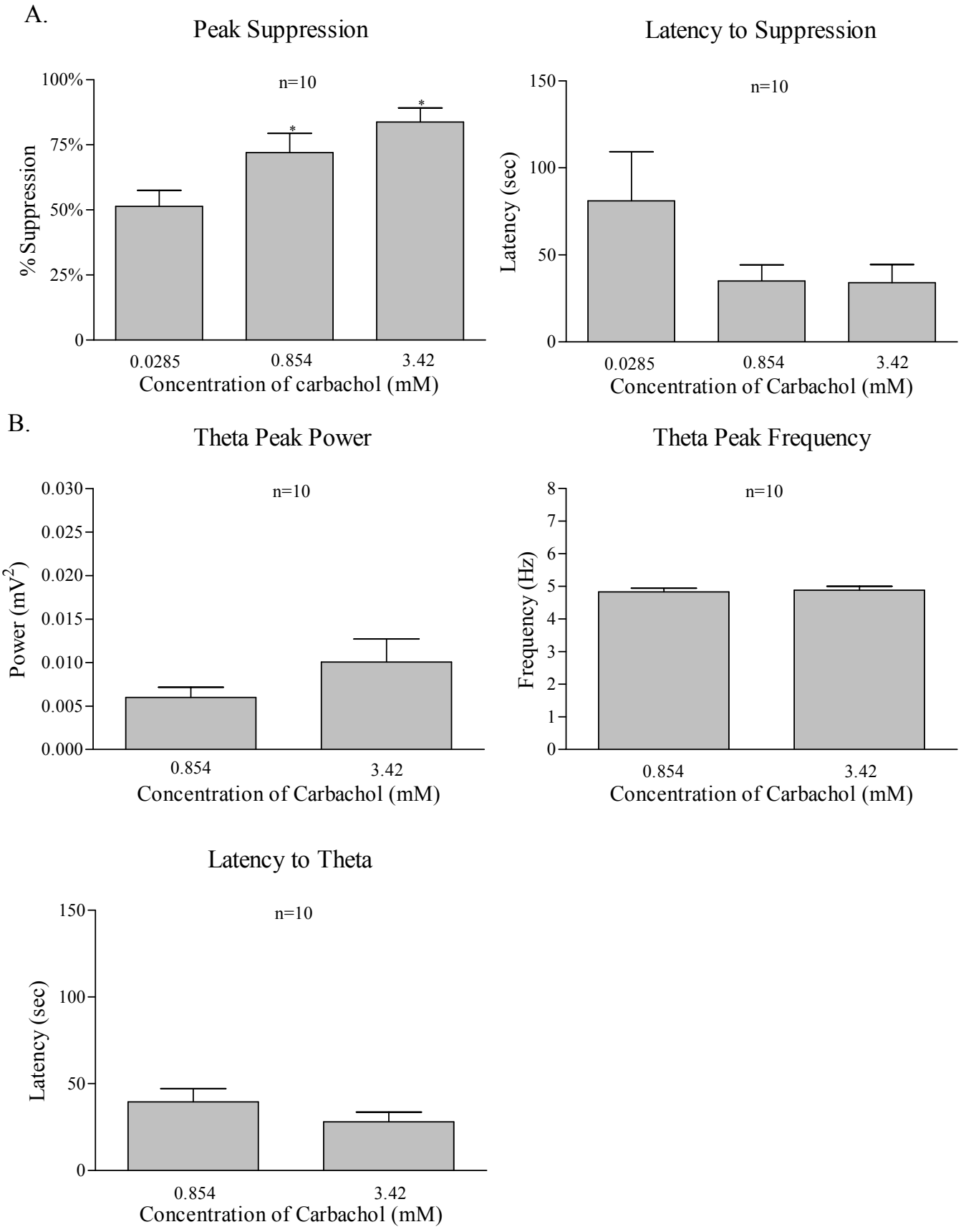
A.
Peak Suppression
n=10
100%
75%
50%
25%
0
% Suppression
*
*
0.0285
0.854
3.42
Concentration of carbachol (mM)
Latency to Suppression
n=10
150
100
50
0
Latency (sec)
0.0285
0.854
3.42
Concentration of Carbachol (mM)
B.
Theta Peak Power
n=10
0.030
0.025
0.020
0.015
0.010
0.005
0.000
Power (mV2)
0.854
3.42
Concentration of Carbachol (mM)
Theta Peak Frequency
n=10
8
7
6
5
4
3
2
1
0
Frequency (Hz)
0.854
3.42
Concentration of Carbachol (mM)
Latency to Theta
n=10
150
100
50
0
Latency (sec)
0.854
3.42
Concentration of Carbachol (mM)

$p < 0.02$, n=10, Fig. 3.15). The mean peak suppression at the two higher concentrations was not different from each other. The latency to suppression at the three concentrations was not different (Concentration, $F_{2, 27}=1.85$, $p > 0.1$, n=10, Fig. 3.15). The suppression of population spike with carbachol was accompanied by decrease in slope of the sfEPSP at the two higher concentrations. The average slopes of sfEPSP in the two minutes before carbachol injection vs. slopes at mean peak suppression of population spike following microinjection of carbachol at concentration of 0.0285-, 0.854- or 3.42-mM were 1.30 ± 0.13 mV/ms vs. 1.24 ± 0.12 mV/ms (two-tail paired T-test, $p > 0.4$), 1.69 ± 0.19 mV/ms vs. 1.40 ± 0.13 mV/ms (two-tail paired T-test, $p < 0.002$, Fig. 3.16A) and 1.13 ± 0.21 mV/ms vs. 0.90 ± 0.15 mV/ms (two-tail paired T-test, $p < 0.009$).

In 10 of the above experiments, following investigations into the effect of microinjection of 0.854 mM of carbachol on ~70% population spike including the investigation of the effect of MS-VLDBB procaine on carbachol-induced suppression (see subsection 3.2.5), the effect of microinjection was monitored on ~25% population spike. Carbachol microinjection also suppressed ~25% population spike (two-tail paired T-test, $p < 0.002$; Fig. 3.16B; mean peak suppression 80.81 ± 6.79%, n = 10). Like with ~70% PS, the mean peak suppression of ~25% population spike were accompanied by decrease in the slope of corresponding sfEPSP (two-tail paired T-test, $p < 0.005$, Fig. 3.16B).

The effective carbachol injection sites in SUM that evoked suppression were mostly in mSUM (all sites at the two higher concentrations and 3 sites at the lowest concentration; Fig. 3.11) with 7 microinjection sites at the lowest concentration localized to the lSUM (Fig.3.11).

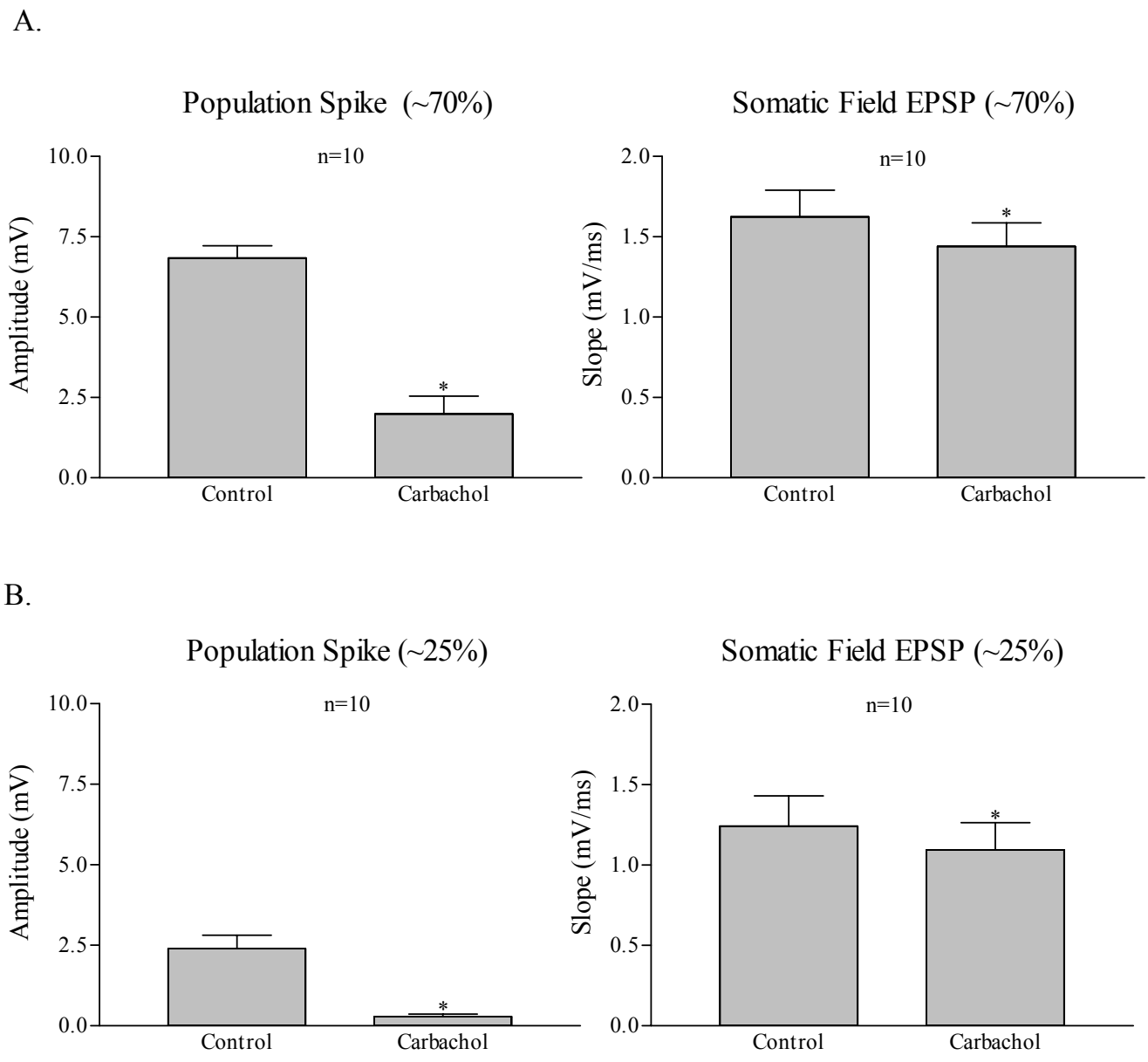

Fig. 3.16: The effect of microinjection of carbachol (0.854 mM) in supramammillary region on somatic field excitatory postsynaptic potentials (sfEPSP) of ~ 70% (A, right) and ~25% (B, right) of maximal and the amplitude of the corresponding population spike (PS; A and B, left). The protocol followed was explained in Fig. 2.1C. Each bar in histogram represents mean ± SEM. The control values are the average PS amplitude and the slope of corresponding sfEPSP in the 2 min prior to carbachol microinjection. The carbachol values are the average PS amplitude and the slope of sfEPSP in 1-min period corresponding to the peak of carbachol effect observed within 5 min following microinjection. Notice that carbachol injection reduced both the population spike amplitude and the corresponding sfEPSP. Significant difference: $p < 0.05$, * vs. control.

Control experiments involved microinjection of 0.01% (w/v) alcian blue dye-saline solution (0.1 μl). All the microinjection sites were in mSUM (n = 5; Fig. 3.12). Unlike carbachol, microinjection of the dye solution did not evoke an immediate effect on the ~70% population spike (Fig. 3.14). Rather a much delayed suppression was observed at 20^{th} and 40^{th} min following microinjection (Time, $F_{13, 57} = 6.87$, $p < 0.0001$, n=5; Fig. 3.14). Individually, the suppression was observed in 2 of 5 experiments, and was accompanied by the appearance of late theta (see the subsection 3.2.3).

In addition to SUM, microinjections of 0.0285 mM of carbachol into SUMX immediately dorsal to mSUM (n = 1; Fig. 3.11), MFB close to lSUM (n = 1; Fig. 3.11), MB near ventral edge of SUM (n = 1; Fig. 3.11) and in PH (n = 3, ipsilateral; Fig. 3.11) evoked a suppression of the ~70% population spike. The suppression observed with microinjection at the above sites was within 5 min of injection and was to the criterion (Time, $F_{13, 70}=3.97$, $p < 0.0001$, n = 6; Fig. 3.19). The latency to suppression for the group was 131.7 ± 28.06 s (PH = 74-214 s, SUMX = 27 s, MB = 173 s, MFB = 144 s). Other microinjection sites in PH (n = 8, 5 ipsilateral and 3 contralateral; Fig. 3.12) and sites in MFB (n=1; Fig. 3.12), SUMX (n=1; Fig. 3.12) and MB (n = 1; Fig. 3.12) that were relatively more dorsal or ventral from SUM than the above comparative sites were without effect (Time, $F_{13, 140}=0.70$, $p > 0.8$, n = 11; Fig. 3.20).

3.2.2 Spatial analysis of effect of carbachol microinjection on CA1 pyramidal cell excitability

Microinjection of the lower concentration of carbachol (0.0285 mM) into the mSUM failed to evoke a significant suppression (Time, $F_{13, 85} = 1.07$, $p > 0.05$, n = 5; Fig. 3.18).

Fig. 3.17: Comparable effect of carbachol (0.854- and 3.42-mM) microinjected into ipsilateral vs. contralateral medial supramammillary region (mSUM; Fig. 3.11) on peak suppression of population spike (A, left), latency to population spike suppression (A, right), the fast Fourier Transform (FFT) theta peak power (B, left upper panel), theta peak frequency (B, right upper panel) and latency to theta activation (B, lower panel). Microinjection into the mSUM was either ipsilateral or contralateral to the recording site. Details as in Fig. 3.15. Each bar in histogram represents mean ± SEM.

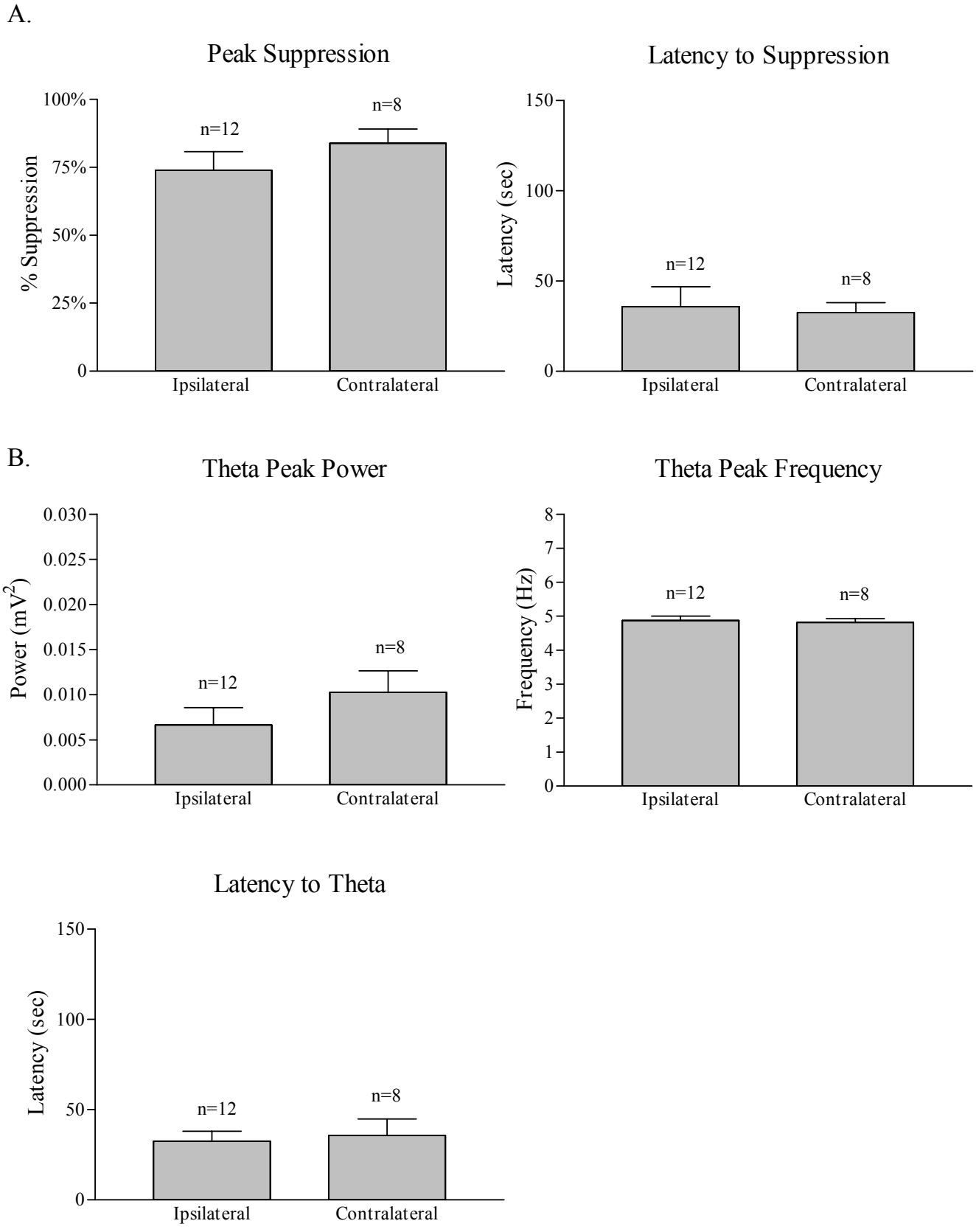
A.
Peak Suppression
% Suppression
100%
75%
50%
25%
0
n=12
n=8
Ipsilateral
Contralateral
Latency to Suppression
Latency (sec)
150
100
50
0
n=12
n=8
Ipsilateral
Contralateral
B.
Theta Peak Power
Power (mV2)
0.030
0.025
0.020
0.015
0.010
0.005
0.000
n=12
n=8
Ipsilateral
Contralateral
Theta Peak Frequency
Frequency (Hz)
8
7
6
5
4
3
2
1
0
n=12
n=8
Ipsilateral
Contralateral
Latency to Theta
Latency (sec)
150
100
50
0
n=12
n=8
Ipsilateral
Contralateral

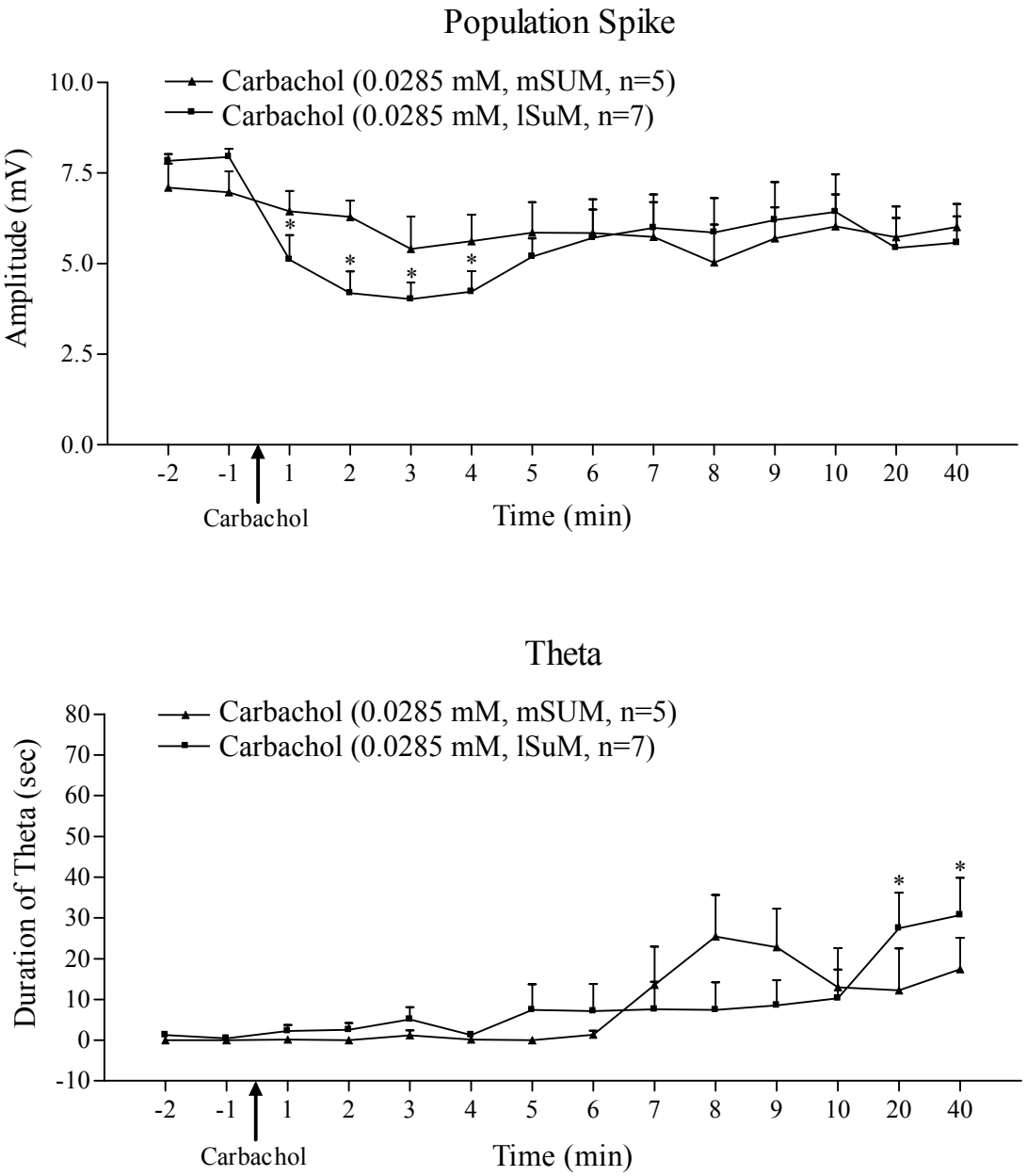

Fig. 3.18: The time course of CA1 population spike amplitude (upper panel) and theta activation (lower panel) following microinjection of carbachol (0.1 µl of 0.0285 mM) into the medial supramammillary (mSUM) region (n=5; sites illustrated in Figs. 3.11 and 3.12) or the lateral supramammillary region (lSUM; n=7, Fig. 3.11). The plots were built as explained for Fig. 3.14. Notice that overall, significant suppression was obtained with lateral but not medial microinjections. Little or no theta activation was observed during the period of suppression with lateral microinjections. The late theta activation seen in the lSUM group may reflect 'spontaneous theta'. Significant differences: $p \leq 0.05$, * vs. -2 and -1 min prior to carbachol injection.

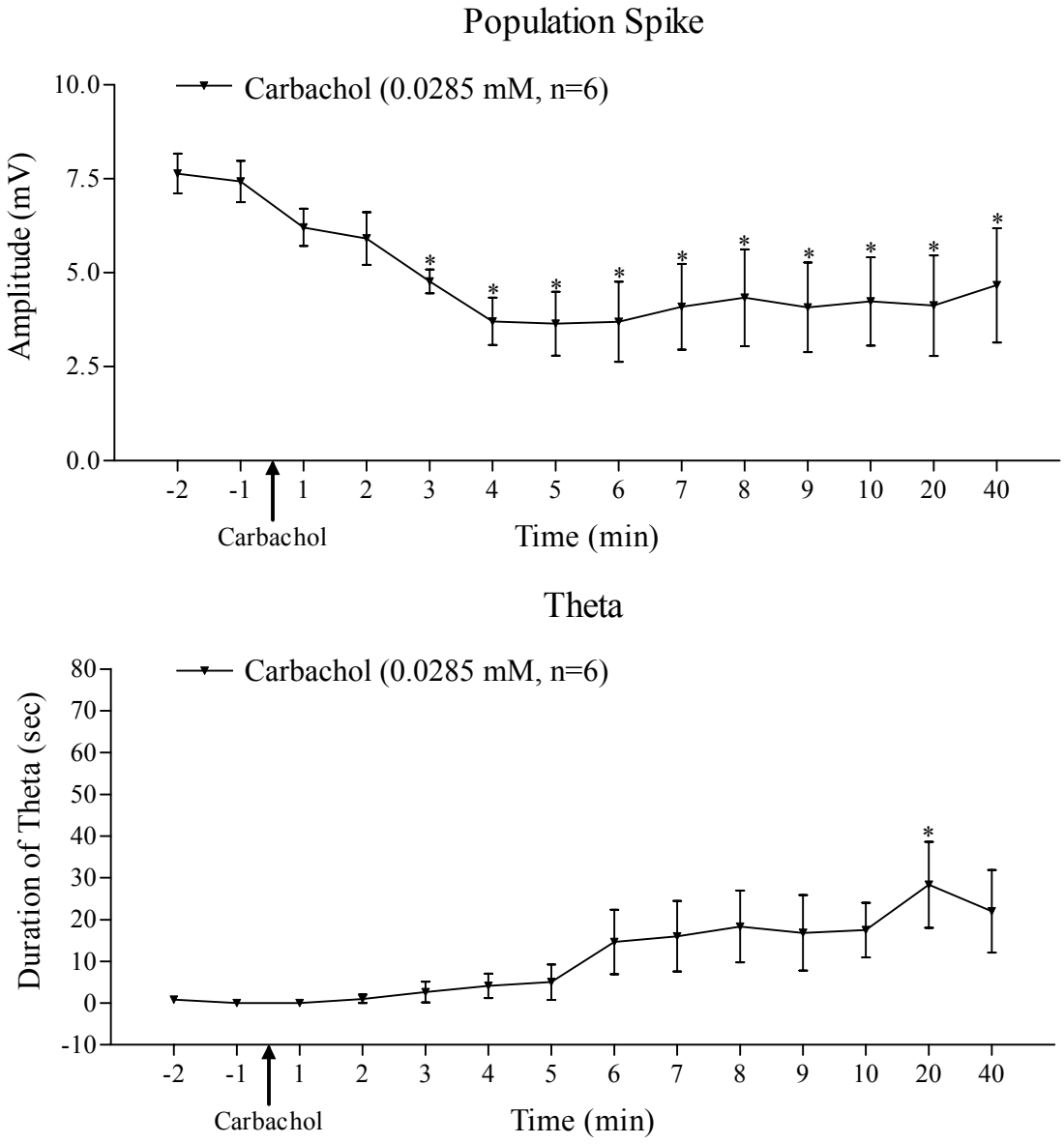

Fig. 3.19: The time course of suppression of CA1 population spike amplitude (upper panel) and theta activation (lower panel) following microinjection of carbachol (0.0285 mM) into posterior hypothalamus, supramammillary decussation, mammillary body and the medial forebrain bundle. The plots were developed as explained for Fig. 3.14. Data are mean ± SEM. The data represented are from sites where microinjection evoked suppression of the population spike to criterion (> 20% decrease from the control amplitude prior to microinjection) which was observed within 5 min of microinjection (Fig. 3.11). Theta activation, although observed, did not parallel suppression and was observed relatively late in time. Robust Theta activation was observed in 3 of 6 cases. Significant difference: $p < 0.05$, * vs. -2 and -1 min prior to carbachol microinjection.

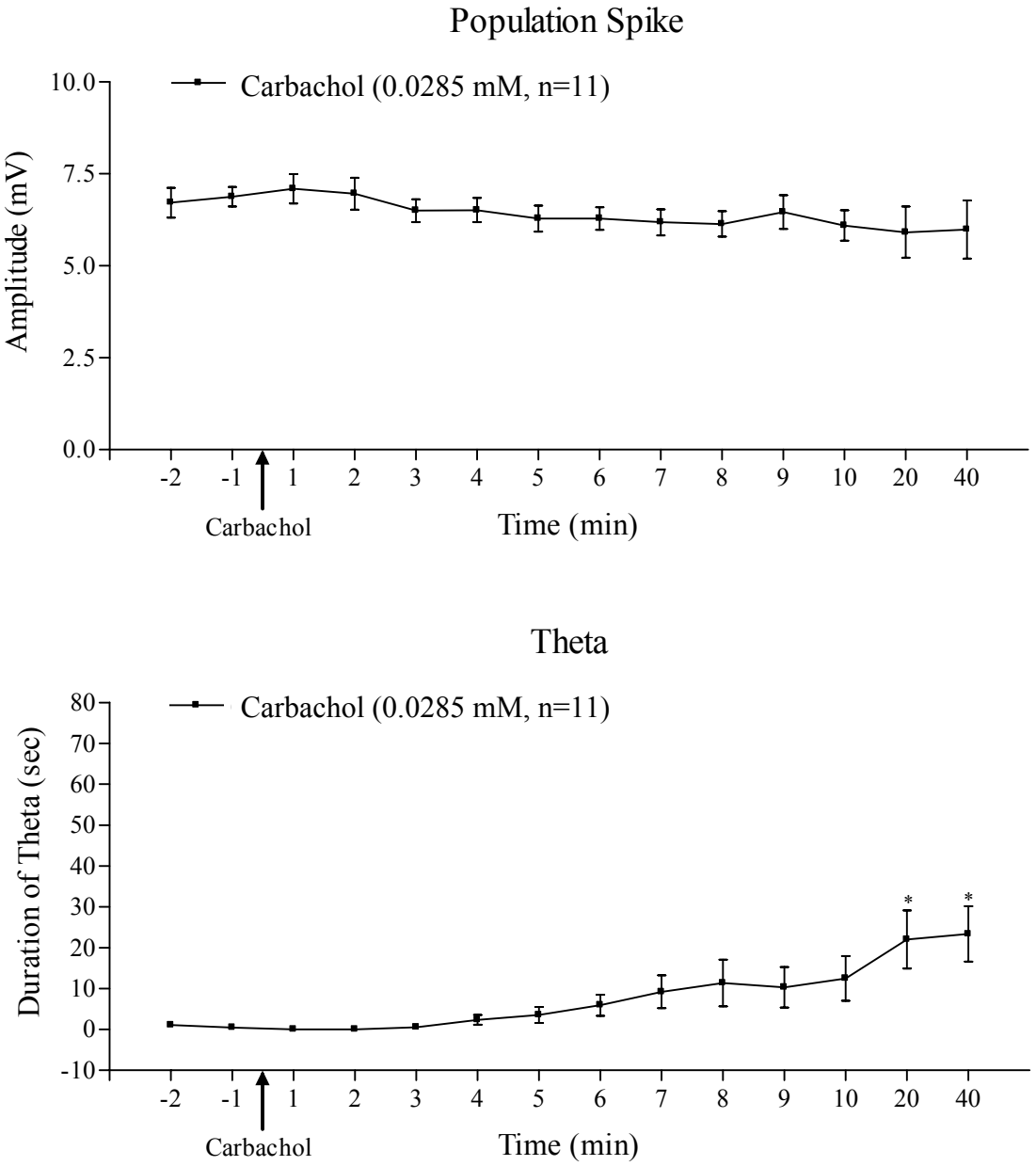

Fig. 3.20: The time course of population spike amplitude (upper panel) and theta activation (lower panel) from experiments where microinjection of carbachol (0.1 µl, 0.0285 mM) was ineffective in suppressing population spike amplitude to the criterion of > 20% decrease from the control amplitude prior to microinjection. These microinjection sites were localized in posterior hypothalamus, medial forebrain bundle, supramammillary decussation, and mammillary body (see Fig. 3.12). The plot is built as explained for Fig. 3.14. Data are mean ± SEM. Delayed theta activation was observed in the group. Significant difference: $p < 0.05$, * vs. -2 and -1 min prior to carbachol microinjection.

Whereas microinjection into lSUM evoked an immediate and robust suppression (Time, $F_{13, 85} = 4.11$, $p < 0.0001$, n = 7) that was significant to at least 4 min after injection (Fig. 3.18). In this group, the mean peak suppression and latency to suppression was 54.43 ± 6.63% and 27.14 ± 4.74 s, respectively. Individually, suppression was observed from 3 of 5 and 7 of 7 sites in the mSUM and lSUM, respectively. However, the latency to suppression in the 2 of 3 sites in mSUM was > 200 s whereas the latency to suppression was less than 80 s for all sites in lSUM (range 10-80 s). A short latency effect (120 s) was observed from the remaining site in mSUM which, however, was close to the principal mammillary tract near the lSUM (Fig. 3.11).

The microinjection sites in the SUM from where the two higher concentrations of carbachol evoked suppression of CA1 population spike were distributed both ipsilateral (n = 12, 5 at concentration of 0.854 mM and 7 at concentration of 3.42 mM) and contralateral (n = 8, 5 at concentration of 0.854 mM and 3 at concentration of 3.42 mM) to the recording site. Given that the effect on suppression with the two higher concentrations of carbachol were similar (noted in the above subsection), the ipsilateral and contralateral injection sites were grouped irrespective of the concentration. Analyses revealed that both the mean peak suppression and the latency to suppression were similar in the ipsilateral vs. contralateral group (two-tail unpaired T-test, $p > 0.3$; two-tail unpaired T-test, $p > 0.8$; Fig. 3.17A).

The following is spread of mean peak suppression, when the effective sites at the two higher concentrations were grouped into medial (<0.5 mm from midline, n = 16, ipsilateral = 9, contralateral = 7) vs. lateral (> 0.5 mm from midline, n =4, ipsilateral = 3,

contralateral = 1) sites. The values for mean peak suppression for the lateral site contralateral to recording side was 92% (n = 1, carbachol concentration of 3.42 mM). The mean peak suppression from medial sites, contralateral to recording side was 82.86 ± 5.92% (n = 7; n = 5 at carbachol concentration of 0.854 mM with mean peak suppression = 83.60 ± 8.5%; n = 2 at carbachol concentration of 3.42 mM with mean peak suppression = 81%). The mean peak suppression from medial sites, ipsilateral to recording side was 66.11 ± 7.50% (n = 9; n = 5 at carbachol concentration of 0.854 mM with mean peak suppression = 60.60 ± 10.38%; n = 4 at carbachol concentration of 3.42 mM with mean peak suppression = 73.0 ± 11.37%; two-tail unpaired t-test indicated that suppression at the two concentrations was not different from each other, $p > 0.4$). The mean peak suppression from lateral sites, ipsilateral to recording side was 97.0 ± 1.53% (n=3, all at carbachol concentration of 3.42 mM). Overall, the values for mean peak suppression for the medial vs. lateral sites was 73.4 % ± 5.23% vs. 95.72 % ± 1.57 % (two-tail unpaired T-test, $p < 0.05$) while the corresponding values for latency to suppression were 37.50 ± 8.39 s vs. 22.5 ± 2.50 s (two-tail unpaired T-test, $p > 0.3$). The mean suppression between medial sites for carbachol concentration of 0.854 mM vs. 3.42 mM were not different from each other (72.06 ± 7.38%, n = 10 vs. 75.63 ± 7.37%, n = 6, two-tail unpaired T-test, $p > 0.7$).

3.2.3 Relationship of carbachol-elicited suppression to generation of theta

Microinjection of 0.854- and 3.42-mM of carbachol into SUM also generated theta waves concomitant with the suppression of the CA1 population spike (Time, $F_{13,}$

$_{126}$=18.97, $p < 0.0001$, n = 10; and Time, $F_{13, 126}$=30.54, $p < 0.0001$, n = 10; Fig. 3.14). The FFT theta peak power and the FFT peak frequency of theta waves at the peak suppression of the population spike observed with the two higher concentrations was similar (two-tail unpaired T-test, $p > 0.05$; Fig. 3.15B). The latency to onset of theta was also comparable at the two higher concentrations (two-tail unpaired T-test, $p > 0.05$) and was similar to the latency to suppression (Fig.3.15B). However, little or no theta activation was observed in the first 5 min following microinjection of the lower dose (0.0285 mM) though some theta activity was observed later in time (Fig. 3.14). Individually, in this group, the relatively late robust theta activation was observed in 6 of 10 experiments. At the peak of carbachol-induced suppression, no theta wave activity was apparent at dose of 0.0285 mM.

The suppression of the population spike with 0.0285 mM of carbachol from effective sites in PH, SUMX, MFB and MB was also not in parallel with theta activation (Fig. 3.19).

In experiments where carbachol (0.0285 mM) microinjection, at sites in PH, SUMX, MFB and MB, did not evoke suppression also did not elicit an immediate theta activity, though late theta activation was observed at 20 and 40 min after microinjection ($F_{13, 140}$=5.47, $p < 0.0001$, n = 10; Fig. 3.20). Individually the delayed theta activation was observed in 7 of 11 experiments.

Finally, late theta activation was also observed following injection of the dye solution,

especially at 20 and 40 min post-microinjection ($F_{13, 56}$=7.76, $p < 0.0001$, n =5; Fig. 3.14). The delayed theta activation that appears with microinjection of dye follows the pattern that is observed following microinjection of 0.0285 mM of carbachol. This suggests that the late responses with carbachol may reflect, at least in part, the 'spontaneous' theta observed under the present experimental conditions involving urethane anaesthesia, surgical manipulation and microinjection. Generally, a decrease in population spike amplitude is observed in correlation with robust 'spontaneous' theta activation in anaesthetized rat and this might explain the late decrease in amplitude observed with microinjection of the dye solution and carbachol (0.0285 mM) in the SUM region (Fig. 3.14).

3.2.4 Comparison of strength of suppression evoked with microinjection of carbachol vs. reticular stimulation

In order to compare the strength of maximal suppression evoked with reticular stimulation vs. microinjection of carbachol, the following comparisons was made: mean peak suppression evoked with T and T+1 volt RPO stimulation vs. mean peak suppression evoked upon microinjection of 0.854- and 3.42-mM carbachol into mSUM. The mean peak suppression at T volt RPO stimulation was grouped with that observed with T+1 volt stimulation since these were not different from each other (see subsection 3.1.1). Likewise the mean peak suppression observed following microinjection of carbachol at concentration of 0.854 mM was grouped with that observed following microinjection of carbachol at concentration of 3.42 mM (see subsection 3.2.1). Comparisons indicated that the maximal suppression evoked with RPO stimulation at T and T+1 volt stimulation was significantly less vs. that evoked with the higher

concentrations of carbachol (mean peak suppression of 61.73 ± 3.30%, n = 14 vs. 77.91 ± 4.65%, n = 20; two-tail unpaired T-test, $p < 0.02$; Fig. 3.21). On the other hand, the mean theta peak frequency, theta peak power evoked with T + 1 volt RPO stimulation, but not T volt stimulation, was stronger than that induced following microinjection of 0.854- and 3.42-mM of carbachol ($F_{3, 30}=7.35$, $P < 0.0009$; $F_{3, 30}=4.82$, $P < 0.008$). In this analysis the values at T volt and T+1 volt RPO stimulation were not combined since these were different from each other (see subsection 3.1.2). The values obtained following microinjection of the two concentrations of carbachol (see subsection 3.2.3) was also not grouped together.

3.2.5 Effect of microinjection of procaine in the MS-VLDBB region on carbachol-induced suppression

The procaine microinjection sites are illustrated in Fig. 3.22. In 6 experiments the microinjection site was in the MS-VLDBB region, midline or ipsilateral to the recording side. In another 3 experiments the microinjection was lateral to the MS-VLDBB region, ipsilateral (n =2) or contralateral (n = 1) to the recording side.

The effect of procaine microinjected in the MS-VLDBB region on carbachol-induced population spike suppression is illustrated in Fig. 3.23. The protocol used in these experiments is as described in Fig. 2.1C. Briefly, after monitoring the effect of the first microinjection of 0.854 mM of carbachol into the SUM region (control in Fig. 3.23), the carbachol microinjection was repeated 5 minutes (post-procaine 5 min in Fig. 3.23) and about 1 hour (post-procaine 1hr in Fig. 3.23) after microinjection of the local anaesthetic

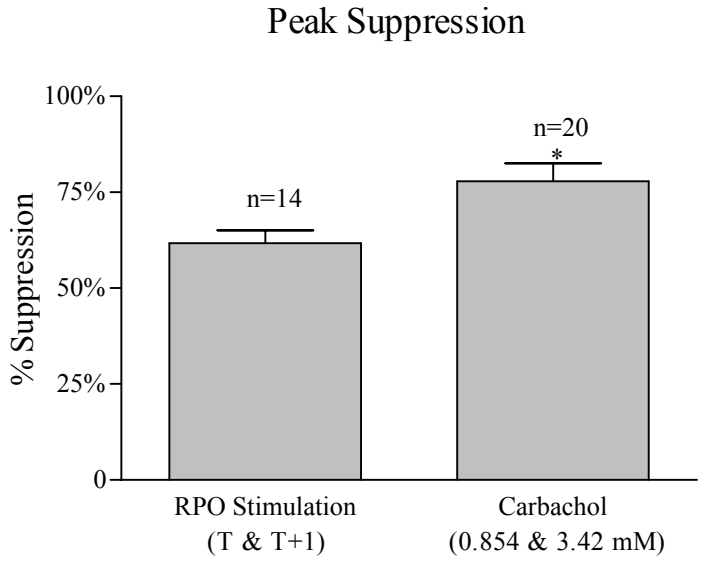

Fig. 3.21: Comparison of the reticularly-elicited vs. carbachol-induced suppression of population spike. The peak suppression evoked at T volt and T+1 volt reticular (region of reticular nucleus pontis oralis or RPO) stimulation were grouped together and compared with the peak suppression observed with carbachol at concentration of 0.854- and 3.42-mM microinjected into the medial supramammillary region. Data are mean ± SEM. Notice that significantly greater suppression was obtained with carbachol microinjections. Significant difference: $p < 0.05$, * vs. RPO stimulation.

Medial Septum-Vertical Limb of the Diagonal Band of Broca (MS-VLDBB)

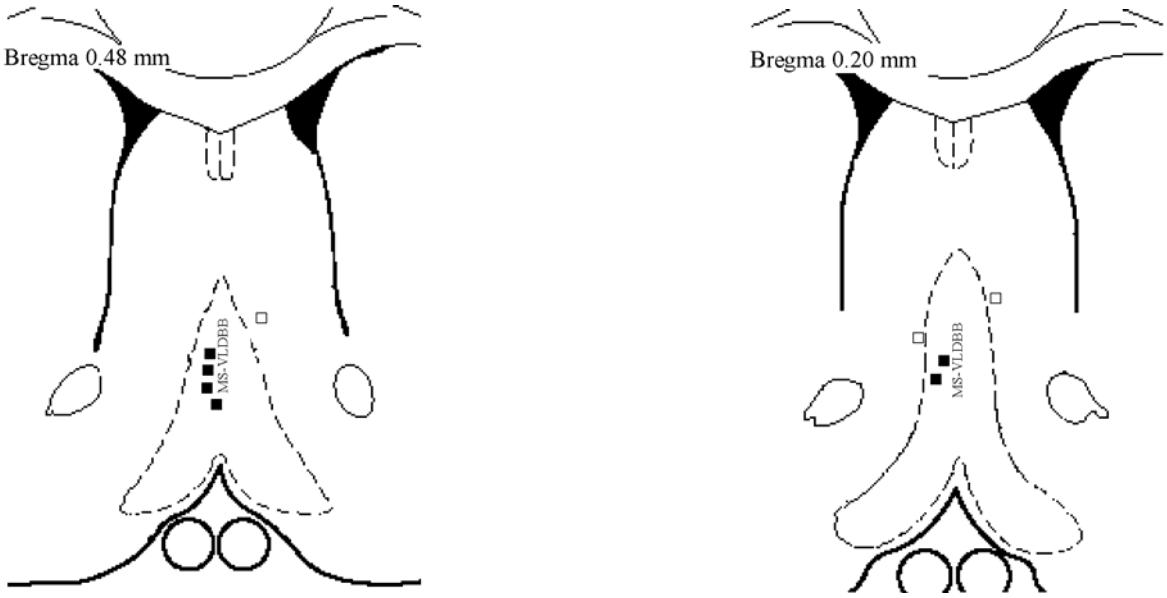

Fig. 3.22: Diagrammatic representation of procaine microinjection (0.5 µl, 20% w/v in 0.01% alcian blue dye solution in saline) sites in the medial septum-vertical limb of the diagonal band of Broca (MS-VLDBB) region. The coronal sections represented are adapted from Paxinos and Watson (1982). The filled squares within the MS-VLDBB region indicate the sites (n = 6) where procaine microinjection attenuated the suppression of CA1 population spike induced upon microinjection of carbachol (0.854 mM) into the medial supramammillary region (mSUM). The procaine microinjection sites within the MS-VLDBB region were either ipsilateral to the CA1 recording side or around midline. The open squares indicate sites outside the MS-VLDBB region where procaine microinjection was without significant effect on mSUM carbachol-induced suppression of CA1 population spike.

Fig. 3.23: A. The time course of the effect of procaine (0.5 μl, 20% w/v) microinjected into the medial septum-vertical limb of the diagonal band of Broca (MS-VLDBB) region (see Fig. 3.22) on carbachol (0.1 μl, 0.854 mM)-induced population spike suppression (upper panel) and theta activation (lower panel). Carbachol was injected into medial supramammillary region (see Fig. 3.11). The protocol is as explained in Fig. 2.1C. The plots are built as explained in Fig. 3.14. Data are mean ± SEM. The control plot represents the values obtained following carbachol microinjection prior to procaine administration into the MS-VLDBB region. The post-procaine 5 min and post-procaine 1 hr plots represents the changes observed when carbachol microinjection was repeated 5 min and 1hr after microinjection of procaine into MS-VLDBB region, respectively. B. Reversible attenuation by MS-VLDBB procaine of carbachol-induced population spike suppression (Peak Suppression; left) and the corresponding theta peak power (Theta Peak Power; right) by MS-VLDBB region procaine. The histograms are built as explained for Fig. 3.15. Data are mean ± SEM. Carbachol was microinjected as explained for A. Significant theta activation was not observed when carbachol was microinjected 5 min after procaine and thus the theta peak power for this microinjection is not illustrated. Significant differences: $p < 0.05$, * vs. –2 and –1 min prior to carbachol microinjection before or 5 min post-procaine in A or vs. control in B; @ vs. -2 and -1 min prior to microinjection of carbachol at 1 hr post-procaine in A; # vs. 5 min post-procaine in B.

A.

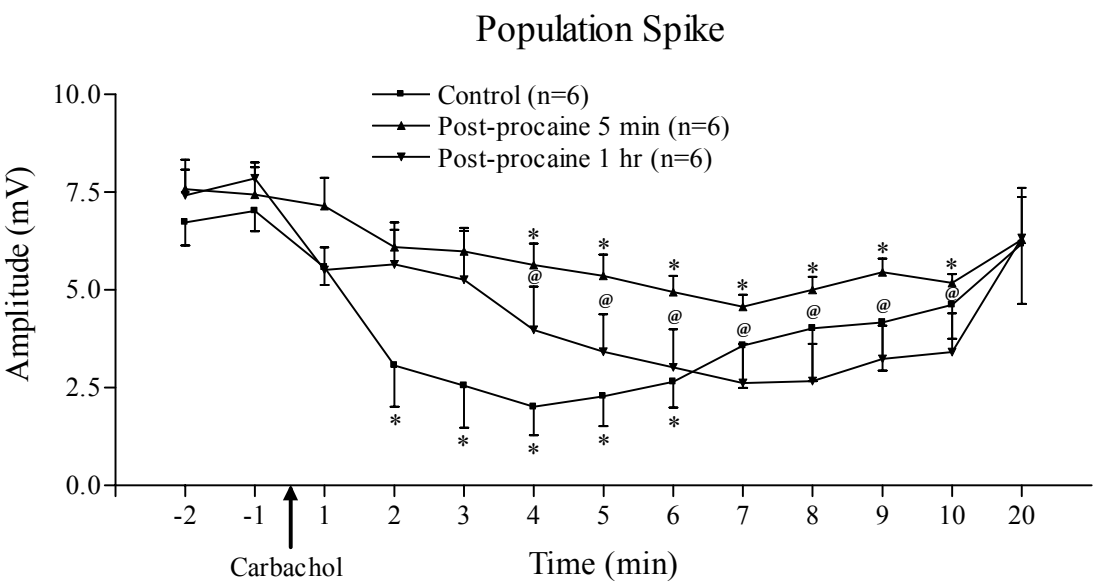
Population Spike
Control (n=6)
Post-procaine 5 min (n=6)
Post-procaine 1 hr (n=6)
Amplitude (mV)
10.0
7.5
5.0
2.5
0.0
-2
-1
1
2
3
4
5
6
7
8
9
10
20
Carbachol
Time (min)

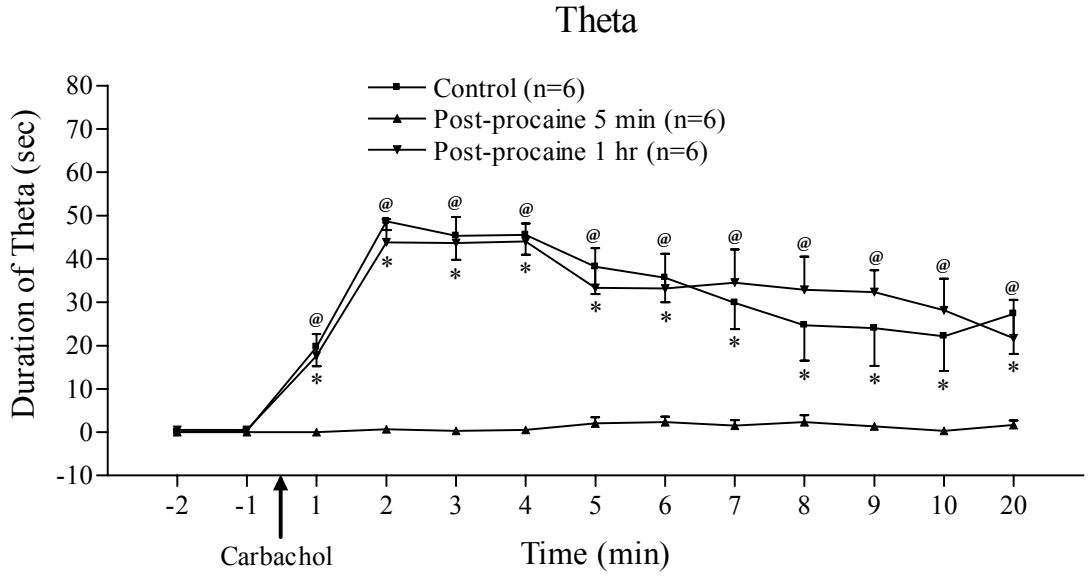
Theta
Control (n=6)
Post-procaine 5 min (n=6)
Post-procaine 1 hr (n=6)
Duration of Theta (sec)
80
70
60
50
40
30
20
10
0
-10
-2
-1
1
2
3
4
5
6
7
8
9
10
20
Carbachol
Time (min)

B.

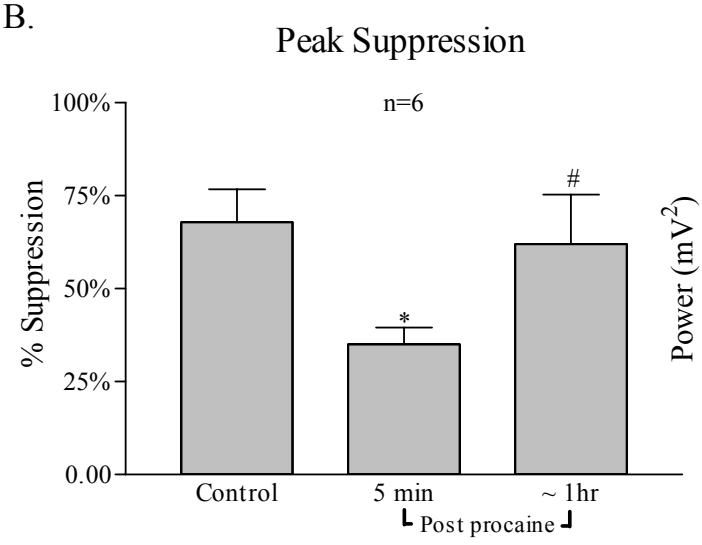
Peak Suppression
n=6
% Suppression
100%
75%
50%
25%
0.00
Control
5 min
~ 1hr
Post procaine

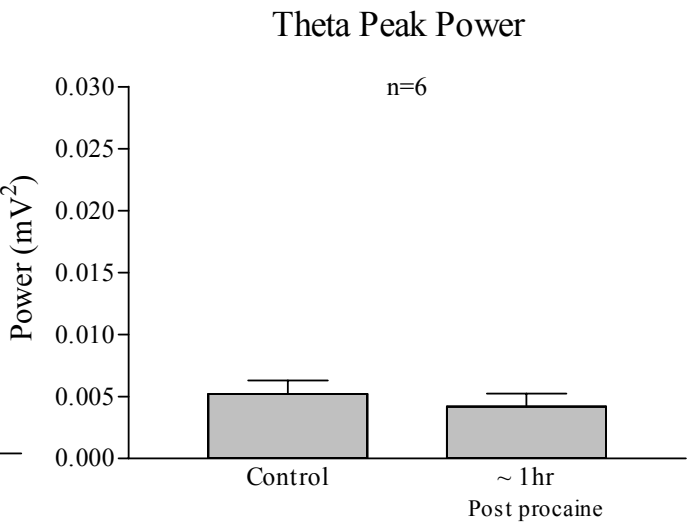
Theta Peak Power
n=6
Power (mV2)
0.030
0.025
0.020
0.015
0.010
0.005
0.000
Control
~ 1hr
Post procaine

procaine (0.5 µl, 20% w/v in 0.01% alcian blue dye solution in saline). The effect of carbachol was continually monitored for 10 min after each microinjection and at least an additional 1min from 19-20 min post injection.

Microinjection of carbachol, before (control) or 5 min after procaine (post-procaine 5 min) evoked a suppression of the population spike (Time, $F_{12, 65} = 10.19$, $p < 0.0001$, n = 6, control; Time, $F_{12, 65} = 12.3$, $p < 0.0001$, n = 6, post procaine 5 min; Fig. 3.23A). However, compared to the control mean peak suppression (67.85 ± 8.88%; Fig. 3.23B), the carbachol induced mean peak suppression was attenuated post-procaine 5 min (35.08 ± 4.45%; Fig. 3.23B) that had recovered towards control when the drug was microinjected around 1 hour after procaine (post-procaine 1 hr; Time, $F_{2, 15} = 4.73$, $p < 0.04$, n = 6; Fig. 3.23B). The average PS amplitude in 2 min before carbachol in the control situation (6.88 ± 0.54 mV), 5 min (7.51 ± 0.79 mV) and ~1 hr after procaine (7.64 ± 0.64 mV) were not different from each other (Concentration, $F_{2, 15}=0.61$, $P > 0.5$, n=6).

The attenuation of suppression by procaine was accompanied by a strong attenuation of theta activation that was otherwise induced on microinjection of carbachol into the SUM (Time, $F_{2, 15} = 33.84$, $p < 0.001$, control; Time, $F_{2, 15}=1.34$, $p > 0.05$, post-procaine 5min; Fig. 3.23). Recovery of theta was observed with microinjection of carbachol post-procaine 1 hr (Time, $F_{12, 65}=9.41$, $p < 0.0001$; Fig. 3.23)

In two experiments out of the three with procaine microinjected into the sites outside of MS-VLDBB region (Fig. 3.22), administration of procaine did not attenuate carbachol-induced suppression. In the remaining experiment procaine was injected in the region

just outside of the border of the MS-VLDBB region. Such procaine microinjection did attenuate suppression but only for brief period. The group data is illustrated in Fig. 3.24 that indicates a robust suppression of population spike following carbachol microinjection before (Time, $F_{11, 24}=4.37$, $p < 0.002$) and after procaine (Time, $F_{11, 24}=36.17$, $p < 0.0001$). In the group, carbachol induced theta activation before (Time, $F_{11, 24}=26.28$, $p < 0.0001$) and after (Time, $F_{11, 24}=5.12$, $p < 0.0006$) procaine. However, theta activation was apparently reduced with carbachol microinjection after procaine.

3.2.6 Effects of atropine on carbachol vs. pinch-induced suppression and theta activation

In four of 10 experiments that involved microinjection of carbachol (0.854 mM) into the SUM, investigations were carried out to determine whether carbachol-induced effects were sensitive to antagonism by the cholinergic muscarinic-receptor antagonist atropine. These experiments were carried out after the investigations with reversible inactivation of MS-VLDBB region with procaine and subsequent investigation of effect of SUM carbachol on ~25% population spike. For the experiments with atropine, the PS amplitude was ~70% of maximal and, as before, the various manipulations were performed against the background of at least 2 min of irregular EEG. About one hour after the last carbachol injection atropine was administered intraperitoneally. Mild pinch to the tail was applied around 5 min before and 15 and 30 min after atropine. Carbachol (0.854 mM) was microinjected into mSUM 20 and 35 min after atropine administration. Comparable mean peak suppression ($F_{2, 9}=2.81$, $p > 0.1$; Fig. 3.25A), theta peak power ($F_{2, 9}=2.76$, $p > 0.1$; Fig. 3.25A) and theta peak frequency ($F_{2, 9}=0.72$, $p > 0.5$; Fig. 3.25A) were observed with pinch before and after atropine. Similarly, the mean peak

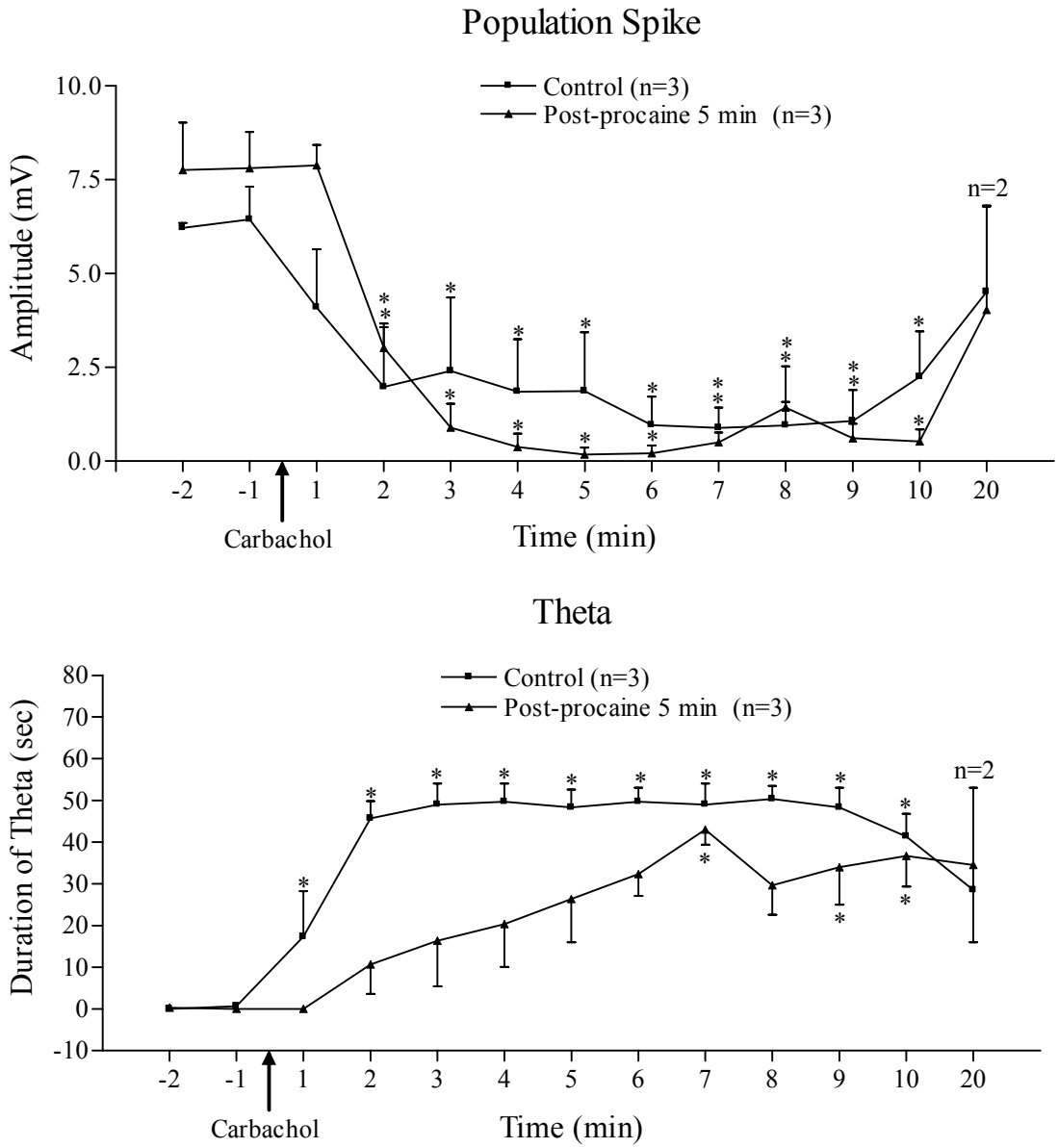

Fig. 3.24: Lack of effect of procaine microinjected outside the medial septum-vertical limb of diagonal band of Broca region on carbachol-induced suppression of population spike (upper panel). However, decreased theta activation was observed with carbachol microinjection following procaine administration (lower panel). The figure is built as explained for Fig. 3.14. Data are mean ± SEM. Carbachol was microinjected as explained in Fig.3.23. Significant differences: $p < 0.05$, * vs. –2 and –1 min prior to carbachol microinjection.

Fig. 3.25: Atropine attenuated carbachol- (B, on right) but not tail pinch-induced (A, on left) population spike suppression (Peak Suppression) and theta activation (Theta Peak Power and Theta Peak Frequency). In these experiments, atropine was administered intraperitoneally (i.p.) at dose of 5 mg/kg. Light pinch was applied to the distal 1-cm end of the tail either before, 15 min or 30 min following atropine. The tail was pinched using forceps for 5 s at similar intensity each time. Carbachol (0.1 µl, 0.854 mM) was microinjected into medial supramammillary region 5 min later following each pinch. The histogram bars were built as explained for Fig. 3.15. Data are mean ± SEM. The % suppression of population spike was calculated from the suppression observed in the minute following pinch or from the maximal suppression observed within 5 min of carbachol microinjection before (control) or 20 and 35 min after atropine administration. The fast Fourier Transform (FFT) analysis was performed on theta waves in the minute following pinch and in the 1-min block corresponding to peak suppression following carbachol microinjection. The FFT data for carbachol microinjected 35 min after atropine is not illustrated since at this stage clear theta was observed in only one of four experiments following microinjection. Significant differences: $p < 0.05$, * vs. control.

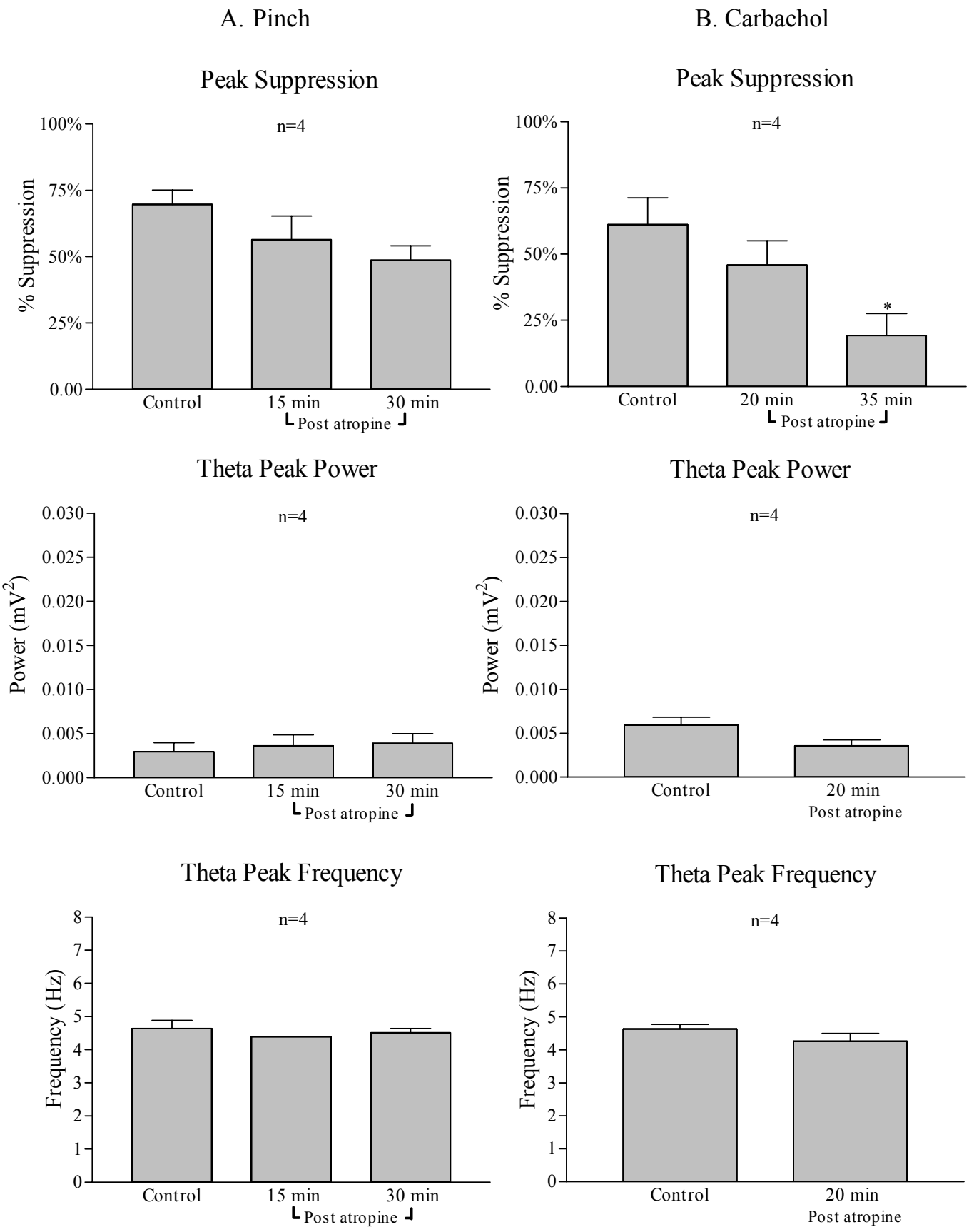
A. Pinch
B. Carbachol
Peak Suppression
n=4
100%
75%
50%
25%
0.00
% Suppression
Control
15 min
30 min
20 min
35 min
Post atropine
*
Theta Peak Power
0.030
0.025
0.020
0.015
0.010
0.005
0.000
Power (mV2)
Theta Peak Frequency
8
7
6
5
4
3
2
1
0
Frequency (Hz)

suppression observed with carbachol microinjection 20 min following atropine was comparable to that observed with the first carbachol (control) early in the experiment (Fig. 3.25B). The theta peak power and frequency was also not different from that observed with the first carbachol microinjection (two-tail paired T-test, $p > 0.05$; Fig. 3.25B). However, the suppression of PS was attenuated when carbachol was microinjected 35 min after atropine (Time, $F_{2, 9}=5.36$, $p < 0.05$; Fig. 3.25B). Furthermore, theta activation was not observed in 3 out of 4 experiments.

CHAPTER IV DISCUSSION

4.1 Findings of present study

The objectives of present study were as follows: (1) investigate the effect of RPO stimulation on CA1 synaptic excitability, (2) investigate whether RPO-elicited changes in CA1 synaptic excitability involved neural components in SUM and MS-VLDBB regions. The latter two regions include components of the ascending theta-synchronizing pathway from RPO, and (3) explore the effect of direct chemical stimulation of PH-SUM region with microinjection of carbachol on CA1 pyramidal cell excitability and determine whether such PH-SUM stimulation-induced changes involve the MS-VLDBB region. The sensitivity of carbachol-induced changes to antagonism by the cholinergic-muscarinic antagonist, atropine, was also investigated and compared with that evoked upon tail pinch.

Data from the study demonstrated that RPO stimulation induced suppression of CA1 pyramidal cell population spike that was accompanied by decrease in the slope of sfEPSP and the dfEPSP. Furthermore, the RPO-stimulation induced suppression was attenuated by microinjection of the local anaesthetic procaine either into SUM or MS-VLDBB region or with the injection of the inhibitory ligand gamma aminobutyric acid (GABA) into the SUM region. Direct chemical stimulation of the PH-SUM region, especially the SUM region, with local microinjection of carbachol also suppressed CA1 population spike and the corresponding sfEPSP. The carbachol-induced suppression was reversibly antagonized by microinjection of procaine into the MS-VLDBB region. The carbachol-induced suppression was generally observed at short latency following microinjection with maximal suppression within 5 min of microinjection. Further, the suppression of population spike and the corresponding sfEPSP was carbachol

concentration-dependent and was attenuated by systemic administration of atropine in dose (5 mg/kg, i.p.) that did not affect tail pinch elicited suppression, suggesting a selective attenuation by atropine of carbachol effect.-

4.2 Stimulation intensity-dependent effect of RPO stimulation on CA1 pyramidal cell excitability

With respect to the influence of RPO stimulation on CA1 synaptic responses, the results show that both brief (non-theta generating) and relatively prolonged (theta generating) stimulation in the RPO evoked a decrease in the amplitude of the CA1 population spike when it was initially set to ~25% or ~70% of the maximal amplitude. That the prolonged stimulation was more effective in evoking suppression of the ~70% population spike suggests that such stimulation evoked a greater recruitment of the neural substrate(s) underlying suppression. Further investigation indicated that the suppression is stimulation intensity-dependent and can be accompanied by a decrease in the slope of the sfEPSP and dfEPSP. The population spike amplitude and the dfEPSP recovered to control levels in the minute after stopping reticular stimulation, indicating that a long-term decrease in pyramidal cell excitability is not evoked with this protocol.

Interestingly, the reticularly-elicited decrease in the slope of the sfEPSP was dependent upon the basal amplitude of the population spike such that a small but significant decrease was observed in the slope of the sfEPSP when this was initially set to ~25%, but not when it was set to ~70% of the maximal population spike. The differences in the effect on the sfEPSP might simply reflect the relative ability of the given reticular drive to influence the strength of the excitatory CA3 afferent drive underlying the submaximal

(~25%) and near maximal (~70%) population responses. Indeed, Leung and Au (1994) reported that the plot representing the slope of dfEPSP vs. CA3 stimulus intensity had a significantly higher rise rate in the lower than in the upper half. This indicates that a given small change in CA3 afferent drive evokes a greater change in submaximal than near maximal dfEPSP. Accordingly, at CA3 stimulation intensities that evoked a nearer maximal (~70%) population spike, small changes in sfEPSP with reticular stimulation might be obscured in comparison with the effect of reticular influence on submaximal sfEPSP of ~25% population spike. The suppression of the ~25% population spike with a corresponding decrease in the sfEPSP and also a decrease in the slope of the dfEPSP indicates that suppression of CA1 pyramidal cell excitability with RPO stimulation is, at least partly, linked to a suppression of synaptic transmission.

Although not evaluated systemically, RPO stimulation at T-1 volt might also suppress large slow wave activity (see Fig.3.1) which is suggested to be generated intrinsically by hippocampus (Leung et al., 1982; Leung, 1998). The suppression of such activity by reticular stimulation is reminiscent of diminishing of the amplitude of the EEG in the hippocampus during awakening of an animal from sleep (Leung et al., 1982; Leung, 1998).

While in the present study reticular stimulation elicited suppression of synaptic transmission across apical dendrites of CA1 pyramidal cells, the evoked effect might vary with synapse in the hippocampus. For example, reticular stimulation elicited facilitation of granule cell population spike evoked by stimulation of perforant pathway (Winson, 1981). On speculative note, the effect of reticular stimulation on synaptic transmission at basal dendrites of CA1 pyramidal cells might also be different from the

effect observed at apical dendrites of CA1 pyramidal neurons. Indeed, the synaptic transmission at basal dendrites is affected differently by conditions that decrease synaptic excitation across the apical dendrites. In this regard, while transmission at apical synapse was reduced in parallel with theta generation during walking as compared to that during immobility, the basal dendrite fEPSP was not significantly affected and basal dendritic population spike was enhanced (Leung, 1980).

4.3 SUM and MS-VLDBB regions mediate suppression of CA1 excitability

The present evidence indicates that neural elements that are juxtaposed, at least in part, to the ascending synchronizing pathway in SUM and MS-VLDBB region mediate suppression of CA1 excitability. This is suggested by the following lines of evidences. One, microinjection of procaine in the MFB region, in and around lateral SUM and medial SUM and MS-VLDBB reversibly attenuated RPO elicited suppression and theta in a coincident fashion. Indeed, procaine microinjected into the ipsilateral MFB-SUM and MS-VLDBB regions attenuated both RPO theta activation and population spike suppression, while microinjections dorsal to ipsilateral MFB-SUM region (around Fr) and in contralateral area in and around SUM region that did not attenuate theta, also did not affect the suppression of CA1 synaptic response.

The effects of procaine microinjection in the MFB region and medial SUM on theta generation were similar to that reported previously with such microinjections (Kirk and McNaughton, 1993; Thinschmidt et al., 1995). In this context, microinjections of procaine in the MFB region (and also lateral SUM) sites reduced the reticularly elicited

theta amplitude but not the frequency prior to the loss of theta, whereas microinjection in medial SUM reduced frequency prior to loss of theta. Here, it is notable that the effect of procaine in MFB on amplitude is linked to reduction in the number of afferents carrying information from PH-medial SUM to MS-VLDBB region, while the effect on frequency with medial SUM procaine is suggested to be due to the action of the agent on reticular inputs to the region (Kirk and McNaughton, 1993).

Two, GABA microinjected into the PH-SUM region produced effects on both the RPO elicited theta and suppression that might be ascribed to a relatively selective action of the agent on synaptic transmission in the region. In addition, the effect of GABA points to the medial SUM as a region in the posterior hypothalamus that contributes to RPO elicited suppression. In the above context, microinjection of GABA (unlike procaine) in and around MFB or in the supramammillary decussation that contain predominantly fibres of passage did not affect theta generation and population spike suppression. On the other hand, GABA microinjection into the medial SUM region attenuated both RPO elicited theta and population spike suppression.

The effect of medial SUM GABA on RPO elicited theta was marked by an initial decrease in amplitude, but not frequency, which was followed by loss of theta. The latter is expected because synapses in the PH-medial SUM region are suggested to contribute to theta generation, including with reticular stimulation in anaesthetized rat (Kirk and McNaughton, 1993; Oddie et al., 1994; Bland et al., 1994; McNaughton et al., 1995; Bland and Oddie, 1998; Kirk, 1998). Interestingly, McNaughton et al. (1995) in their study of the role of synapses in medial SUM reported that such microinjection of a benzodiazepine decreased the frequency of reticularly elicited theta. This contrasts with

the present findings that theta frequency is not affected with microinjection of GABA into the medial SUM. The different outcomes between the present and the previous report (McNaughton et al., 1995) might be linked to the different neural effects of the microinjected agents. For example, benzodiazepines act at the benzodiazepine-GABA-chloride ionophore complex to enhance the effects of endogenously released GABA. Thus, the reduction in theta frequency with application of benzodiazepine might be because the agent increased the duration of phasic inhibition impinging on theta generating circuits by prolonging the effects of endogenous GABA. On the other hand, the effects of exogenous GABA in the present study represent continuous-tonic inhibition. This would be expected to reduce the overall population response but not the duration of rhythmic inhibition of the theta generating circuit in the medial SUM. As a consequence, the theta amplitude, but not theta frequency, is affected.

Three, an effect of SUM region procaine and GABA on population spike suppression and theta generation was observed with ipsilateral, but not contralateral injections. This is consistent with the evidence that the relay from this region to the MS-VLDBB is predominantly ipsilateral (Vertes, 1992; Leranth and Kiss, 1996; Borhegyi et al., 1998; Kiss et al., 2000; Vertes and McKenna, 2000).

Four, direct chemical activation of SUM with carbachol elicited a suppression of CA1 excitability that was evoked in parallel with theta activation with the two higher concentrations of the drug. The carbachol-induced suppression was attenuated by reversible inactivation of the MS-VLDBB region with microinjection of procaine.

4.4 Distinct neural elements modulate the suppression vs. theta activation

Despite the above evidence for close anatomical proximity, different lines of evidence from the study suggest that suppression of population spike amplitude involves at least some distinct neurons from those controlling theta generation. In this regards, (1) suppression of CA1 synaptic excitability could be evoked upon RPO stimulation in the absence of dominant extracellular theta rhythmic activity; (2) the population spike suppression reached its maximum at an RPO stimulation voltage that was only at the threshold for theta and was not increased further with increases in voltage that did increase the frequency and amplitude of theta waves; (3) carbachol microinjection at the lowest concentration in lateral SUM region evoked robust suppression without concomitant theta activation; (4) the maximal suppression evoked with higher concentrations of carbachol was greater than the maximal suppression evoked on RPO stimulation. However, the frequency and power of theta on T+1 volt RPO stimulation was significantly greater than that evoked at maximal suppression with the higher concentrations of carbachol. The dissociation of the suppression of population spike and theta generation is also in line with published data in behaving rat (Leung and Vanderwolf, 1980). These authors reported that systemic administration of atropine attenuated suppression of fEPSP and population spike but not theta rhythm observed during animal exploratory behavior.

The time course of the effects of microinjection on RPO elicited responses provides similar evidence. The effects of medial SUM GABA and MFB-SUM region procaine on PS suppression by RPO stimulation both preceded the loss of theta rhythm. Likewise,

microinjection of procaine into MS-VLDBB, especially in the lateral regions, attenuated suppression with no apparent loss of theta. Further, while the onset of effect of MS-VLDBB procaine on suppression paralleled the decrease in amplitude of RPO elicited theta, the population spike suppression recovered to control even though the amplitude of theta remained strongly reduced. Additionally, the recovery of suppression of PS from drug microinjection in the medial SUM region, which was fully monitored in experiments with microinjection of GABA, preceded the recovery of theta amplitude. Indeed, the population spike suppression recovered to levels recorded prior to microinjection while the amplitude of theta remained suppressed at levels observed with onset of effect of GABA. If suppression of pyramidal cell excitability and generation of theta amplitude depended on the same neurons, then the time course of the recovery should have been the same.

Likewise, the strength of effect of MS-VLDBB procaine on SUM carbachol induced suppression and theta activation was also not in parallel. In this context, MS-VLDBB procaine partially reduced SUM carbachol-induced suppression while evoking a loss of theta that was otherwise observed in parallel with suppression on microinjection of the higher concentration of carbachol.

Furthermore, the effect of microinjection of GABA on RPO elicited suppression was observed from relatively fewer sites as compared to the effect of the agent on theta activation. In this context, microinjections into the lateral SUM region and lateral-ventral sites in PH did not effect suppression although the RPO elicited theta amplitude was reduced. This raises the possibility that a relatively limited population of neurons from the PH-SUM region contributes to the reticular stimulation-evoked suppression in

anaesthetized rat. The lack of effect of GABA at lateral sites in SUM contrasts with the effects of procaine and suggests that cell bodies of neurons in SUM that mediate RPO elicited suppression are located medially and send their axons laterally to join the MFB.

4.5 Cholinergic mechanisms in SUM mediate CA1 suppression

The findings that carbachol evoked concentration-dependent suppression of CA1 population spike that was antagonized by atropine suggest that cholinergic-muscarinic mechanisms in SUM trigger suppression of CA1 synaptic excitability. The suppression of population spike was accompanied by decrease in the slope of the corresponding sfEPSP suggesting, at least partly, suppression in CA3-CA1 synaptic transmission. The identity of neurons in SUM region that might be cholinoceptive and underlie the suppression is not clear. However, the marked potency of lSUM microinjection of the lowest carbachol concentration in eliciting suppression at relatively short latency suggests that a critical population of neurons is positioned laterally in the SUM region, which is consistent with the anatomical evidence of a relatively strong projection from the region to MS-VLDBB (Vertes, 1988; Leranth and Kiss, 1996; Borhegyi et al., 1998; Kiss et al., 2000). With the lower concentration of carbachol, medial injections, as whole, were ineffective in contrast to lateral injections. Individually, in some instances medial injection evoked suppression. However, the suppression was observed at very long-latencies or if the microinjection site was close to the lateral SUM region. The relatively long-latency effect with medial carbachol suggests delayed recruitment of neurons following diffusion of drug over relatively larger area. Perhaps, the density of neural elements that subserve carbachol suppression is relatively low in the mSUM region. Indeed, tracer studies indicate a gradient in the projection to MS-VLDBB from

SUM that increases from medial to lateral regions (Vertes, 1992; Leranth and Kiss, 1996; Borhegyi et al., 1998; Kiss et al., 2000; Vertes and Mckenna; 2000).

While the relatively lateral microinjections of carbachol in mSUM at the higher concentrations evoked a greater suppression than the relatively medial microinjections at those concentrations, overall the effective sites were distributed throughout the medial-lateral extent of the SUM. Robust suppression at comparable short latencies was observed, including from the most lateral of the contralateral site. The above is consistent with the notion that with microinjection of the higher concentrations into the SUM significant amount of carbachol diffused rapidly and perhaps, bilaterally in the SUM region to affect the neural population in the region. A bilateral diffusion is suggested because unilateral spread of the drug only on the side of microinjection does not explain the robust suppression observed with contralateral carbachol, given that the MS-VLDBB projection from the SUM is predominantly ipsilateral (Vertes, 1992; Leranth and Kiss, 1996; Borhegyi et al., 1998; Kiss et al., 2000; Vertes and Mckenna, 2000; also see subsection 4.3). The recruitment of SUM mechanism with the higher concentration of carbachol was more extensive than with RPO because the mean peak suppression elicited with carbachol microinjection was significantly greater than that evoked on RPO stimulation.

The pattern of selective recruitment of SUM mechanisms to elicit CA1 suppression in anaesthetized rat suggests that neural mechanisms in SUM that mediate CA1 pyramidal cell suppression are organized, at least in part, in modules of which RPO region stimulation selectively recruited a module in mSUM region while carbachol influenced a lateral module with greater potency (Fig. 4.1). Whether a medial module is recruited

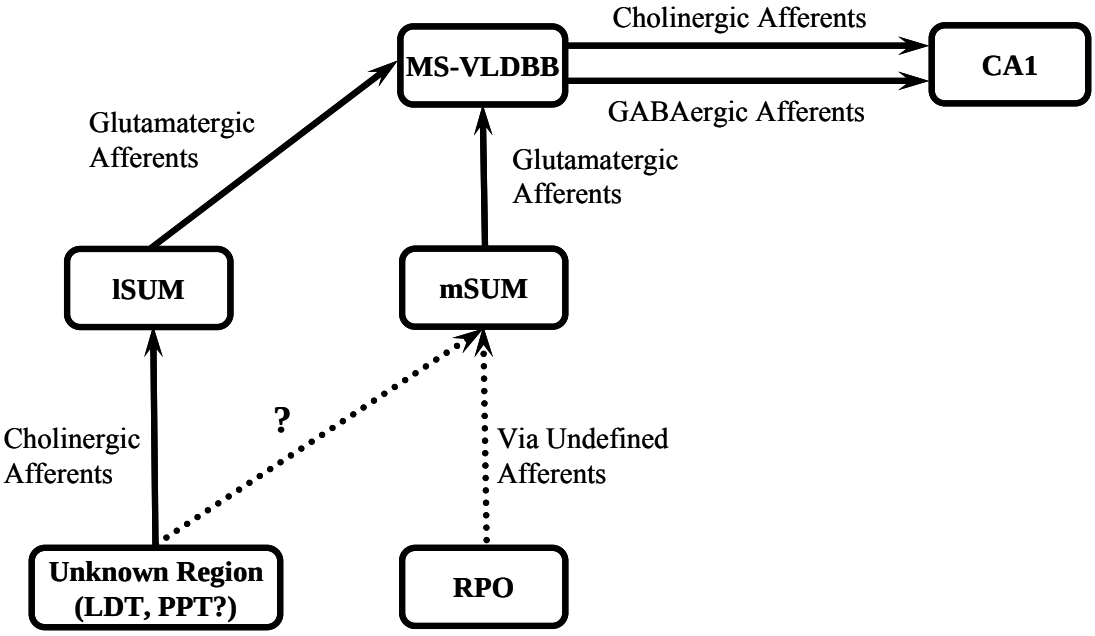

Fig. 4.1: Schematic representation of the proposed ascending pathways from the supramammillary (SUM) region that are involved in the suppression of CA1 pyramidal cell excitability. The proposed pathways overlap with that involved in generation of theta activity in the hippocampus. The SUM, both medial (mSUM) and lateral (lSUM) project to the medial septum-vertical limb of the diagonal band of Broca (MS-VLDBB) region, though the projection from lSUM is more robust (Vertes, 1992; Leranth and Kiss, 1996; Borhegyi et al., 1998; Kiss et al., 2000; Vertes and Mckenna; 2000). The projection from the SUM region to MS-VLDBB is, at least in part, glutamatergic (Kiss et al., 2000). The MS-VLDBB region in turn sends afferents, including cholinergic and GABAergic afferents to the hippocampus and dentate gyrus (Meibach and Siegel, 1977; Swanson and Cowan, 1979; Monmaur and Thomson, 1983; Nyakas et al., 1987; Gaykema et al., 1990; Yoshida and Oka, 1995; Dutar et al., 1995). Activation of both the cholinergic and GABAergic neurons in MS-VLDBB region is involved in generation of theta rhythm in the hippocampus (Buzsáki, 2002). Present findings indicate that stimulation of reticular formation in the region of the reticular pontis oralis (RPO) nucleus preferentially excites neurons in the mSUM to evoke suppression of CA1 pyramidal cell excitation on field CA3 stimulation. In this context, GABA microinjection in mSUM, but not lSUM attenuated RPO-elicited suppression. Furthermore, current findings also indicate that cholinergic agonist recruit lSUM mechanisms with higher potency. Such recruitment also evokes a suppression of CA1 pyramidal cell synaptic excitability. The lSUM- and mSUM-mediated suppression was reversibly attenuated with local anaesthetic block of MS-VLDBB suggesting a relay via the MS-VLDBB region. Interestingly, previous evidence indicates that septohippocampal cholinergic afferents mediates suppression of CA1 pyramidal cell excitability (Rovira et al., 1983; Zheng and Khanna, 2001) which raises the possibility that the SUM mediated suppression is via population of septohippocampal cholinergic neurons. The endogenous cholinergic afferents that activate SUM remains unclear. However, cholinergic afferents to the SUM from cholinergic nuclei such as laterodorsal tegmental nucleus (LTD; Gonzalo-Ruiz et al., 1999) and/or pedunculopontine tegmentum (PPT; Bland and Oddie, 1998) have been identified.

with carbachol is at present ambiguous. Interestingly, tracer studies indicate that cholinergic neurons from laterodorsal tegmental nucleus, medial septum, and the vertical and horizontal limb of the diagonal band of Broca project to SUM (Gonzalo-Ruiz et al., 1999). However, it remains unclear whether these projection neurons show topographic selectivity in the innervation of the SUM region.

Whether there are other modules in the SUM or in the wider PH-SUM region is unclear. In context of the latter, microinjection of the lower concentration of carbachol in the PH region was relatively ineffective in eliciting suppression. Indeed, CA1 pyramidal cell suppression was observed in only 3 of 9 experiments following microinjection of the lower concentration of carbachol into the PH region. Further, the suppression that was observed was evoked at long-latencies. Evaluation of the literature indicates that the PH region receives afferents from cholinergic nuclei (Abrahamson and Moore, 2001) and is recruited by carbachol. For example, infusion of large volume of high concentration of carbachol in the PH region evoked hippocampal theta activation in an atropine-sensitive fashion (Bland et al., 1994). On the other hand, microinjection of carbachol at concentrations lower than currently used evoked concentration-dependent increases in blood pressure when microinjected along the anterior-posterior and dorsal-ventral extent of the PH (Buccafusco and Brezenoff, 1979; Martin et al., 1988; Martin, 1996). This effect was observed both in behaving and anaesthetized rat. The comparisons with published data suggests that the relative inconsistent effect of PH carbachol on CA1 pyramidal cell excitability in the present study might be because of one or combination of the following reasons: (a) carbachol microinjections in the current study were generally not in the relevant region of PH that influences hippocampal CA1 pyramidal cell excitability. In this context, carbachol infusion sites that induced hippocampal theta

were mostly in the anterior and dorsal PH region (Bland et al., 1994), (b) the neural substrate that underlies the regulation of hippocampal excitability is organized diffusely in PH and requires higher concentration of carbachol that diffuses over larger volume to influence significant population of neurons, and (c) the sensitivity of PH neural mechanisms to carbachol is less than that for mechanisms underlying autonomic changes.

4.6 Possible neuronal type that underlies suppression

The dissociation of suppression from theta rhythm generation induced by both reticular stimulation and carbachol microinjection suggests that the suppression is not mediated by the theta-related rhythmic discharge of neurons in medial SUM region and MS-VLDBB (Bland, 1986; Kirk and McNaughton, 1991; Kocsis and Vertes, 1994; Bland et al., 1995; Kirk et al., 1996; Vertes and Kocsis, 1997; Bland and Oddie, 1998; Kirk, 1998). Rather, the strength of the presynaptic inhibition that impinges on CA1 pyramidal cells may depend upon principles such as the population size and/or the discharge rates of the neurons recruited with reticular stimulation or carbachol injection. The neural connections between the SUM, MS-VLDBB and CA1 that are brought into play to evoke suppression of CA1 pyramidal cells on reticular stimulation and carbachol injection remains to be elucidated. Anatomically, a direct projection has been delineated from both medial- and lateral SUM to MS-VLDBB (Vertes, 1992; Kiss et al., 2000). Based on retrograde transport of [^{3}H] D-aspartate this medial and lateral SUM projections are suggested to be excitatory (Kiss et al., 2000). While the synaptic contacts made in the MS-VLDBB region by the medial SUM neurons have not been separately defined, anterogradely labeled neurons from the lateral SUM region were

observed to make synaptic contacts with both cholinergic and parvalbumin positive (i.e. GABAergic) neurons of MS-VLDBB (Borhegyi et al., 1998).

It is notable that while activation of septohippocampal GABAergic neurons evoked disinhibition of CA pyramidal neurons in vitro (Toth et al., 1997; see introduction), stimulation of the septohippocampal cholinergic neurons evoked a cholinergic-mediated depression of CA1 synaptic transmission at commissural/Schaffer-collateral synapses in vivo (Rovira et al., 1983). Indeed, iontophoretic application of the cholinergic transmitter, acetylcholine, in the apical dendrites depressed the Schaffer-collateral stimulation-evoked synaptic EPSP in pyramidal neurons recorded intracellularly (Valentino and Dingledine, 1981). This action of acetylcholine was suggested to be due to presynaptic inhibition of transmitter release. Given the above background, it is conceivable that reticular stimulation and carbachol microinjection activates a relay from the neuronal population of medial and/or lateral SUM to a population of MS-VLDBB cholinergic neurons. Excitation of these cholinergic neurons may, in turn, contribute to suppression of CA1 pyramidal cell excitability. Indeed, previous evidence suggests that MS-VLDBB cholinergic neurons are involved in behavior- and sensory stimulation-induced suppression of CA1 pyramidal cell excitability that is observed in correlation with theta activation (Leung and Vanderwolf, 1980; Zheng and Khanna, 2001). It is an intriguing possibility that the both medial and lateral SUM also contributes to behavior- and sensory stimulation-induced suppression of CA1 synaptic responses.

4.7 Functional significance of the present findings

The functional significance of SUM mediated suppression of CA1 pyramidal cells remains to be elucidated. However, the overlap, at least partially, of the neural components underlying the suppression with theta generating ascending synchronizing pathway (Fig. 4.1) suggests an importance of these neural components in influencing the theta functional state of the hippocampus. It is possible that the SUM region mediated inhibitory regulation is a neural basis for the decrease in the excitability of CA1 pyramidal cells that accompanies the 'switch' to theta functional state of the hippocampus from non-theta state. For example, the change from non-theta to theta state is accompanied by suppression of sharp waves recorded from field CA1 (Buzsáki et al., 1983). The sharp waves are evoked as result of synaptic excitation of CA1 pyramidal cells by synaptic input from field CA3 (Buzsáki et al., 1983; Buzsáki, 1989; Moser and Paulsen, 2001). Similarly, the excitability of CA1 pyramidal cells to random, non-theta wave-linked, CA3 stimulation is suppressed with sensory- or behavior-induced change in the state of the hippocampus from non-theta to theta (Leung and Vanderwolf, 1980; Zheng and Khanna, 2001).

Interestingly, the hippocampal formation projects to the PH-SUM region via a polysynaptic descending limb that includes projections from the hippocampal formation to population of neurons at the border of lateral septum and medial septum which in turn project to the PH-SUM region (Vertes, 1992; Leranth and Kiss, 1996; Borhegyi and Freund, 1998; Leranth et al., 1999). The projection from the septum has a strong GABAergic component (Borhegyi and Freund, 1998; Leranth et al., 1999). The present findings that SUM microinjection of GABA attenuates, at least partly, SUM

mechanisms that inhibit CA1 pyramidal cell synaptic excitability raises the possibility that the GABAergic descending fibers from the forebrain inhibit SUM during the non-theta functional state of the hippocampus. Indeed, Kirk et al. (1996) have reported that inactivation of septum enhanced the activity of SUM neurons to RPO stimulation.

In conclusion, the present study provides evidence that the SUM region exercises an inhibitory influence on the excitability of CA1 pyramidal cells. The inhibitory influence is mediated via the MS-VLDBB region and might play a role in 'signal-to-noise' processing during the theta functional state of the hippocampus.

REFERENCES

Abrahamson, E.E. and Moore, R.Y. (2001) The posterior hypothalamic area: chemoarchitecture and afferent connections. *Brain Res*., 889(1-2): 1-22

Albertson, T.E. and Joy, R.M. (1987) Increased inhibition in dentate gyrus granule cells following exposure to GABA-uptake blockers. *Brain Res.*, 435(1-2): 283-292.

Alger, B.E. and Nicoll, R.A. (1982) Feed-forward dendritic inhibition in rat hippocampal pyramidal cells studied in vitro. *J. Physiol.*, 328: 105-123.

Ali, A.B., Deuchars, J., Pawelzik, H. and Thomson, A.M. (1998) CA1 pyramidal to basket and bistratified cell EPSPs: dual intracellular recording in rat hippocampal slices. *J. Physiol*., 507: 201-217.

Amaral, D.G., Dolorfo, C., and Alvarez-Royo, P. (1991) Organization of CA1 projectios to the subiculum: A PHA-L analysis in the rat. *Hippocampus,* 1(4) : 415-436.

Amaral, D.G. and Kurz, J. (1985) An analysis of the origins of the cholinergic and noncholinergic septal projections to the hippocampal formation of the rat. *J. Comp. Neurol*., 240(1): 37-59.

Amaral, D.G. and Witter, M.P. (1989) The three-dimensional organization of the hippocampal formation: a review of anatomical data. *Neuroscience*, 31(3): 571-591.

Amaral, D.G. and Witter M.P. (1995) Hippocampal formation. In: The rat nervous system (2nd edition). Paxinos G. (Ed). *Academic Press*, 443-493.

Andersen, P. (1960) Interhippocampal impulses. II. Apical dendritic activation of CAI neurons. *Acta. Physiol. Scand*., 48: 178-208.

Andersen, P., Bliss, T.V.P. and Skrede, K.K., (1971) Unit analysis of hippocampal population spikes. *Exp. Brain Res.*, 13: 208-221.

Andersen, P., Eccles, J.C. and Loyning, Y. (1964a) Location of postsynaptic inhibitory synapses on hippocampal pyramids. *J. Neurophysiol*., 27: 592-607.

Andersen, P., Eccles, J.C. and Loyning, Y. (1964b) Pathway of postsynaptic inhibition in the hippocampus. *J. Neurophysiol*., 27: 608-619.

Andersen, P., Soleng, A.F. and Raastad, M. (2000) The hippocampal lamella hypothesis revisited. *Brain Res*., 886(1-2): 165-171.

Ashwood, T.J., Lancaster, B. and Wheal, H.V. (1984) In vivo and in vitro studies on putative interneurones in the rat hippocampus: possible mediators of feed-forward inhibition. *Brain Res.,* 293(2): 279-91.

Auerbach, J.M. and Segal, M. (1996) Muscarinic receptors mediating depression and long-term potentiation in rat hippocampus. *J. Physiol.,* 492 (Pt 2): 479-493.

Azouz, R., Jensen, M.S. and Yaari, Y. (1996) Ionic basis of spike after-depolarization and burst generation in adult rat hippocampal CA1 pyramidal cells. *J. Physiol.,* 492 (Pt 1): 211-223.

Ben-Ari, Y., Krnjevic, K., Reinhardt, W. and Ropert, N. (1981) Intracellular observations on the disinhibitory action of acetylcholine in the hippocampus. *Neuroscience,* 6(12): 2475-2484.

Blackstad, T.W., Brink, K., Hem, J. and Jeune, B. (1970) Distribution of hippocampal mossy fibers in the rat. An experimental study with silver impregnation methods. *J. Comp. Neurol.,* 138(4): 433-449.

Blackstad, T.W. and Kjaerheim, A. (1961) Special axo-dendritic synapses in the hippocampal cortex: electron and light microscopic studies on the layer of mossy fibers. *J. Comp. Neurol.,* 117: 133-159.

Bland, B.H. (1986) The physiology and pharmacology of hippocampal formation theta rhythm. *Prog. Neurobiol*., 26: 1-54.

Bland, B.H., Anderson, P., Ganes, T. and Sveen, O. (1980) Automated analysis of rhythmicity of physiologically identified hippocampal formation neurons. *Exp. Brain Res.*, 38: 205-219.

Bland, B.H., Konopacki, J. and Dyck, R.H. (2002) Relationship between membrane potential oscillations and rhythmic discharges in identified hippocampal theta-related cells. *J. Neurophysiol.* 88(6): 3046-3066.

Bland, B.H., Konopacki, J., Kirk, I.J., Oddie, S.D. and Dickson, C.T. (1995) Discharge patterns of hippocampal theta-related cells in the caudal diencephalon of the urethane-anesthetized rat. *J. Neurophysiol*., 74(1): 322-333.

Bland, B.H. and Oddie, S.D. (1998) Anatomical, electrophysiological and pharmacological studies of ascending brainstem hippocampal synchronizing pathways. *Neurosci. Biobehav. Rev*., 22, 259-273.

Bland, B.H., Oddie, S.D., Colom, L.V. and Vertes, R.P. (1994) Extrinsic modulation of medial septal cell discharges by the ascending brainstem hippocampal synchronizing pathway. *Hippocampus*, 4(6): 649-460.

Bland, B.H., and Whishaw, I..Q. (1976) Generators and topography of hippocampal theta (RSA) in the anaesthetized and freely moving rat. *Brain Res.,* 118(2): 259-280.

Blasco-Ibanez, J.M. and Freund, T.F. (1995) Synaptic input of horizontal interneurons in stratum oriens of the hippocampal CA1 subfield: structural basis of feed-back activation. *Eur. J. Neurosci.,* 7: 2170-2180.

Bolshakov, V.Y. and Siegelbaum, S.A. (1995) Regulation of hippocampal transmitter release during development and long-term potentiation. *Science*, 269(5231): 1730-1734.

Borhegyi, Z. and Freund, T.F. (1998) Dual projection from the medial septum to the supramammillary nucleus in the rat. *Brain Res. Bull*., 46(5): 453-459.

Borhegyi, Z., Magloczky, Z., Acsady, L. and Freund, T.F. (1998) The supramammillary nucleus innervates cholinergic and GABAergic neurons in the medial septum-diagonal band of broca complex. *Neuroscience*, 82: 1053-1065.

Borhegyi, Z. and Leranth, C. (1997) Distinct substance P- and calretinin-containing projections from the supramammillary area to the hippocampus in rats: a species difference between rats and monkeys. *Exp. Brain Res.,* 115(2): 369-374.

Brankack, J., Stewart, M. and Fox, S.E. (1993) Current source density analysis of the hippocampal theta rhythm: associated sustained potentials and candidate synaptic generators. *Brain Res.*, 615(2): 310-327.

Buccafusco, J.J. and Brezenoff, H.E. (1979) Pharmacological study of a cholinergic mechanism within the rat posterior hypothalamic nucleus which mediates a hypertensive response. *Brain Res.,* 165(2): 295-310.

Buhl, E.H., Halasy, K. and Somogyi, P. (1994a) Diverse sources of hippocampal unitary inhibitory postsynaptic potentials and the number of synaptic release sites. *Nature*, 368(6474): 823-828.

Buhl, E.H., Han, Z.S., Lorinczi, Z., Stezhka, V.V., Karnup, S.V. and Somogyi P. (1994b) Physiological properties of anatomically identified axo-axonic cells in the rat hippocampus. *J. Neurophysiol*., 71(4): 1289-1307.

Buzsáki, G. (1983) Cellular bases of hippocampal EEG in the behaving rat. *Brain Res.,* 287(2): 139-171.

Buzsáki, G. (1986) Hippocampal sharp weaves: their origin and significance. *Brain Res.,* 398: 242-252.

Buzsáki, G. (1984) Feed-forward inhibition in the hippocampal formation. *Prog Neurobiol.,* 22(2): 131-153.

Buzsáki, G. (1989) Two-stage model of memory trace formation: a role for 'noisy' brain states. *Neuroscience,* 31: 551-570.

Buzsáki, G. (2002) Theta oscillations in the hippocampus. *Neuron*, 33: 325-340.

Buzsáki, G. and Eidelberg, E. (1982) Direct afferent excitation and long-term potentiation of hippocampal interneurons. *J. Neurophysiol.,* 48: 597-607.

Buzsáki, G. and Eidelberg, E. (1983) Phase relations of hippocampal projection cells and interneurons to theta activity in the urethane anaesthetized rat. *Brain Res*., 266, 334-338.

Buzsáki, G., Leung, L.W. and Vanderwolf, C.H. (1983) Cellular bases of hippocampal EEG in the behaving rat. *Brain Res.* 287(2): 139-171.

Buzsáki, G., Penttonen, M., Nadasdy, Z. and Bragin, A. (1996) Pattern and inhibition-dependent invasion of pyramidal cell dendrites by fast spikes in the hippocampus in vivo. *Proc. Natl. Acad. Sci*. U S A. 93(18): 9921-9925.

Cao, F. and Leung, L.S. (1991) Behavior-dependent paired-pulse responses in the hippocampal CA1 region. *Exp. Brain Res*., 87: 553-561.

Carre, G.P. and Harley, C.W. (1991) Population spike facilitation in the dentate gyrus following glutamate to lateral supramammillary nucleus. *Brain Res.,* 568: 307-310.

Claiborne B.J., Amaral, D.G. and Cowan, W.M. (1986) A light and electron microscope analysis of the mossy fibers of the rat dentate gyrus. *J. Comp. Neurol.,* 246: 435-458.

Cobb, S.R., Buhl, E.H., Halasy, K., Paulsen, O. and Somogyi, P. (1995) Synchronization of neuronal activity by individual GABAergic interneurons. *Nature*, 378: 75-98.

Colom, L.V., Ford, R. D. and Bland, B.H. (1987) Hippocampal formation neurons code the level of activation of the cholinergic septohippocampal pathway. *Brain Res*., 410: 12-20.

Csicsvari, J., Hirase, H., Czurko, A., Mamiya, A. and Buzsáki, G. (1999) Oscillatory coupling of hippocampal pyramidal cells and interneurons in the behaving Rat. *J. Neurosci.,* 19(1): 274-287.

Dutar, P., Bassant, M.H., Senut, M.C. and Lamour, Y. (1995) The septohippocampal pathway: structure and function of a central cholinergic system. *Physiol. Rev*., 75: 393-427.

Fernandez de Sevilla, D. and Buno, W. (2003) Presynaptic inhibition of Schaffer collateral synapses by stimulation of hippocampal cholinergic afferent fibers. *Eur. J. Neurosci.*, 17(3): 555-558.

Finch, D.M., Nowlin, N.L., and Babb, T.L. (1983) Demonstration of axonal projection of neurons in the rat hippocampus and subiculum by intracellular injections of HRP. *Brain Res*., 271: 201-216.

Fox, S.E. and Ranck, J.B.Jr (1975) Localization and anatomical identification of theta and complex spike cells in dorsal hippocampal formation of rats. *Exp. Neurol.,* 49: 299-313.

Fox, S.E. and Ranck, J.B.Jr (1981) Electrophysiological characteristics of hippocampal complex-spike cells and theta cells. *Exp. Brain Res.,* 41: 399–410.

Fox, S.E., Wolfson, S. and Ranck, J.B.Jr (1986) Hippocampal theta rhythm and the firing of neurons in walking and urethane anesthetized rats. *Exp. Brain Res*., 62: 495-580.

Freund, T.F. (1989) GABAergic septohippocampal neurons contain paravalbumin. *Brain Res*., 478: 375-381.

Freund, T.F. and Antal, M. (1988) GABA-containing neurons in the septum control inhibitory interneurons in the septum control inhibitory interneurons in the hippocampus. *Nature,* 336: 170-173.

Freund, T.F. and Buzáki, G. (1996) Interneurons of the hippocampus. *Hippocampus*, 6: 347-470.

Freund, T.F., Gulyás, A.I., Acsady, L., Gorcs, T., and Toth, K. (1990) Serotonergic control of the hippocampus via local inhibitory interneurons. *Proc. Natl. Acad. Sci*. USA, 87: 8501-8505.

Fricke, R. and Cowan, W.M. (1978) An autoradiographic study of the commissural and ipsilateral hippocampo-dentate projections in the adult rat. *J. Comp. Neurol.*, 181(2): 253-269.

Frotscher, M. and Leranth, C. (1985) Cholinergic innervatio of the rat hippocampus as revealed by choline acetylrtansferase immunocytochemistry: a combined light and electron microscopic study. *J. Comp. Neurol.,* 239: 237-246.

Gaarskjaer, F.B. (1978) Organization of the mossy fiber system of the rat studied in extended hippocampi. I. Terminal area related to number of granule and pyramidal cells. *J. Comp. Neurol.*, 178(1): 49-72.

Gaykema, R.P., Luiten, P.G., Nyakas, C. and Traber, J. (1990) Cortical projection patterns of the medial septum-diagonal band complex. *J. Comp. Neurol*., 293(1): 103-124.

Gonzalo-Ruiz, A., Morte, L., Flecha, J.M. and Sanz, J.M. (1999) Neurotransmitter characteristics of neurons projecting to the supramammillary nucleus of the rat. *Anat Embryol* (Berl). 200(4): 377-92

Green, K.F. and Rawlins, J.N.D. (1979) Hippocampal theta in rats under urethane: generators and phase relations. *Electroencephalogr. Clin. Neurophysiol*., 47: 420-429

Gulyás, A.I., Miles, R., Sik, A., Tóth, K., Tammmaki, N. and Freund, T.F. (1993) Hippocampal pyramidal cells excite inhibitory neurons through a single release site. *Nature*, 366: 683-687.

Haglund, L., Swanson, L.W. and Kohler, C. (1984) The projection of the supramammillary nucleus to the hippocampal formation: an immunohistochemical and anterograde transport study with the lectin PHA-L in the rat. *J. Comp. Neurol*., 229(2): 171-185.

Halasy, K. and Somogyi, P. (1993) Subdivisions in the multiple GABAergic innervation of granule cells in the dentate gyrus of the rat hippocampus. *Eur. J. Neurosci*., 5: 411-429.

Han, Z.S, Buhl, E.H., Lorinczi, Z. and Somogyi, P. (1993) A high degree of spatial selectivity in the axonal and dendritic domains of physiologically identified local-circuit neurons in the dentate gyrus of the rat hippocampus. *Eur. J. Neurosci.,* 5: 395-410.

Herreras, O. (1990) Propagating dendritic action potential mediates synaptic transmission in CA1 pyramidal cells in situ. *J. Neurophysiol*., 64(5): 1429-1441.

Herreras, O., Solis, J.M., Herranz, A.S., Martin, del Rio R. and Lerma, J. (1988) Sensory modulation of hippocampal transmission. II. Evidence for a cholinergic locus of inhibition in the Schaffer-CA1 synapse. *Brain Res*., 461(2): 303-313.

Hjorth-Simonsen, A. (1973) Some intrinsic connections of the hippocampus in the rat: an experimental analysis. *J. Comp. Neurol.,* 147(2): 145-161.

Holscher, C., Anwyl, R. and Rowan, M.J. (1997) Stimulation on the positive phase of hippocampal theta rhythm induces long-term potentiation that can be depotentiated by stimulation on the negative phase in area CA1 in vivo. *J. Neurosci*., 17(16): 6470-6477.

Holsheimer, J., Feenstra, B.W.A. and Nijkamp, J.M. (1979) Distribution of field potentials and their relationships during theta and beta activity in the hippocampus and the overly- ing neocortex of the rat. In '*E.J. Speckman and H. Caspers*' (Eds.), Origin of Cerebral Field Potentials, Thieme, Stuttgart.

Hyman, J.M., Wyble, B.P., Goyal, V., Rossi, C.A. and Hasselmo, M.E. (2003) Stimulation in hippocampal region CA1 in behaving rats yields long-term potentiation when delivered to the peak of theta and long-term depression when delivered to the trough. *J. Neurosci.*, 23(37): 11725-11731.

Jensen, M.S., Azouz, R. and Yaari, Y. (1996) Spike after-depolarization and burst generation in adult rat hippocampal CA1 pyramidal cells. *J. Physiol*., 492 (Pt 1): 199-210.

Kamondi, A., Acsady, L., Wand X.J. and Buzsáki, G. (1998) Theta oscillations in soma and dendrites of hippocampal pyramidal cell *in vitro*: activity-dependent phase-precession of action potentials. *Hippocampus,* 8: 244-261.

Kandel, E.R., Spencer, W.A. and Brinley, F.J. Jr. (1961) Electrophysiology of hippocampal neurons. I. Sequential invasion and synaptic organization. *J. Neurophysiol.,* 24: 225-242.

Khanna S. (1997) Dorsal hippocampal field CA1 pyramidal cell responses to a persistent versus an acute nociceptive stimulus and their septal modulation. *Neuroscience*, 77: 713-721.

Khanna, S. and Sinclair, J.G. (1992) Responses in the CA1 region of the rat hippocampus to a noxious stimulus. *Exp. Neurol*., 117(1), 28-35.

Kirk I.J. (1997) Supramammillary neural discharge patterns and hippocampal EEG. *Brain Res. Bull.* 42(1): 23-26

Kirk, I.J. (1998) Frequency modulation of hippocampal theta by the supramammillary nucleus, and other hypothalamo-hippocampal interactions: mechanisms and functional implications. *Neurosci. Biobehav. Rev*., 22(2): 291-302.

Kirk, I.J. and McNaughton, N. (1991) Supramammillary cell firing and hippocampal rhythmical slow activity. *Neuroreport*, 2: 723-725.

Kirk, I.J. and McNaughton, N. (1993) Mapping the differential effects of porcaine on frequency and amplitude of reticularly elicited hippocampal rhythmical slow activity. *Hippocampus*, 3: 517-526.

Kirk, I.J., Oddie, D. D., Konopacki, J. and Bland, B. H. (1996) evidence for differential control of posterior hypothalamic, supramammillary, and medial mammillary theta-related cellular discharge by ascending and descending pathways. *J. Neurosci*., 16: 5547-5554.

Kiss, J., Csaki, A., Bokor, H., Shanabrough, M. and Leranth, C. (2000) The supramammillo-hippocampal and supramammillo-septal glutamatergic/aspartatergic projections in the rat: a combined [3H]D-aspartate autoradiographic and immunohistochemical study. *Neuroscience*, 97(4): 657-669.

Kiss, J., Magloczky, Z., Somogyi, J. and Freund, T.F. (1997) Distribution of calretinin-containing neurons relative to other neurochemically identified cell types in the medial septum of the rat. *Neuroscience*, 78(2): 399-410.

Kiss, J., Patel, A. J. and Freund, T. F. (1990) Distribution of septohippocampal neurons containing parvalbumin or choline acetyltransferase in the rat brain. *J. Com. Neurol*., 298: 362-372.

Klausberger, T., Magill, P.J., Marton, L.F., Roberts, J.D., Cobden, P.M., Buzsáki, G. and Somogyi, P. (2003) Brain-state- and cell-type-specific firing of hippocampal interneurons in vivo. *Nature*, 421(6925): 844-848.

Kloosterman, F., Peloquin, P. and Leung, L.S. (2001) Apical and basal orthodromic population spikes in hippocampal CA1 in vivo show different origins and patterns of propagation. *J. Neurophysiol*., 86(5): 2435-2444.

Knowles, W.D and Schwartzkroin, P.A. (1981) Local circuit synaptic interactions in hippocampal brain slices. *J. Neuroscience*, 3: 318-322.

Kocsis, B. and Vertes, R.P. (1994) Characterization of neurons of the supramammillary nucleus and mammillary body that discharged rhythmically with the hippocampal theta rhythm in the rat. *J. Neurosci*., 14: 7040-7052.

Krnjevic, K. and Ropert, N. (1982) Electrophysiological and pharmacological characteristics of facilitation of hippocampal population spikes by stimulation of the medial septum. *Neuroscience*, 7(9): 2165-2183.

Lacaille, J.C., Mueller, A.L., Kunkel, D.D. and Schwartzkroin, P.A. (1987) Local circuit interactions between oriens/alveus interneurons and CA1 pyramidal cells in hippocampal slices: electrophysiology and morphology. *J. Neurosci.,* 7(7): 1979-1993.

Laurberg, S. (1979) Commissural and intrinsic connections of the rat hippocampus. *J. Comp. Neurol.* 184(4): 685-708.

Lee, M.G., Chrobak, J.J., Sik, A., Wiley, R.G. and Buzsáki, G. (1994) Hippocampal theta activity following selective lesion of the septal cholinergic system. *Neuroscience,* 62 (4): 1033-1047.

Leranth, C. and Kiss, J. (1996) A population of supramammillary area calretinin neurons terminating on medial septal area cholinergic and lateral septal area calbindin-containing cells are aspartate/glutamatergic. *J. Neurosci*., 16(23): 7699-7710.

Leung, L.S. (1980) Behavior-dependent evoked potentials in the hippocampal CA1 region of the rat. I. Correlation with behavior and EEG. *Brain Res*., 198: 95-117.

Leung, L.S. (1984a) Pharmacology of theta phase shift in the hippocampal CA1 region of freely moving rats. *Electroencephalogr. Clin. Neurophysiol*., 58(5): 457-466.

Leung, L.S. (1984b) Model of gradual phase shift of theta rhythm in the rat. *J. Neurophysiol.,* 52: 1051-1065.

Leung, L.S. (1985) Spectral analysis of hippocampal EEG in the freely moving rat: effects of centrally active drugs and relations to evoked potentials. *Electroencephal. Clin. Neurophysiol*., 60: 65-77.

Leung, L.S. (1998) Generation of theta and gamma rhythms in the hippocampus. *Neurosci. Biobehav. Rev*., 22: 275-290.

Leung, L.S., Shen, B., Rajakumar, N. and Ma, J. (2003) Cholinergic activity enhances hippocampal long-term potentiation in CA1 during walking in rats. *J. Neurosci*., 23(28): 9297-304.

Leung, L.S. and Vanderwolf, C.H. (1980) Behavior-dependent evoked potentials in the hippocampal CA1 region of the rat. II. Effect of eserine, atropine, ether and pentobarbital. *Brain Res*., 198: 119-133.

Leung, L.S. and Yim, C. Y. (1984) Intracellular theta in hippocampal CA1 pyramidal cells in the urethane-anesthetized rat (Abstract). Proc. Can. Fed. *Biol. Soc*., 27(40).

Leung, L.S. and Au, A.S. (1994) Long-term potentiation as a function of test pulse intensity: a study using input/output profiles. *Brain Res. Bull*., 33: 453-460.

Li, X.G., Somogyi, P., Ylinen, A. and Buzsáki, G. (1994) The hippocampal CA3 network: an in vivo intracellular labeling study. *J. Comp. Neurol*., 339(2): 181-208.

Lisman, J.E. (1997) Bursts as a unit of neural information: making unreliable synapses reliable. *Trends Neurosci.,* 20(1): 38-43.

Lorente de Nó, R. (1934) Studies on the structure of the cerebral cortex. II. Continuation of the study of the ammonic system. *J. Psychol. Neurol*., 46, 113-177.

Maccaferri, G. and McBain, C.J. (1995) Passive propagation of LTD to stratum oriens-alveus inhibitory neurons modulates the temporoammonic input to the hippocampal CA1 region. *Neuron,* 15(1): 137-145.

Magee, J.C. (2001) Dendritic mechanisms of phase precession in hippocampal CA1 pyramidal neurons. *J. Neurophysiol.,* 86(1): 528-532.

Magloczky, Z., Acsady, L. and Freund, T.F. (1994) Principal cells are the postsynaptic targets of supramammillary afferents in the hippocampus of the rat. *Hippocampus*, 4(3): 322-334.

Martin, J.R. (1996) Mechanisms of the cardiovascular response to posterior hypothalamic nucleus administration of carbachol. *J. Cardiovasc. Pharmacol.,* 27(6): 891-900.

Martin, J.R., Beinfeld, M.C.and Westfall, T.C. (1988) Blood pressure increases after injection of neuropeptide Y into posterior hypothalamic nucleus. *Am. J. Physiol*., 254(5 Pt 2): H879-888.

Martin, J.L. and Sloviter, R.S. (2001) Focal inhibitory interneuron loss and principal cell hyperexcitability in the rat hippocampus after microinjection of a neurotoxic conjugate of saporin and a peptidase-resistant analog of Substance P. *J. Comp. Neurol*., 436(2): 127-152.

McNaughton, N., Logan, B., Panickar, K.S., Kirk, I.J., Pan, W.X., Brown, N.T. and Heenan, A. (1995) Contribution of synapses in the medial supramammillary nucleus to the frequency of hippocampal theta rhythm in freely moving rats. *Hippocampus*, 5(6): 534-545.

Meibach, R.C. and Siegel, A. (1977) Efferent connections of the septal area in the rat: an analysis utilizing retrograde and anterograde transport methods. *Brain Res.,* 119(1): 1-20.

Milner, T.A. and Amaral, D.G. (1984) Evidence for a ventral septal projection to the hippocampal formation of the rat. *Exp. Brain Res*., 55(3): 579-585.

Mitzdorf, U. (1985) Current source-density method and application in cat cerebral cortex: investigation of evoked potentials and EEG phenomena. *Physiol. Rev*., 65: 37-100.

Mizumori, S.J.Y., McNaughton, B.A. and Barnes, C.A. (1989) A comparison of surpamammillary and medial septal influences on hippocampal field potentials and single-unit activity. *J. Neurophysiol.*, 61: 15-31.

Monmaur, P. and Thomson, M.A. (1983) Topographic organization of septal cells innervating the dorsal hippocampal formation of the rat: special reference to both the CA1 and dentate theta generators. *Exp Neurol*. 82(2): 366-378.

Moser, E.I. and Paulsen, O. (2001) New excitement in cognitive space: between place cells and spatial memory. *Curr. Opin. Neurobiol*., 11(6): 745-51.

Nakanishi, K., Saito, H. and Abe, K. (2001) The supramammillary nucleus contributes to associative EPSP-spike potentiation in the rat dentate gyrus in vivo. *Eur. J. Neurosci.,* 13(4): 793-800.

Nyakas, C., Luiten, P.G.M., Spencer, D.G. and Traber, J. (1987) Detailed projection patterns of septal and diagonal band efferents to the hippocampus in the rat with emphasis on innervation of CA1 and dentate gyrus. *Brain Res. Bull.,* 18: 533-545.

Oddie, S.D., Bland, B.H., Colom, L.V. and Vertes, R. P. (1994) The midline posterior hypothalamic region comprises a critical part of the ascending brainstem hippocampal synchronizing pathway. *Hippocampus*, 4: 454-473.

O'keefe, J. and Recce, M.L. (1993) Phase relationship between hippocampal place units and the EEG theta rhythm. *Hippocampus*, 3: 317-330.

Olbrich, H.G. and Braak, H. (1985) Ratio of pyramidal cells verse non-pyramidal cells in sector CA1 of the human Ammons horn. *Anat. Embryol.,* 173: 105-110.

Otto, T., Eichenbaum, H., Wiener, S.I. and Wible CG. (1991) Learning-related patterns of CA1 spike trains parallel stimulation parameters optimal for inducing hippocampal long-term potentiation. *Hippocampus*, 1(2): 181-192.

Paulsen, O. and Sejnowski, T.J. (2000) Natural patterns of activity and long-term synaptic plasticity. *Curr. Opin. Neurobiol.,* 10(2): 172-179.

Pike, F.G., Meredith, R.M., Olding, A.W. and Paulsen, O. (1999) Rapid report: postsynaptic bursting is essential for 'Hebbian' induction of associative long-term potentiation at excitatory synapses in rat hippocampus. *J. Physiol*., 518 (Pt 2): 571-576.

Radpour, S. and Thomson A.M. (1992) Synaptic enhancement induced by NMDA and Qp receptors and presynaptic activity. *Neurosci. Lett.,* 13, 138(1): 119-122.

Ramón y Cajal, S. (1893) Estructura del asta de Ammon y fascia dentata. *Ann. Soc. Esp. Hist. Nat.* 22.

Rawlins, J.N. and Green, K.F. (1977) Lamellar organisation in the rat hippocampus. *Exp. Brain. Res.*, 28(3-4): 335-344.

Reece, L. and Schwartzkroin, P.A. (1991) Effects of cholinergic agonists on two non-pyramidal cell types in rat hippocampal slice. *Brain Res.,* 140: 315-332.

Richardson, T.L., Turner, R.W.and Miller, J.J. (1984) Extracellular fields influence transmembrane potentials and synchronization of hippocampal neuronal activity. *Brain Res*., 294(2): 255-262.

Richardson, T.L., Turner, R.W. and Miller, J.J. (1987) Action-potential discharge in hippocampal CA1 pyramidal neurons: current source-density analysis. *J. Neurophysiol.,* 58(5): 981-996.

Rose, G. and Pang, K. (1985) Pharmacological differentiation of hippocampal neurons. In '*Electrical activity of the archicortex*', Eds., G. Buzsáki and G.H. Vanderwolf, Akademiai Kiado, Budapest, pp. 191-204.

Rovira, C., Ben-Ari, Y. and Cherubini, E. (1983) Dual cholinergic modulation of hippocampal somatic and dendritic field potentials by the septo-hippocampal pathway. *Exp. Brain Res*., 49(1): 151-155.

Saji, M., Kobayashi, S., Ohno, K. and Sekino, Y. (2000) Interruption of supramammillohippocampal afferents prevents the genesis and spread of limbic seizures in the hippocampus via a disinhibitory mechanism. *Neuroscience*, 97: 437-445.

Sayin, U,, Osting, S., Hagen, J., Rutecki, P. and Sutula, T. (2003) Spontaneous seizures and loss of axo-axonic and axo-somatic inhibition induced by repeated brief seizures in kindled rats. *J. Neurosci.,* 23(7): 2759-2768

Sayin, U., Rutecki, P.A., Mellanby, J. and Sutula, T.P. (2001) Gamma-vinyl GABA reduces paired pulse inhibition in the rat dentate gyrus in vivo and in vitro. *Epilepsy Res*., 44(2-3): 109-117.

Schaffer, J. (1892) Uber Drusen im Epithel der Vasa efferentia testis beim menschen. *Anat. Anz*., 7: 711-717.

Schwartzkroin, P.A. (1975) Characteristics of CA1 neurons recorded intracellularly in the hippocampal in vitro slice preparation. *Brain Res*., 85(3): 423-436.

Sík, A., Penttonen, M., Ylinen, A., Buzsáki, G. (1995) Hippocampal CA1 interneurons: an in vivo intracellular labeling study. *J. Neurosci.,* 15: 6651-6665.

Smythe, J.W., Cristie, B.R., Colom, L.V., Lawson, V.H. and Bland, B.H. (1991) Hippocampal theta field activity and theta-on/theta-off cell discharges are controlled by an ascending hypothalamo-septal pathway. *J. Neurosci.,* 11(7): 2241-2248.

Soltész, I. and Deschénes,M. (1993) Low- and high-frequency membrane potential oscillations during theta activity in CA1 and CA3 pyramidal neurons of the rat hippocampus under ketamine-xylazine anesthesia. *J. Neurophysiol.,* 10: 97-116.

Spencer, W.A. and Kandel, E.R. (1961) Hippocampal neuron responses to selective activation of recurrent collaterals of hippocampofugal axons. *Expl. Neurol*. 4: 149-161.

Spruston, N., Schiller, Y. Stuart, G. and Sakmann, B. (1995) Activity-dependent action potential invasion and calcium influx into hippocampal CA1 dendrites. *Science*, 268(5208): 297-300.

Steffensen, S.C. and Henriksen, S.J. (1991) Effects of baclofen and bicuculline on inhibition in the fascia dentata and hippocampus regio superior. *Brain Res.,* 538(1): 46-53.

Stewart, M. and Fox, S.E. (1990) Do septal neurons pace theta hippocampal theta rhythm? *Trends Neuronsci.,* 13: 163-168.

Stewart, M., Luo, Y. and Fox, S.E. (1992) Effects of atropine on hippocampal theta cells and complex-spike cells. *Brain Res*., 591(1): 122-128.

Swanson, L.W. and Cowan, W.M. (1979) The connections of the septal region in the rat. *J. Comp. Neurol.,* 186: 621-656.

Swanson, L.W., Sawchenko P.E. and Cowan,W.M. (1978) An autoradiographic study of the organization of intrahippocampal association pathways in the rat. *J. Comp. Neurol.,* 181: 681-716.

Swanson, L.W., Sawchenko, P.E. and Cowan, W.M. (1981) Evidence for collateral projections by neurons in Ammon's horn, the dentate gyrus, and the subiculum: a multiple retrograde labeling study in the rat. *J. Neurosci.,* 1(5): 548-559.

Taylor, C.P. and Dudek, F.E. (1984) Excitation of hippocampal pyramidal cells by an electrical field effect. *J. Neurophysiol.* 52(1): 126-142.

Thinschmidt, J.S., Kinney, G.G., and Kocsis, B. (1995) The supramammillary nucleus: is it necessary for the mediation of hippocampal theta rhythm? *Neuroscience*, 67(2): 301-312.

Thomas, M.J., Watabe, A.M., Moody, T.D., Makhinson, M. and O'Dell, T.J. (1998) Postsynaptic complex spike bursting enables the induction of LTP by theta frequency synaptic stimulation. *J. Neurosci.,* 18(18): 7118-7126.

Tóth, K., Freund, T.F and Miles, R. (1997) Disinhibition of rat hippocampal pyramidal cells by GABAergic afferents from the septum. *J. Physiol.,* 500: 463-474.

Turner, R.W., Meyers, D.E. and Barker, J.L. (1989) Localization of tetrodotoxin-sensitive field potentials of CA1 pyramidal cells in the rat hippocampus. *J. Neurophysiol*. 62(6): 1375-1387

Turner, R.W., Meyers, D.E., Richardson, T.L. and Barker, J.L. (1991) The site for initiation of action potential discharge over the somatodendritic axis of rat hippocampal CA1 pyramidal neurons. *J. Neurosci.,* 11(7): 2270-2280.

Umbriaco, D., Garcia, S., Beaulieu, C., and Descarries, L. (1995) Relational features of acetylcholine, noradrenaline, serotonin and GABA axon terminals in the stratum radiatum of adult rat hippocampus (CA1). *Hippocampus,* 5(6): 605-620.

Valentino, R.J. and Dinglendine, R. (1981) Presynaptic inhibitory affect of acetylchoine in the hippocampus. *J. Neurosci*., 1: 784-792.

Vanderwolf, C.G. (1969) Hippocampal electrical activity and voluntary movement in the rat. *Electroencephalogr. Clin. Neurophysiol.,* 26: 407-418.

Vertes, R.P. (1988) Brainstem afferents to the basal forebrain in the rat. *Neuroscience,* 24(3): 907-935.

Vertes, R.P. (1992) PHA-L analysis of projections from the supramammillary nucleus in the rat. *J. Comp. Neurol.*, 326: 595-622.

Vertes, R.P., Crane, A.M., Colom, L.V. and Bland, B.H. (1995) Ascending projections of the posterior nucleus of the hypothalamus: A PHA-L analysis in the rat. *J. Comp. Neurol*., 359: 90-116.

Vertes, R.P. and Kocsis, B. (1997) Brainstem-diencephalo-septohippocampal systems controlling the theta rhythm of the hippocampus. *Neuroscience*, 81(4): 893-926.

Vertes, R.P and Mckenna, J.T. (2000) Collateral projections from the supramammillary nucleus to the medial septum and hippocampus. *Synapse*, 38: 281-293.

Winson, J. and Abzug, C. (1977) Gating of neuronal transmission in the hippocampus: efficacy of transmission varies with behavioral state. *Science*, 196: 1223-1225.

Winson, J. (1981) Reticular formation influence on neuronal transmission from perforant pathway through dentate gyrus. *Brain Res*., 225: 37-49.

Wong, R.K.S., Numann, R.E., Miles, R. and Traub, R.D. (1986) Hippocampal pyramidal cells: ionic conductance and synaptic interactions. In '*Neural mechanisms of conditioning*', Eds., D.L. Alkon and C.D. Woody, Plenum Press, NY, pp. 311-318.

Wong, R.K. and Prince, D.A. (1978) Participation of calcium spikes during intrinsic burst firing in hippocampal neurons. *Brain Res.,* 159(2): 385-390.

Wong, R.K., Traub, R.D. and Miles, R. (1986) Cellular basis of neuronal synchrony in epilepsy. *Adv. Neurol.* 44: 583-592.

Woolf, N.J., Eckenstein, F., and Butcher, L.L. (1984) Cholinergic systems in the rat brain: I. projections to the limbic telencephalon. *Brain Res. Bull*., 13(6): 751-784.

Ylinen, A., Soltesz, I., Bragin, A., Penttonen, M., Sik, A. and Buzsáki,G (1995) Intracellular correlates of hippocampal theta rhythm in identified pyramidal cells, granule cells and basket cells. *Hippocampus,* 5: 78-90.

Yoshida, K and Oka, H. (1999) Topographical projections from the medial septum-diagonal band complex to the hippocampus: a retrograde tracing study with multiple fluorescent dyes in rats. *Neurosci. Res.,* 21(3): 199-209.

Zheng, F. and Khanna, S. (2001) Selective destruction of medial sepal cholinergic neurons attenuates pyramidal cell suppression, but not excitation in dorsal hippocampus field CA1 induced by subcutaneous injection of formalin. *Neuroscience*, 103: 985-998.